

# **Development Strategies and Functional Enhancements of Peptide and Nucleic Acid Aptamers as Covalent Drugs**

“ペプチド・核酸アプタマー型共有結合性薬剤  
の開発戦略とその機能拡張”

**Yudai Tabuchi**

**Department of Engineering Science  
Graduate School of Informatics and Engineering  
The University of Electro-Communications**

**March 2022**

## **Document description**

A thesis submitted to the University of Electro-Communications in accordance with the requirements of the degree of Doctor of Engineering

Title:

Development Strategies and Functional Enhancements of Peptide and Nucleic Acid Aptamers as Covalent Drugs

Author:

Yudai Tabuchi

Approved by the Dissertation Committee:

Chair: Professor Masumi Taki

Professor Takayuki Ishida

Professor Takashi Hirano

Associate Professor Hideki Shirakawa

Associate Professor Shojiro Maki

**Copyright Notice:**

© 2022 Yudai Tabuchi

All Rights Reserved

## Summary in Japanese

近年、標的蛋白質<sup>1</sup>に対して特異的に共有結合を形成し半永久的な薬剤効果を発揮する共有結合性薬剤<sup>2</sup>の開発が脚光を浴びている。共有結合性薬剤は標的以外に不可逆的に結合することで長期的な副作用を引き起こすリスクがあるため、反応特異性の高さが重要となる。そのため、近年では、標的蛋白質に対する高い特異性を持つペプチドや蛋白質<sup>3</sup>などのバイオリジクス<sup>4</sup>に反応基を導入することで高い反応特異性を持つ共有結合性薬剤の開発が行われ始めている。

私は、拡張ファージディスプレイ法<sup>5</sup>による標的特異的なペプチド型共有結合性薬剤の直接的な獲得と、世界で初となる薬効の中和<sup>6</sup>が可能な核酸アプタマー<sup>7</sup>型共有結合性薬剤の開発をそれぞれ行った。さらに、核酸アプタマー型共有結合性薬剤が標的蛋白質に対して共有結合を形成することにより、ヌクレアーゼ<sup>8</sup>による分解から逃れて安定に存在することを実証した。

(参考) 専門用語の補足など：

1. 標的蛋白質と薬剤：病気の原因となる物質は生体内の蛋白質であることが殆どであり、これを標的として結合/阻害するものが薬剤。
2. 従来型共有結合性薬剤の例：解熱鎮痛薬（アセチルサリチル酸；商品名バファリン）
3. ペプチドや蛋白質：分子量が中くらい（数百～一万程度）のポリアミド型生体分子をペプチド、分子量がそれ以上のものを蛋白質と一般に呼ぶ。
4. バイオリジクス：分子量が中くらい以上の生体分子のこと。一般的にはペプチドや蛋白質のほか、核酸(=DNA や RNA)および多糖などを総称してバイオリジクスと呼ぶ。
5. ファージディスプレイ法：多種類（約  $10^9$  種類）の多様性を持つペプチドライブラリーの中から標的蛋白質だけに結合するペプチドを選択する進化分子工学的な手法。
6. 薬効の中和：薬剤が効きすぎたときに行う「解毒」とほぼ同義。
7. アプタマー：標的特異性を持つバイオリジクス。狭義では核酸型のものを、広義ではペプチドまたは核酸型のものを指す。
8. ヌクレアーゼ：体内で働く、核酸（DNA）を分解する酵素。

## Abstract

Biologics (*e.g.*, peptides, proteins, nucleic acids) is attracted attention as a covalent-drug modality for alleviating off-target reactions. However, the methods to develop biologics type covalent drugs are limited, and further, it is challenging to overcome the potential risk of irreversible ADEs yet. Thus desirably, there are needs the additional strategies for the development and functional enhancement of covalent drugs.

Here, I demonstrated novel development strategies and functional enhancements of peptide and nucleic acid aptamers as covalent drugs. Specifically, 1) a novel direct and stringent screening method to obtain a peptidic-covalent binder using T7 phage display, and 2) a novel covalent drug modality that allows the neutralization of permanent drug action at an arbitrary time using the DNA aptamer, were developed in this study. Furthermore, both peptide and nucleic acid aptamer type covalent drugs obtained here showed remarkable reaction specificity, and preferable property of target inhibition activity ( $k_{\text{inact}}/K_i = 25 \pm 5.8 \text{ M}^{-1} \text{ s}^{-1}$  and  $0.21 \pm 0.06 \mu\text{M}^{-1} \text{ s}^{-1}$  respectively). Additionally, the DNA aptamer type covalent drug showed long-term nuclease resistance compared to that of the original nucleic acid aptamer (*i.e.* non-covalent binding aptamer) due to the covalent-binding to the target protein.

I envision that the proposed strategies will apply to a wide range of target proteins and accelerate the development of biologics-type covalent drugs. Furthermore, I believe that my findings will mitigate the major concern of covalent drugs and accelerate their translation to human usage.

# **Development Strategies and Functional Enhancements of Peptide and Nucleic Acid Aptamers as Covalent Drugs**

“ペプチド・核酸アプタマー型共有結合性薬剤  
の開発戦略とその機能拡張”

**Yudai Tabuchi**

**Department of Engineering Science  
Graduate School of Informatics and Engineering  
The University of Electro-Communications**

**March 2022**

## Preface

In recent years, there have been major efforts in the fields of drug discovery and chemical biology to develop covalent drugs. The covalent drugs have a unique drug action mechanism that can form permanent bonds to target proteins and, in theory, eternally exert the drug effect. However, because of the potential risks for irreversible adverse drug effects by covalent binding to off-target, covalent drugs require high target specificity. Therefore, covalent drug modalities in the fundamental research are gradually shifting to middle- or large-molecular-weight biologics (*e.g.*, peptides, proteins, nucleic acids) from the small molecules. In most cases, the biologics type inhibitors are created by rational design such as introducing a warhead (*i.e.*, reactive group) into the targeted biologics at a specific position via bioconjugation or non-natural amino acid incorporation. However, methods to identify the appropriate position of the biologics for introducing a warhead are often time-consuming, and sometimes unsuccessful. Currently, the development would be performed by limited numbers of methodologies, and alternative methods for obtaining biologics type covalent inhibitors are requested. Furthermore, so far many small molecule-, peptide-, and protein-type covalent drugs have been developed. However, to the best of my knowledge, none have overcome the potential risks of irreversible adverse drug effects (ADEs). Under this scientific background, I started the development of an alternative approach to obtain peptidic target-specific covalent binders by using a combinatorial screening method. I also developed the first example of a nucleic-acid-type covalent binder as a novel modality to overcome the potential risks of the irreversible ADEs.

Chapter 1 describes the introduction of recent advances in the development of biologics type covalent drugs and their challenges. Chapter 2 describes the development of a peptide-type covalent drug by using the expanded T7-phage display; I investigated the reactivity of different warheads, and performed a selection using a peptide library possessing the optimized warhead. With this ‘direct’ combinatorial screening, I successfully obtained a target-specific covalent binder. Chapter 3 describes the development of a DNA aptamer-type covalent drug that can reverse its semi-permanent inhibition activity at an arbitrary time. Chapter 4 describes the nuclease resistance of the DNA aptamer after the conjugation with the target protein.

I sincerely hope that this research will contribute to the development of biologics-type covalent drugs and accelerate the translation to human usage of them.

## **Table of contents**

### **CHAPTER 1**

#### **General introduction**

### **CHAPTER 2**

#### **Direct screening of a target-specific covalent binder: stringent regulation of warhead reactivity in a matchmaking environment**

2.1 – Introduction

2.2 - Results and discussion

2.3 - Experimental procedures and additional figures

### **CHAPTER 3**

#### **Inhibition of thrombin activity by a covalently-binding aptamer and reversal by the complementary strand antidote**

3.1 - Introduction

3.2 - Results and discussion

3.3 - Experimental procedures and additional figures

### **CHAPTER 4**

#### **Relative nuclease resistance of DNA-aptamer covalently conjugated to a target protein**

4.1 - Introduction

4.2 - Results and discussion

4.3 - Experimental procedures and additional figures

### **CHAPTER 5**

#### **Concluding remarks**

### **CHAPTER 6**

#### **References**

**List of publications**

**List of presentations**

**List of grants and awards**  
**Acknowledgments**

## Abbreviations

FDA:	Food and Drug Administration
10BASE <sub>d</sub> -T:	gp10 based-thioetherification
BSA:	bovine serum albumin
CBB:	Coomassie Brilliant Blue
CD:	circular dichroism
Da:	dalton
DNA:	deoxyribonucleic acid
DTT:	dithiothreitol
SuFEx:	sulfur fluoride exchange
ESI:	electrospray ionization
gp10:	gene-10 protein
GST:	glutathione <i>S</i> -transferase
HPLC:	high-performance liquid chromatography
D-PBS:	Dulbecco's Phosphate-Buffered Saline
LC:	liquid chromatography
NMR:	nuclear magnetic resonance
MS:	mass spectrometry
PAGE:	polyacrylamide gel electrophoresis
PFU:	plaque-forming units
NGS:	next-generation sequencer
SDS:	sodium lauryl sulfate
TCEP:	tris(2-carboxyethyl)phosphine
TOF:	time-of-flight
Fam:	carboxyfluorescein
UV:	ultraviolet
Alkyl-SO <sub>2</sub> F:	alkyl-sulfonyl fluoride
Aryl-SO <sub>2</sub> F; AFS:	aryl-fulorosulfate
ESF:	ethene sulfonyl fluoride
Br-AFS:	4-bromoacetamide aryl-fluorosulfate
MAFS:	Michael acceptor-type AFS
PDA:	photodiode array
DIPEA:	<i>N,N</i> -diisopropylethylamine
DCM:	dichloromethane

DMF:	<i>N, N</i> -dimethylformamide
PB:	phosphate buffer
GUI:	graphical-user interface
FL-IA:	5-(idodoacetamido)fluorescein
PCR:	polymerase chain reaction
DMSO:	dimethyl sulfoxide
CDNB:	1-chloro-2,4-dinitrobenzene
ADEs:	adverse drug effects
CS:	complementary strand
DS:	double-strand
TBA:	thrombin binding aptamer
SELEX:	Systematic Evolution of Ligands by EXponential enrichment
CuAAC:	copper(I)-catalyzed azide-alkyne cycloaddition
MALDI-TOF/MS:	matrix-assisted laser desorption/ionization time-of-flight mass spectrometry
SPPS	solid-phase peptide synthesis
PBP	penicillin-binding protein
MAO-B	monoamine oxidase B
GABA	gamma-Amino Butyric Acid
DPP-IV	dipeptidyl Peptidase IV
DOPA	aromatic L-amino acid decarboxylase

# **CHAPTER 1**

## **General introduction**

Recently irreversible binding inhibitors (*i.e.*, covalent drugs) have attracted re-attention as therapeutic agents.<sup>1-9</sup> Covalent drugs can form a permanent bond to target proteins and irreversibly inhibit their activity (Fig. 1.1). This prolonged drug effects result in less-frequent drug dosing and in wide therapeutic margins for patients.<sup>6, 8, 9</sup> In addition, the mechanism of covalent binding would improve the inhibition selectivity of protein families and subtypes and reduce the risk of drug resistance in the oncology and infectious fields.<sup>8</sup> However, covalent drugs have potential risks of non-specific covalent binding to off-target biological components, which would induce serious side effects.<sup>6, 8, 10</sup> Thus, the development of covalent drugs in pharmaceutical companies has been avoided for long years.<sup>6</sup> On the contrary of the development trend, one-third of FDA-approved enzyme inhibitors are covalent drugs and clinically used to treat various diseases (Table 1.1)<sup>6</sup>. The reason is that most covalent drugs are obtained by coincidence, not intentionally developed; the mechanism of covalent inhibition has clarified after their usefulness had been confirmed.<sup>6</sup>

From the 2000s, intentional covalent drug developments have started for alleviating off-target reactions by linking warheads (*i.e.*, weakly reactive electrophiles) to high-affinity and selective binding elements.<sup>6-8</sup> The major developments in covalent drugs have been focused on small molecules because of their desirable features such as easy production, lack of immunogenic response, and the possibility of oral administration.<sup>11, 12</sup> So far, many small-molecule-type covalent drugs have been approved by FDA (Fig. 1.2), and the number of publications and patent applications that refer to covalent drugs has increased exponentially since 2010. However, it is known that such small-molecule-type covalent drugs, including FDA-approved ones, tend to cause off-target reactions depending on their concentration; the interaction between the small molecules and a protein is strongly influenced by the hydrophobic effect, which induces off-target binding and reaction.<sup>13, 14</sup> To avoid such problems due to the off-target binding, covalent drug modalities in the fundamental research are gradually shifting to biologics (*e.g.*, peptides, proteins, and nucleic acids), which have high target specificity and selectivity.<sup>15-</sup>

19

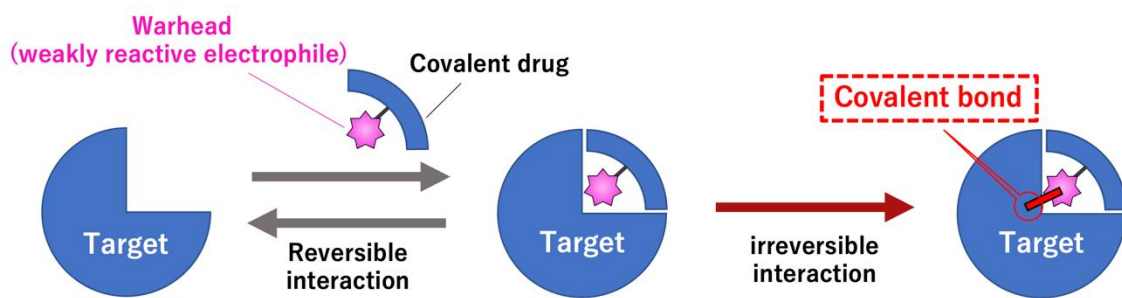


**Fig. 1.1** Inhibition mechanism of covalent drugs. A covalent drug that possesses a reactive moiety (*i.e.*, warhead) reversibly interacts with a target protein (left and middle). A covalent bond is formed between the target protein and the covalent drug (right).

**Table 1.1** List of approved covalent drugs. This table is made by partial modification from supplementary information S1 of a reference.<sup>6</sup>

Compound Name	First Approval	Molecular target	Therapeutic Area	Approved Indication (s)	Was prototype discovered or invented?
Amoxicillin	1982	PBP	Anti-infective	Bacterial infection	Discovered/pathogen screening
Augmentin/Amoxicillin + clavulanic acid	1984	PBP and beta-lactamase	Anti-infective	Bacterial infection	Discovered/pathogen screening
Cefaclor/Ceclor	1988	PBP	Anti-infective	Bacterial infection	Discovered/pathogen screening
Cefprozil/Cefzil	1991	PBP	Anti-infective	Bacterial infection	Discovered/pathogen screening
Ceftriaxibe/Rocephin	1984	PBP	Anti-infective	Bacterial infection	Discovered/pathogen screening
Cefuroxime axetil/Ceftin	1987	PBP	Anti-infective	Bacterial infection	Discovered/pathogen screening
Cephalexin/Keflex	1986	PBP	Anti-infective	Bacterial infection	Discovered/pathogen screening
D-cycloserine/Seromycin	1982	Alanine racemase	Anti-infective	Bacterial infection	Discovered/anti-biotic screening
Fosfomycin/Monurol	1996	UDP-N-acetylglucosamine-3-enolpyruvyl-transferase	Anti-infective	Anti-bacterial	Discovered/anti-biotic screening
Isoniazid	1982	Enol-acyl carrier protein reductase	Anti-infective	Tuberculosis	Discovered/tuberculosis screening
Meropenem	1996	PBP	Anti-infective	Bacterial infection	Discovered/pathogen screening
Ornicef/Cefdinir cefzon	1997	PBP	Anti-infective	Bacterial infection	Discovered/pathogen screening
Penicillin V	1982	PBP	Anti-infective	Bacterial infection	Discovered/pathogen screening

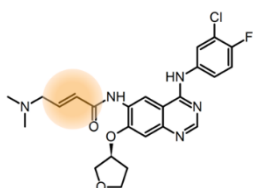
**Table 1.1 (Continued)**

Compound Name	First Approval	Molecular target	Therapeutic Area	Approved Indication (s)	Was prototype discovered or invented?
Azacytidine/Azacytidine	2004	Methyltransferase	Cancer	Anti-cancer	Invented/mechanism based design
Bortezomib/Velcade	2003	Proteasome	Cancer	Anti-cancer	Invented/mechanism based design
Decitabine/AzacD	2006	Methyltransferase	Cancer	Anti-cancer	Invented/mechanism based design
Dutasteride/Avodart	2001	5-alpha-reductase	Cancer	Benign prostatic hypertrophy	Invented/mechanism based design
Exemestane/Aromasin	1999	Aromatase	Cancer	Breast cancer	Discovered
Floxuridine	2000	Thymidylate synthase	Cancer	Anti-cancer	Invented/mechanism based design
Gemcitabine/Gemzar	1996	Ribonucleoside reductase	Cancer	Anti-cancer	Discovered
Proscar/Finasteride	1992	5-alpha-reductase	Cancer	Benign prostatic hypertrophy/hair growth stimulant	Invented/mechanism based design
Plavix/Clopidogrel	1997	BMS/Sanofi	Cardio-vascular	Reduction of risk for stroke and heart attack	Discovered/ex vivo screening
Warfarin	1982	Vitamin K reductase	Cardio-vascular	Anti-coagulant	Discovered
Rasagiline	2006	MAO-B	CNS	Parkinson's disease	Discovered
Rivastigmine/Exelon	2007	MAO-B	CNS	Dementia/Parkinson's disease	Invented/mechanism based design
Selegiline	1989	MAO-B	CNS	Parkinson's disease	Discovered
Vigabatrin	2009	GABA-aminotransferase	CNS	Anti-epileptic	Invented/mechanism based design

**Table 1.1 (Continued)**

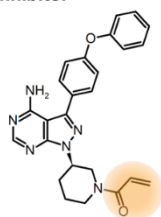
Compound Name	First Approval	Molecular target	Therapeutic Area	Approved Indication (s)	Was prototype discovered or invented?
Nexium/Esomeprazole	2001	H+/K+ ATPase	Gastro-intestinal	Esophageal reflux and heartburn	Discovered/animal screening
Orlistat/Xenical/Alli	1999	Lipase	Gastro-intestinal	Hyperlipidemia	Discovered/enzyme screening
Prevacid/Lansoprazole	1995	H+/K+ ATPase	Gastro-intestinal	Esophageal reflux and heartburn	Discovered
Prilosec/Omeprazole	1989	H+/K+ ATPase	Gastro-intestinal	Esophageal reflux and heartburn	Discovered
Protonix/Pantoprazole	2000	H+/K+ ATPase	Gastro-intestinal	Esophageal reflux and heartburn	Discovered
Aciphex/Rabeprazole	1999	H+/K+ ATPase	Gastro-intestinal	Esophageal reflux and heartburn	Discovered
Aspirin	1982	Cyclooxygenase	Inflammation	Inflammation and stroke prevention	Discovered
Disulfiram/Antabuse	1983	Aldehyde dehydrogenase	Other	Alcoholism	Discovered
Eflornithine	1990	Ornithine decarboxylase	Other	Facial hair retardant and anti-trypanosomiasis	Invented/mechanism based design
Propylthiouracil/Procasil	1982	Thyroxine-5-deiodinase	Other	Hyperthyroidism	Animal screening
Saxagliptin/Onglyza	2009	DPP-IV	Other	Diabetes	Invented/mechanism based design
Vildagliptin/Eugreas	2008	DPP-IV	Other	Diabetes	Invented/mechanism based design
Phenoxy-benzamine hydrochloride	1982	Alpha adrenoceptor	Cardio-vascular	Phenochromocytoma	Invented/mechanism based design
Mercaptopurine/Purinthol	1982	Purine nucleotide synthesis	Cancer	Acute lymphatic leukemia	Discovered
Carbidopa/Lodosyn	1982	DOPA decarboxylase	CNS	Parkinson's disease	Invented/mechanism based design

**EGFR inhibitor :**



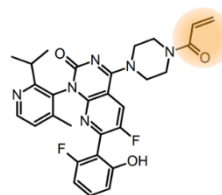
**Afatinib**  
FDA approval in 2013

**BTK inhibitor :**

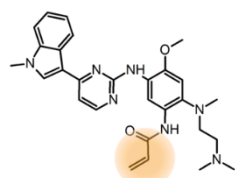


**Ibrutinib**  
FDA approval in 2013

**Kras G12C inhibitor :**



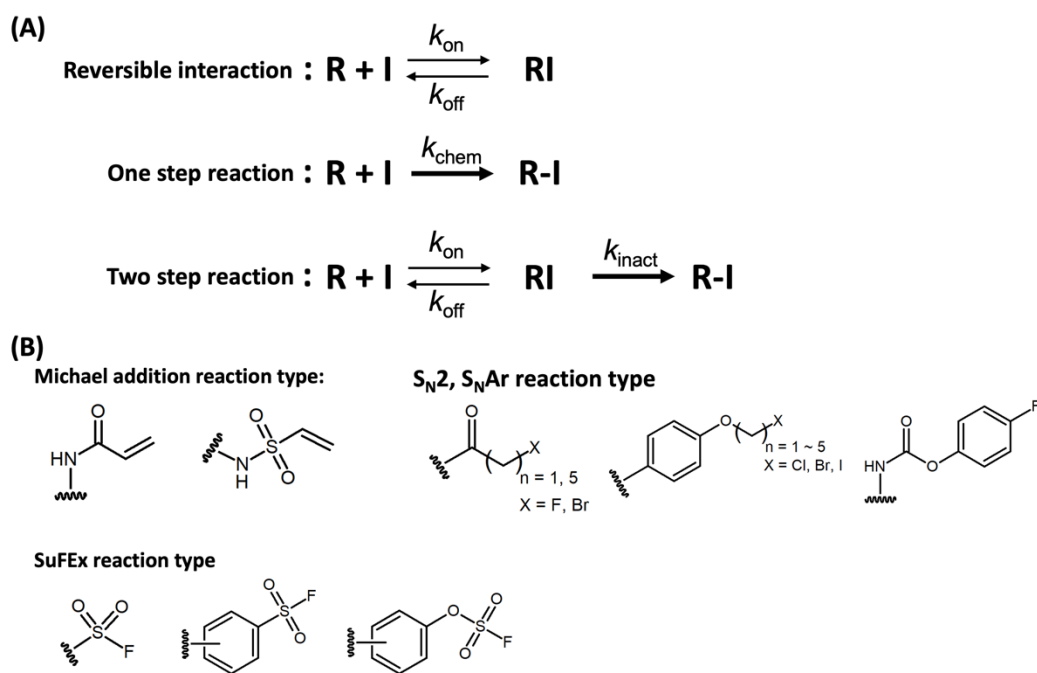
**Sotorasib**  
FDA approval in 2021



**Osimertinib**  
FDA approval in 2015

**Fig. 1.2** Rationally designed covalent drugs in which FDA approved.

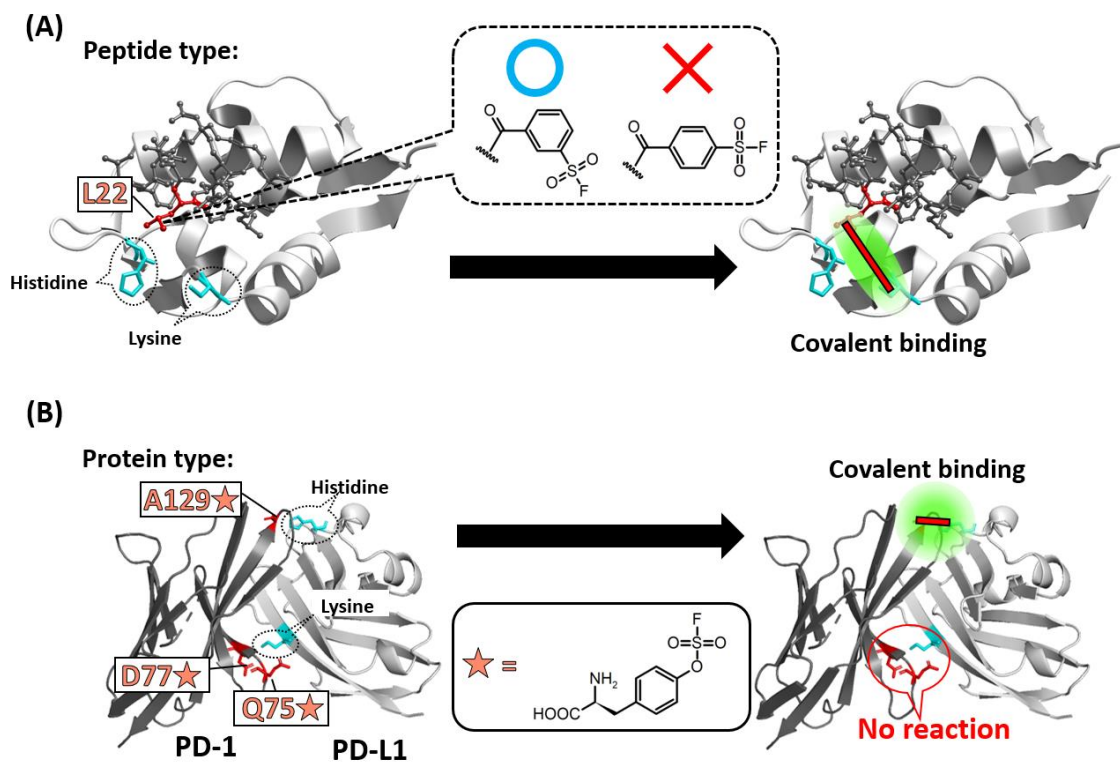
Adjusting warhead electrophilicity is the key for developing covalent drugs, regardless of the modality (*e.g.*, low molecular or biologics type); too much electrophilicity would induce non-specific reactions to any nucleophilic functional groups of any target-unrelated protein (Fig. 1.3A, one step reaction). Thus, weak electrophilic warheads which do not react with the nucleophilic functional group at a dilute concentration are needed.<sup>7</sup> By introducing such a warhead to an appropriate position of the binding element, the location of the warhead becomes closer to a destined nucleophilic amino acid of the target protein. This proximity effect increases the local effective concentration of the warhead / nucleophilic amino acid, and promotes the appropriate covalent binding reaction (Fig. 1.3A, two step reaction).<sup>6-8, 18</sup> So far, Michael-addition-, conventional nucleophilic substitution- ( $S_N2$ ,  $S_NAr$ ), or sulfur fluoride exchange- (SuFEx) reaction-type warheads have been used in developments of biologics-type covalent inhibitors (Fig. 1.3B).<sup>18</sup> In most cases, the biologics-type covalent inhibitors are created by rational design, such as introducing these warheads into the targeted biologics at specific positions via bioconjugation or unnatural amino acid (Uaa) incorporation.<sup>15-19</sup> Specifically, the developments of peptide-type covalent inhibitors have started at an early stage (*i.e.*, in the middle of 1960s) because position-specific chemical modification of the warhead can be easily performed through the historically-established solid-phase peptide synthesis<sup>20</sup> (SPPS) followed by the post-synthesis bioconjugation. In contrast, the developments of the protein-type covalent inhibitors have been delayed because the specific chemical modification of a protein is a huge challenge; only the Uaa incorporation methodology is performed.<sup>21-23</sup> However, the warhead on the Uaa would promiscuously react to off-target biologics components, resulting in interruption of translation or cytotoxicity.<sup>18</sup> This promiscuous reaction has been overcome elegantly by Xiang in 2013 through fine-tuning of the Uaa-warhead electrophilicity on the basis of proximity-enabled reactivity; the Uaa does not react with off-target-natural amino acids and other biomolecules under physiological conditions.<sup>24</sup> After this breakthrough, protein-type covalent inhibitors have been actively reported.<sup>18</sup>



**Fig. 1.3** (A) Interaction mechanism between the target (R) and the inhibitor (I) of non-covalent type (top), conventional alkylation-type (middle), or targeted covalent-type (bottom). (B) Warhead structures used in biologics-type covalent inhibitors.

Now, a major challenge of developing biologics-type covalent inhibitors is determining most appropriate position(s) of the warhead to be introduced. In most cases, the position is determined based on the three-dimensional structure of a biologics/target complex. However, such position determination is often time-consuming, and the covalent bond can not necessarily form by introducing a warhead to biologics. In fact, when a SuFEx-type warhead, which can theoretically react with any nucleophilic amino acids<sup>25-32</sup>, was introduced into 22nd leucine (L22) position of a Mdm2/4-binding staple peptide, a covalent bond did not form despite the presence of histidine and lysine in the vicinity on the target protein; unpredictably, the expected covalent bond formed when a regioisomer of the warhead was used (Fig. 1.4A).<sup>33</sup> Furthermore, when a SuFEx type Uaa-warhead was rationally introduced into the 75th glutamine, 77th asparagine, and 129th alanine (Q75, D77, A129) of PD-1 protein, respectively, only A129-mutated PD-1 reacted with PD-L1 (Fig. 1.4B).<sup>24</sup> These results suggested that such a simple point mutation is not often enough to facilitate the covalent reaction; stringent proximity and orientation between the warhead and the nucleophilic amino acid are needed. Currently, the methods addressing such problems are limited, thus desirably, there is a need for the development of an alternative approach.

Meanwhile, combinatorial screening methods are widely used to discover binders as they allow for the rapid generation of a candidate library with a large diversity.<sup>34</sup> Furthermore, the candidates of the combinatorial library could possess a specific function by incorporating a common structure. As an example, I successfully generated a fluorescent library by incorporating a Schiff-base structure, and obtained a targeted fluorescent binder.<sup>35</sup> Theoretically, in a similar way, covalent drugs should be obtained by combinatorial screening methods by incorporating a warhead structure into a designated position of a biologics library. However, they are rarely reported because regulation of the warhead reactivity during the library construction and selection is difficult; the warhead in the library often forms promiscuous covalent bonds between biologics.<sup>36</sup> To avoid this, my group reported an *indirect* combinatorial method to obtain a covalent binder by using a bait-incorporated peptide library on the T7 phage, which is followed by alteration of the bait to a warhead (Fig. 1.5A).<sup>36</sup> In 2021, *direct* combinatorial screening methods were independently reported by Bogyo's group and my group (Fig. 1.5B, C). Bogyo's group elegantly designed novel least-reactive warheads to minimize the promiscuous reactions between the biologics, and successfully selected the peptide type covalent binder using M13 phage display.<sup>37</sup> To minimize the promiscuous reaction during the selection, I took another strategy to design the warhead, to perform an affinity/proximity/ reactivity-based co-selection as shown in the next chapter.<sup>38</sup>



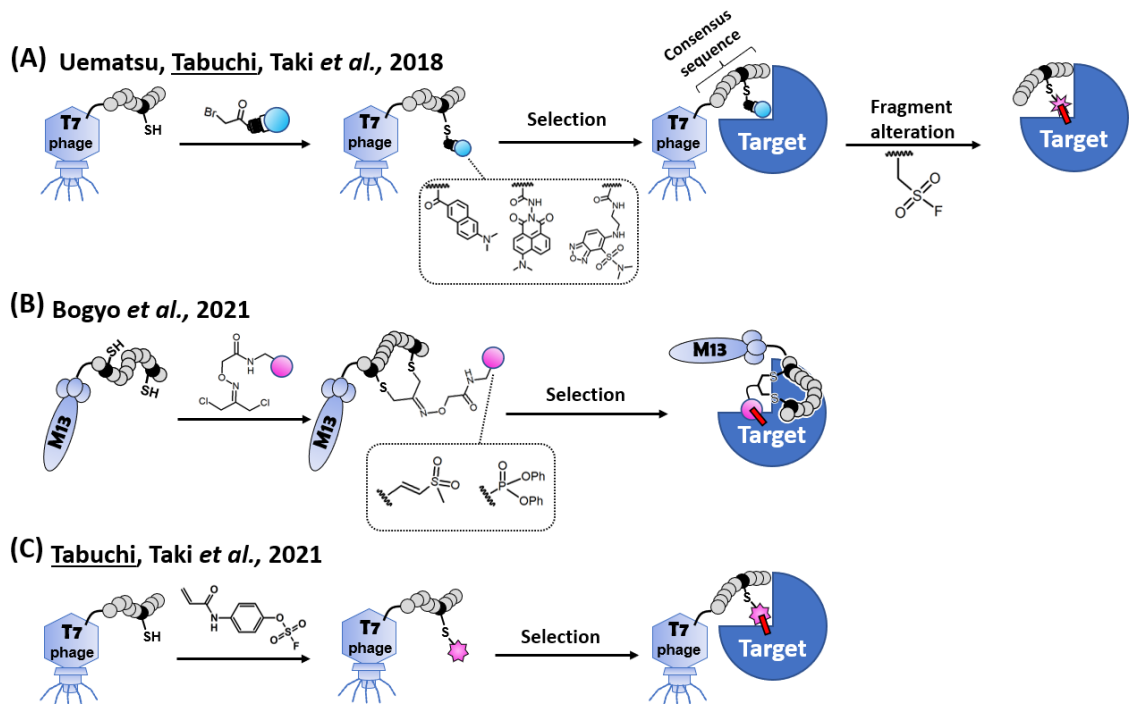


**Fig. 1.5** All of the reported methods in the combinatorial screening of peptide-type covalent binders. (A) Indirect screening. Library peptide on the T7 phage is modified by each bait fragment respectively. After the selection for a target protein, a consensus sequence of a peptide fragment is obtained. The bait fragment of the peptide is alternated to a SuFEx-type warhead for obtaining a covalent binder. (B) Bogyo's direct screening method. A cysteine-reactive vinyl sulfone or a serine-reactive diphenylphosphonate is introduced to the library peptide on the M13 phage. A covalent binder is directly selected from the warhead modified cyclic peptide library. (C) My direct screening method. Aryl-fluorosulfate (AFS) warhead is introduced to the library peptide on the T7 phage. A covalent binder is directly selected from the AFS-modified peptide library.

## **CHAPTER 2**

**Direct screening of a target-specific covalent binder:  
stringent regulation of warhead reactivity in a  
matchmaking environment**

## ■ 2.1 Introduction

As described in the previous Chapter, direct combinatorial screening of biologics type covalent inhibitors is still challenging. Thus, further structural optimization of the warhead is needed to regulate its reactivity during library construction and selection. One strategy is to minimize its reactivity; Bogyo *et al.* have just reported a direct screening using the M13 phage<sup>37</sup> by synthesizing a cysteine-reactive vinyl sulfone and a serine-reactive diphenylphosphonate<sup>26</sup> as the ‘least reactive’ warheads.<sup>37</sup> Another strategy is to turn-on its reactivity only in a matchmaking microenvironment<sup>7, 25</sup> (Fig. 2.1); the screening using a warhead-modified peptide library would destine both the reactivity of the warhead and the target affinity of the covalent binder to be selected. A turn-on warhead was synthesized here and introduced into designated cysteines of a peptide library on the T7 phage to construct such a library.<sup>39, 40</sup> With this library, I directly screened the covalent binder by the reactivity/affinity-based co-selection.

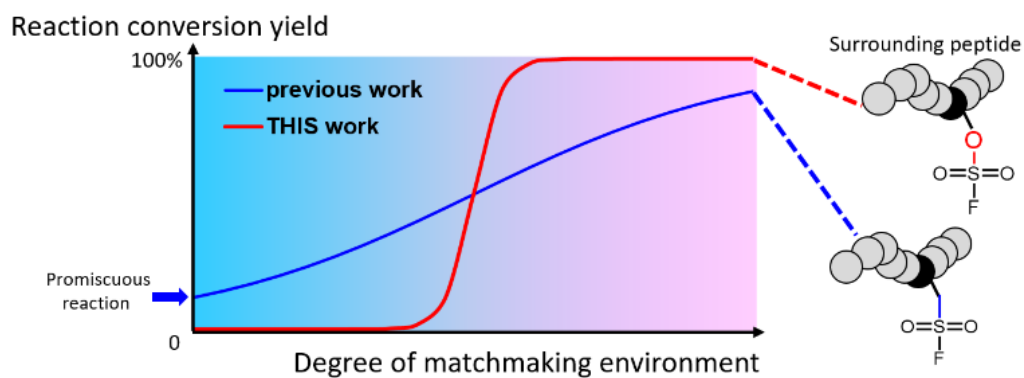


**Fig. 2.1** Stringent regulation of warhead reactivity in a matchmaking microenvironment created between a target protein and a warhead-modified peptide for direct screening of a target-specific covalent binder. Previous work (blue line): sulfonyl fluorides form promiscuous covalent bonds between biologics.<sup>36</sup> This work (red line): a turn-on warhead (*i.e.*, aryl-fluorosulfate) possessed exquisite reactivity which allowed us to perform reactivity/affinity-based co-selection against a target protein.

## ■ 2.2 Results and discussion

First, I decided the appropriate structure of the turn-on warhead on the basis of reactivity optimization in the sulfur fluoride exchange (SuFEx) catalytic microenvironment.<sup>25-32</sup> As a model target protein, I used glutathione-*S*-transferase (GST) so that I can compare all the results of this work with those of the peptidic GST covalent binder obtained by an indirect screening.<sup>36</sup> As the SuFEx-based warhead candidates, three major structures can be considered: alkyl-sulfonyl fluoride (alkyl-SO<sub>2</sub>F), aryl-SO<sub>2</sub>F, and aryl-fluorosulfate (aryl-OSO<sub>2</sub>F; AFS) which can react with any nucleophilic amino acid residues (*i.e.*, serine, threonine, lysine, tyrosine, cysteine, and histidine).<sup>25</sup> Among them, I excluded aryl-SO<sub>2</sub>F as it forms promiscuous bonds<sup>36</sup> because of its higher reactivity.<sup>16, 25</sup> Here, by introducing ethene sulfonyl fluoride (ESF) and 4-bromoacetamide aryl-fluorosulfate (Br-AFS), respectively, at the designated cysteine (underlined), I compared the reaction conversion yields of alkyl-SO<sub>2</sub>F and AFS on a GST binder (*i.e.*, LNYCDGW) (Fig. 2.2A).<sup>36</sup> Each warhead-modified peptide was covalently bound to the same tyrosine of GST (Fig. 2.2B and C), and the reaction conversion yield of AFS-modified peptide was over 90%, whereas that of ESF-modified peptide was only 60% (Fig. 2.3). The AFS-modified peptide would be inert in the presence of target-unrelated proteins,<sup>25</sup> and fortunately, the warhead was resistant against hydrolysis (Fig. 2.4).<sup>16</sup> Therefore, I determined AFS to be the ideal turn-on warhead and used it for further experiments. On the contrary, the incomplete reaction of the ESF-modified peptide could not be overcome by elongating the reaction time or increasing the peptide concentration. I suppose this is most probably caused by instability of alkyl-SO<sub>2</sub>F against hydrolysis.<sup>41</sup>

Second, I confirmed the introduction of the turn-on warhead to the designated cysteines of a model peptide (–GSRVS-C-GGRDRPG-C-LSV) on a T7 phage monoclonal.<sup>39</sup> Surprisingly, Br-AFS did not react even at 55°C (Fig. 2.5A). When I changed the haloacetyl group of Br-AFS into an acryloyl one, the expected thioetherification of the cysteines with the Michael acceptor-type AFS (MAFS) was occurred at 37°C (Fig. 2.5B and C).

Third, I constructed a warhead-modified peptide library (–SGGG-X<sub>3</sub>-C\*-X<sub>4-10</sub>-C\*-X<sub>3</sub>; where X and C\* represent amino acids and MAFS-modified cysteine, respectively) on the T7 phage, and performed a direct screening against GST-immobilized magnetic beads (Fig. 2.6A). Before the screening, I determined stringent washing conditions during the biopanning in order to eliminate unfavorable non-covalent interactions between GST and any target-unrelated peptides in a denatured state. Unexpectedly, the T7 phage did not lose

its infectivity<sup>39,42</sup> when it was treated with a stringent washing buffer made from 1% (w/v) sodium dodecyl sulfate (SDS), 4 M urea, 150 mM NaCl, and 50 mM dithiothreitol (DTT) in Dulbecco's Phosphate-Buffered Saline (D-PBS) under sonication.<sup>43</sup> After the complete washing during the 1<sup>st</sup> round of biopanning, I evaluated the number of GST-bound phages by a plaque assay; only when the peptide library was modified with MAFS, remarkable phage enrichment was observed (Fig. 2.6B, right). On the contrary, regardless of MAFS modification, enrichment of the model peptide-displayed monoclonal phage never happened (Fig. 2.6B, left). This suggests that the SuFEx reaction was conducted exclusively in the matchmaking environment and was not caused by a non-specific interaction of the warhead on the target-unrelated peptide. Then, another round of the biopanning was performed, and the amino acid sequences of the polyclonal GST covalent binders were analyzed by a next-generation sequencer (NGS). A unique sequence (LESCAWYVHDNTLMCDTF) was predominantly condensed, and no consensus sequence was found among the top 11 most abundant candidates (Fig. 2.6C).

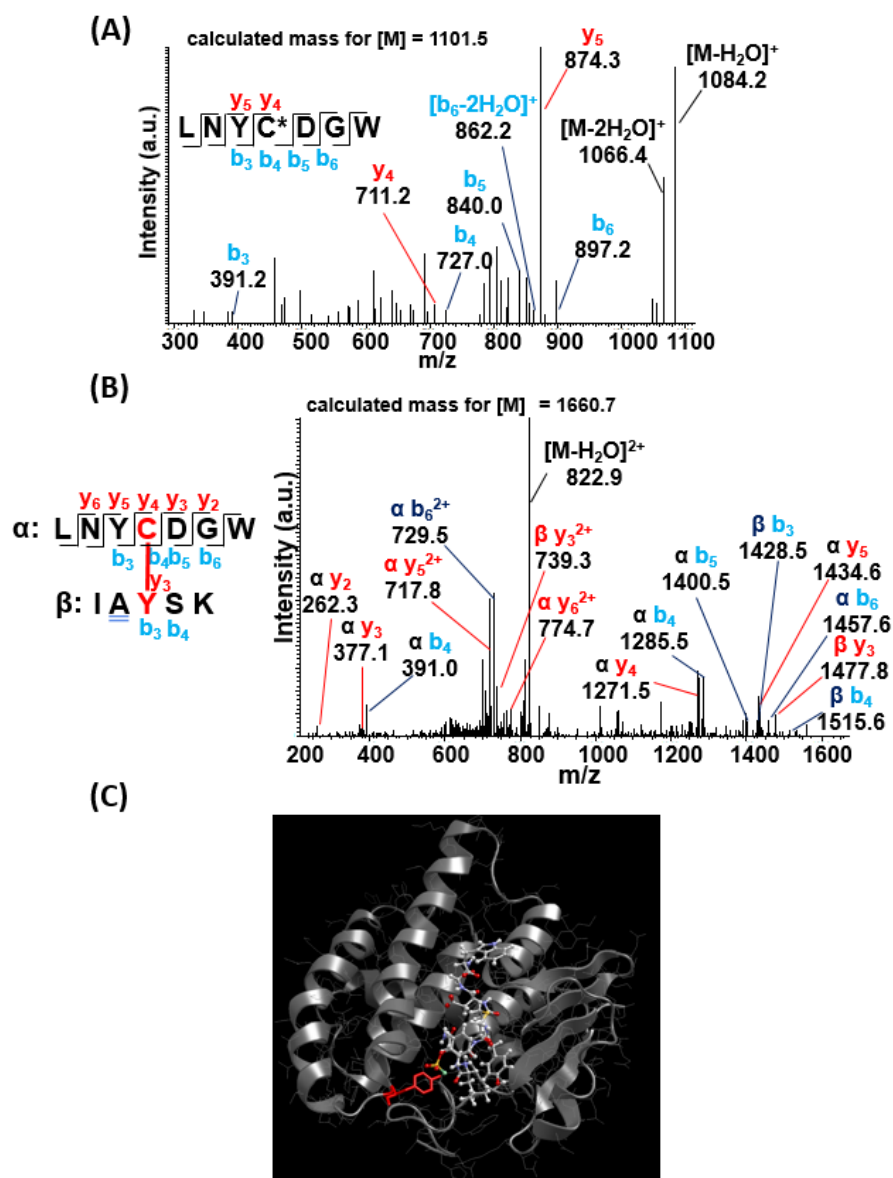


**Fig. 2.2** (A) Identification of the purified LNYC\*DGW peptide via MS/MS analysis; C\* represents AFS-modified cysteine. (B) Identification of covalently-binding position on GST using the AFS-modified binder by the trypsinization/LC-MS/MS analysis; 111<sup>th</sup> tyrosine of GST was exclusively modified. (C) Molecular docking simulation of the AFS-modified binder (shown as a stick) to GST (PDB ID: 1UA5) using sievGene of myPreSt. Fluorine atom in the warhead and the conjugated 111<sup>th</sup> tyrosine were colored in cyan and dark red, respectively. GST was shown as a cartoon with side chains as a line description. The distance between fluorine atom in the warhead and the oxygen atom in 111<sup>th</sup> tyrosine was deduced to be ca. 3.4 Å.

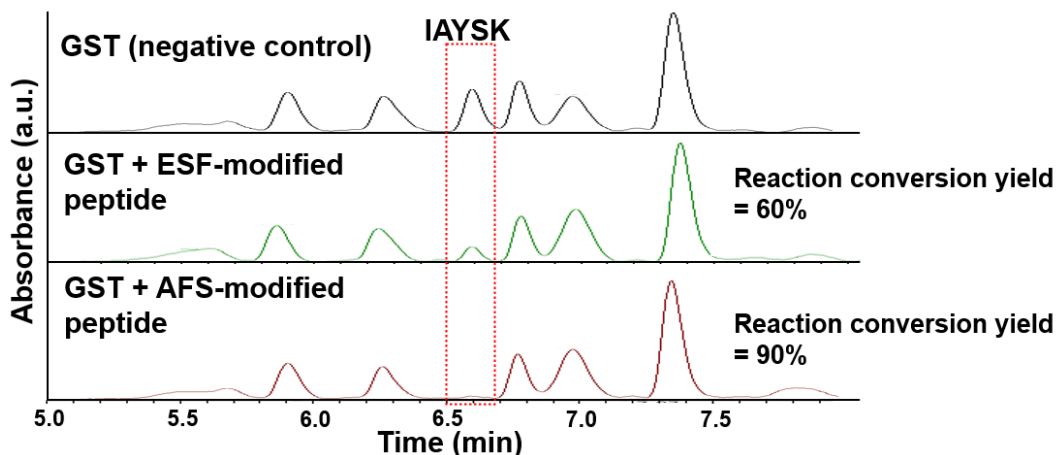


**Fig. 2.3** LC absorbance profiles of trypsinized fragments of GST before (top) and after the reaction with the ESF- (middle) or AFS- (bottom) modified covalent binder (*i.e.*, LNYC\*DGW). The reaction conversion yield was calculated from a disappearance of the GST fragment containing 111<sup>th</sup> tyrosine (*i.e.*, IAYSK at 6.6 minutes; Y should react with each warhead<sup>24</sup>). Other detected GST fragments were used as internal standards.

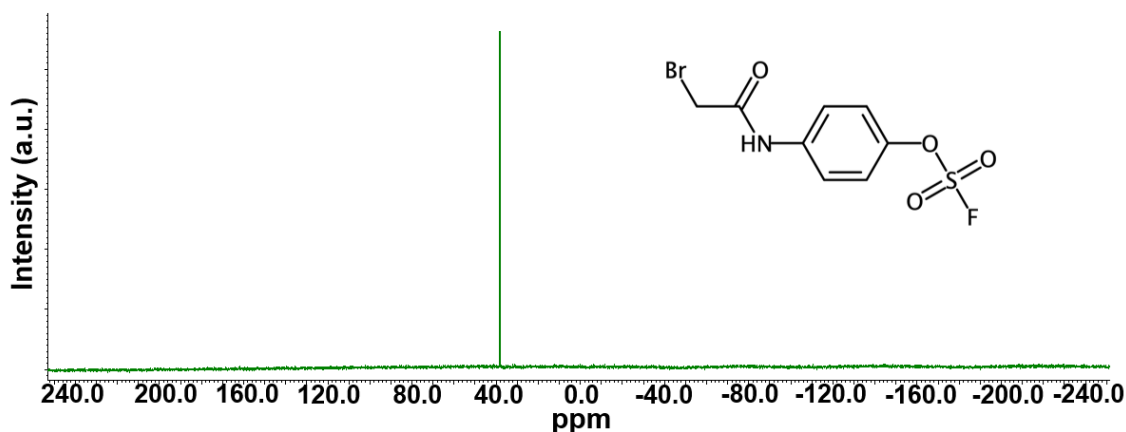


**Fig. 2.4** <sup>19</sup>F NMR spectrum of Br-AFS after incubation for 48 hours at 37°C in 50 mM PB (Na<sub>2</sub>HPO<sub>4</sub>/NaH<sub>2</sub>PO<sub>4</sub> in D<sub>2</sub>O, pH 7.4) / 50% (v/v) DMSO-*d*<sub>6</sub>, to prove its excellent stability against hydrolysis of the warhead. Any unfavorable peaks of hydrolyzed products (*e.g.*, hydrogen fluoride; ca. -200 ppm), could not be seen.

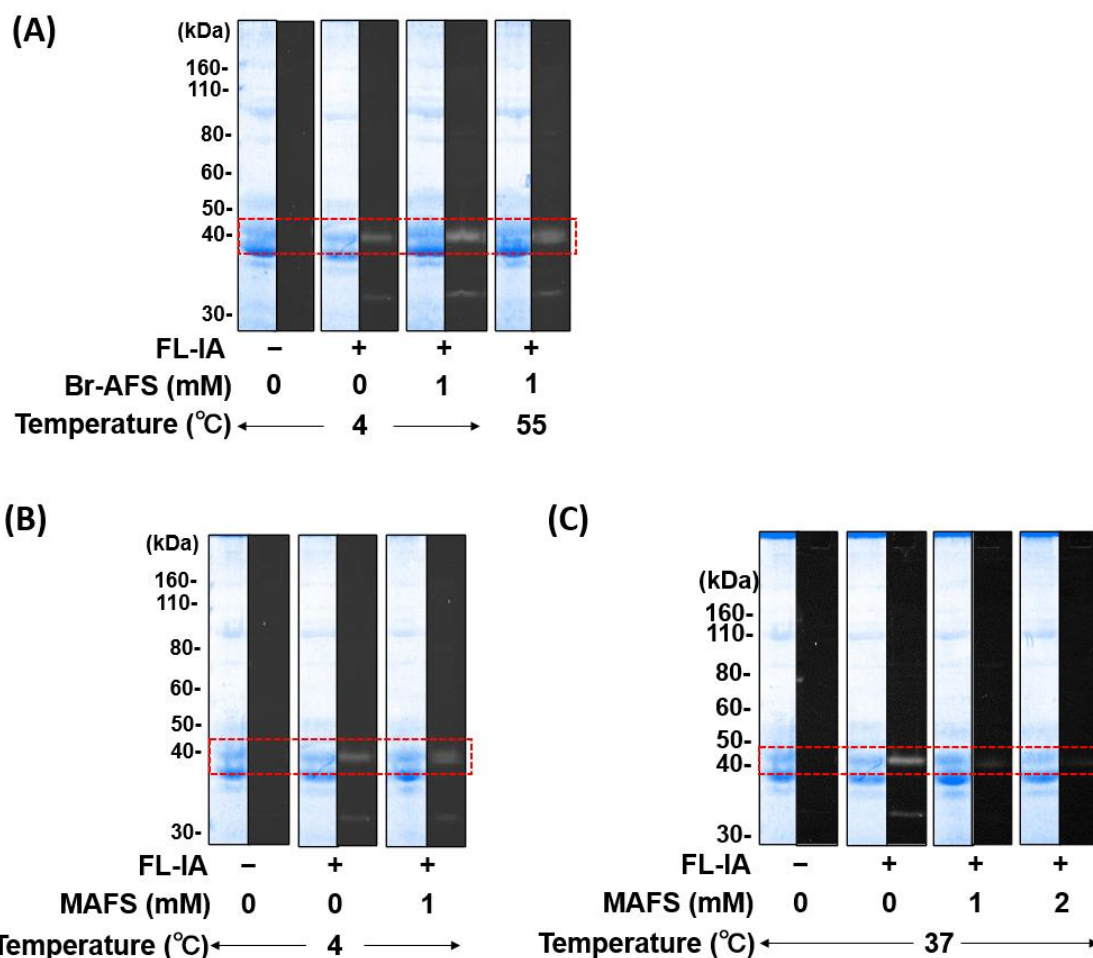


**Fig. 2.5** Evaluation of thioetherification between each warhead and designated cysteines of the model peptide on T7 phage by fluorescent densitometric analysis / CBB staining. A single fluorescent band could be seen at an appropriate molecular weight (*ca.* 44 kDa; red rectangle) of the peptide-fused gp10 when the warhead (*i.e.*, Br-AFS or MAFS) was absent. This control experiment indicates that the thioetherification with FL-IA exclusively occurred at the peptide-fused gp10.<sup>46</sup> (A) Br-AFS introduction. Even when Br-AFS was present, the fluorescent band did not disappear at each temperature. This suggests that Br-AFS did not react with the designated cysteines even at the elevated temperature. (B, C) MAFS introduction at ice temperature and 37°C, respectively. When incubated at 37°C, the fluorescent band disappeared in a concentration-dependent manner. This indicates that the introduction was successful at an optimal molar concentration of 1.0 mM, and FL-IA no longer reacted with the designated cysteines.<sup>44</sup>

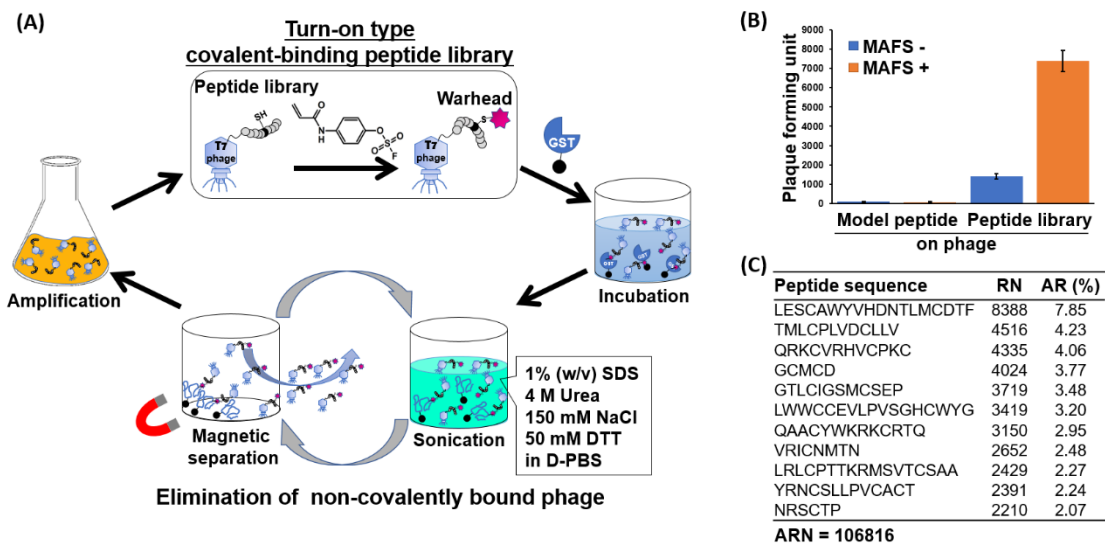


**Fig. 2.6** (A) Schematic diagram of reactivity/affinity-based co-selection. Top: A MAFS-modified peptide library was constructed on the T7 phage. Right: The library was incubated with GST-immobilized magnetic beads; MAFS formed a covalent bond in the matchmaking environment. Bottom: Non-covalently bound phages were completely removed by a stringent washing under sonication. Left: The GST-bound phages were amplified and used for the next round of biopanning. (B) A plaque assay to quantify the GST-bound phages after the 1st round of biopanning. Values are mean SD from 3 independent experiments. Remarkable phage enrichment was observed only when MAFS was conjugated to the library. (C) GST-specific covalent binders identified by a NGS after 2 rounds of biopanning. RN, ARN, and AR stand for reading number, all read number, and abundance ratio (defined as  $100 \times \text{RN}/\text{ARN}$ ), respectively.

Next, I chemically synthesized a representative MAFS-modified peptide whose sequence was LESC\*AWY, and its covalently-binding position on GST was investigated; this sequence was chosen since it is a part of the predominantly enriched peptide, and the other part (*i.e.*, TLMC\*DTF) was impossible to synthesize. First, the representative MAFS-modified peptide and GST were incubated, and SDS polyacrylamide gel electrophoresis (SDS-PAGE) was performed. Then, the GST band in the gel was excised and digested with trypsin. The resulting peptide fragments were analyzed by liquid chromatography-tandem mass spectrometry (LC-MS/MS). An intense absorbance in the chromatogram was newly detected after the incubation (Fig. 2.7A), and by MS and MS/MS analyses, it was identified as the GST-conjugated covalent binder (Fig. 2.7B and C). The covalently bound amino acid was tyrosine in an IAYSK sequence, which is located at the 111<sup>th</sup> position from the N-terminus (underlined).<sup>36</sup> Furthermore, the conjugation of the covalent binder was rationalized by a protein–ligand docking simulation using MolDesk Basic/myPresto.<sup>45</sup> The lowest energy docking model suggested that the warhead was buried deep inside the hydrophobic region of the glutathione binding pocket and located very close to the covalently bound tyrosine at the 111<sup>th</sup> position; the distance between the fluorine atom in the warhead and the oxygen atom in Y111 was deduced to be ca. 7.2 Å (Fig. 2.7D).

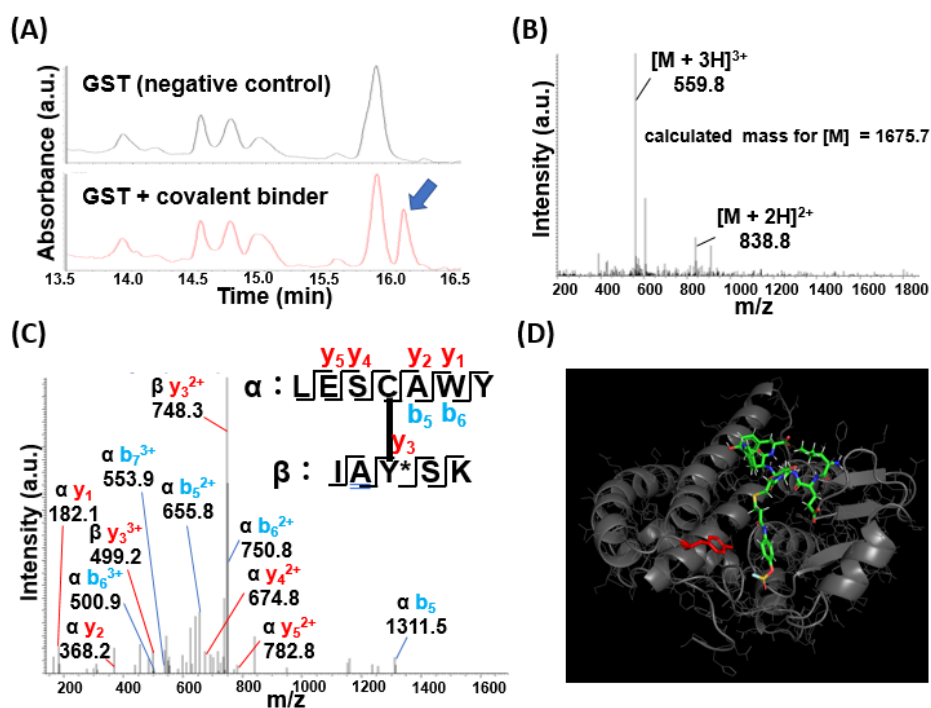


**Fig. 2.7** Identification of fragments derived from covalent binder-conjugated GST by LC-MS/MS analysis. (A) LC absorbance profiles of trypsin-digested peptide fragments derived from conjugated and unconjugated GST by the covalent binder. (B) MS and (C) MS/MS spectra of the newly appeared peak (indicated by an arrow in A). All the detected fragments were consistent with the theoretical  $m/z$  values of the represented structure. The peptide fragment of IAYSK was derived from a constituent of the glutathione binding pocket of the GST protein. Y\* stands for the conjugated 111th tyrosine. (D) Molecular docking simulation of the covalent binder (shown in a stick form) and GST (PDB ID: 1UA5) using SievGene in myPresto; the best docking model is shown. The fluorine atom in the warhead and the conjugated tyrosine in GST are colored in cyan and dark red, respectively. GST is shown as a cartoon with the side chains shown as lines.

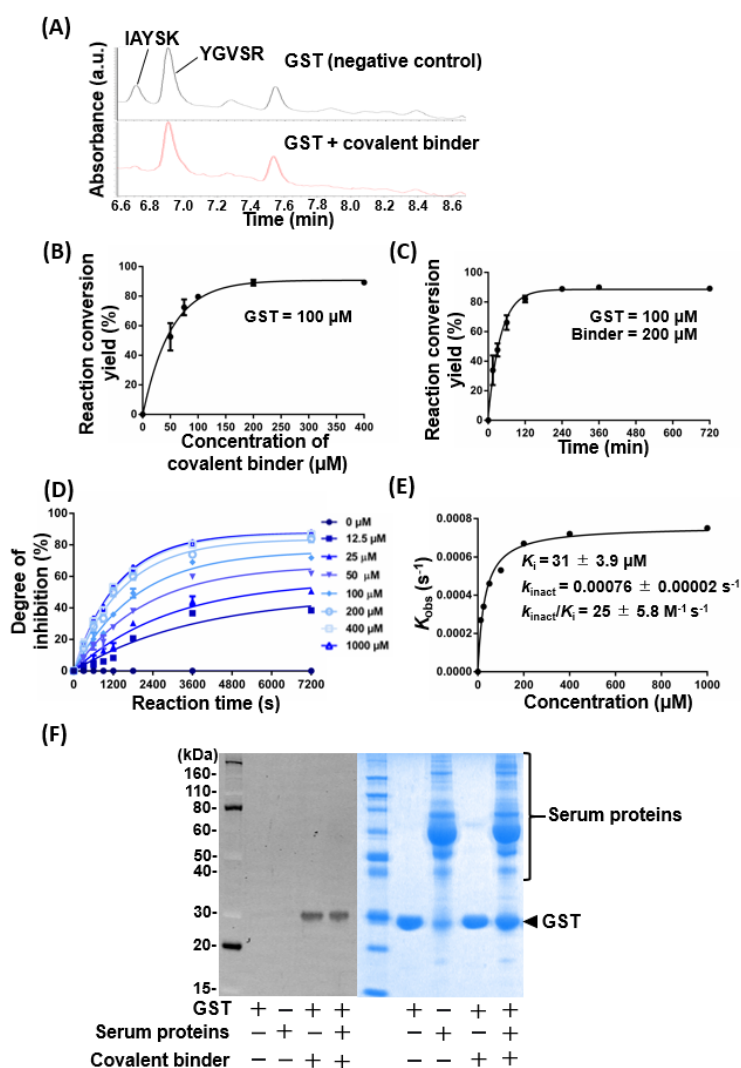


**Fig. 2.8** (A) LC absorbance profiles of trypsinized fragments of GST before and after the reaction with the directly obtained covalent binder (*i.e.*, LESCOAWY where the cysteine was modified with MAFS). (B, C) Concentration- or time-dependent conversion of the covalent binder. The reaction conversion yield was calculated from the peak ratios of the reacted IAYSK and unreacted YGVSR (*i.e.*, an internal standard). (D) The degree of GST-activity inhibition at each reaction time was monitored by the colorimetric activity assay under different concentrations of the covalent binder. The pseudo-first-order rate constant,  $k_{\text{obs}}$ , was calculated for each covalent-binder concentration using nonlinear regression analysis in GraphPad Prism 6. I The obtained  $k_{\text{obs}}$  were plotted against each covalent-binder concentration to afford the second-order rate constant  $k_{\text{inact}}/K_i$ .<sup>7</sup> (F) GST-specific conjugation of the covalent binder in the presence of serum proteins, confirmed by 12% (w/v) SDS-PAGE/fluorescence imaging. Whole proteins were visualized by CBB staining (right), and proteins conjugated with the fluorescently-labelled covalent binder were visualized in the same gel (left).

Finally, I estimated the reaction conversion yield, kinetics, and target-specificity of the covalent binder. From the LC absorbance peak ratio changes of reacted IAYSK and unreacted YGVSR derived from the trypsinized fragments of GST (Fig. 2.8A), I found that the conversion reached ca. 90% in a concentration- and time-dependent manner (Fig. 2.8B and C). Furthermore, GST activity inhibition by the covalent binder was monitored by a colorimetric activity assay.<sup>46</sup> As I expected, the covalent binder inhibited GST by up to ca. 90% in a time- and concentration-dependent manner (Fig. 2.8D) and possessed a  $k_{\text{inact}}/K_i$  value of  $25 \pm 5.8 \text{ M}^{-1} \text{ s}^{-1}$  (Fig. 2.8E). Next, I chemically synthesized Fam-GG-LESC\*AWY (Fam, GG, and C\* represent carboxyfluorescein, the glycylglycine spacer, and MAFS-modified cysteine, respectively), and its GST-specific covalent binding in the presence of human serum was confirmed by SDS-PAGE followed by fluorescence imaging/Coomassie Brilliant Blue (CBB) staining. A single fluorescence band was seen at an appropriate molecular weight (*ca.* 29 kDa) for the peptide-fused GST, and such fluorescence bands could not be seen for any human serum proteins (Fig. 2.8F). This indicates that more specific covalent binding occurred, compared with the previous GST-targeted covalent binder obtained by an indirect screening.<sup>24</sup> I suppose that the whole structure of the warhead-modified peptide was more appropriately optimized during the reactivity/affinity-based co-selection. Of note, the fluorescent band was maintained its intensity even in the presence of human serum, which suggests that peptide type covalent binder might be resisted peptidase digestion via covalent binding to the target protein.

In summary, I demonstrated a direct and stringent screening strategy to obtain a covalent binder from a turn-on type covalently-binding peptide library on the T7 phage. The turn-on warhead only reacted when a matchmaking microenvironment was created between the target protein and the warhead-modified peptide having an appropriate sequence. Non-specific/non-covalent interactions between target-unrelated biologics were completely eliminated during the washing process under severe protein-denaturing conditions where the robust T7 phage still retained its infectivity. I envision that the direct screening method developed here is the fastest and easiest way to obtain custom covalent binders, because the AFS-type warhead on the library peptide can potentially adapt its specificity to any one of the nucleophilic amino acids<sup>16, 25, 47</sup> in a wide range of proteins, including structure-unknown or mutational ones.

## ■ 2.3 Experimental procedures and additional figures

### *General*

All the reagents, kits, and solvents were purchased commercially and used without further purification. *S. japonicum* glutathione-*S*-transferase (GST) was prepared according to the reported procedure.<sup>39</sup> Peptides (*i.e.*, LESCOAW, Fam-GG-LESCOAW, LNYCDGW, and Fam-GG-LNYCDGW; Fam represents carboxyfluorescein) were synthesized, purified, and characterized by GenScript Inc. Warhead-modified peptides were purified with reverse-phase high performance liquid chromatography (LC-20AD, Shimadzu, Japan) equipped with a Xterra prep MS C18 column (10 × 50 nm, Waters). Each conjugate was separated using a 0–100% linear gradient of methanol containing 0.1% (v/v) formic acid during 10 minutes at a flow rate of 4 mL per minute.

NMR experiments were performed at 25°C using a 500 MHz spectrometer (JNM-ECA500, Jeol Resonance,). Liquid chromatography (LC) analysis was performed on an Agilent 1100 HPLC system (Agilent Technologies, USA) using a 0–100% gradient of acetonitrile containing 0.1% (v/v) formic acid at a flow rate of 300 µL per minutes, equipped with a C18 reverse-phase column (Hypersil GOLD, 2.1 × 100 mm, Thermo Fisher Scientific) connected to a photodiode array (PDA) and/or a LCQ-Fleet ion trap mass spectrometer. Electrospray ionization-time-of-flight-mass spectrometry (ESI-TOF-MS; JMS-T100 AccuTOF, Jeol Resonance) was performed by dissolving the analyte in methanol and directly injecting into the instrument.

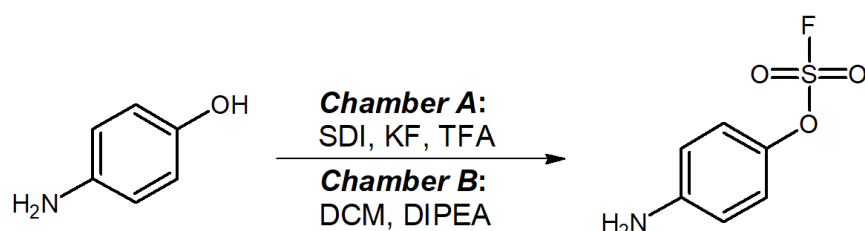
All images of stained gel and in-gel fluorescence were captured by ChemDoc XRS+ (BioRad Laboratories Inc.), and band intensities were quantified using Image Lab software (BioRad).

For protein digestion and analysis by LC-MS/MS, a 12% (w/v) sodium dodecyl sulfate-polyacrylamide gel electrophoresis (SDS-PAGE) was performed, and the gel was stained with Rapid Stain CBB kit (Nacalai tesque). The stained protein bands were excised from the gel. Proteins in the gel were reduced with 25 mM dithiothreitol (DTT) at 60°C for 10 minutes, and then alkylated with 55 mM iodoacetamide at 25°C for 60 minutes in the dark. Digestion was carried out with modified trypsin (Promega, #V5111) at 37°C overnight. The resulting peptides were analyzed using the above LC-MS/PDA system. The trypsinized peptides were separated using a 0%–50% gradient of acetonitrile containing 0.1% (v/v) formic acid during 55 minutes at a flow rate of 300 µL per minute, and then eluted peptides were directly sprayed into the mass spectrometer. The mass spectrometer was operated in the data-dependent mode and externally calibrated. Survey MS scans were fragmented with collision-induced dissociation in the ion trap. A dynamic exclusion window was applied within 30 s. All tandem mass spectra were collected

using normalized collision energy of 40%. Data were obtained and analyzed with Xcalibur software v. 2.07 (Thermo Fisher Scientific).

### Syntheses of turn-on warheads

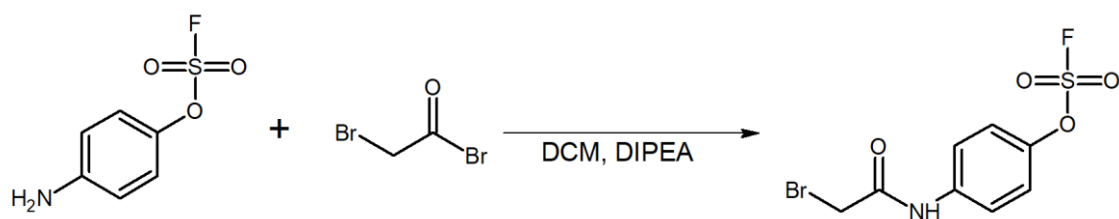
#### Synthesis of warhead precursor<sup>48</sup>



The warhead precursor was synthesized on a preparative scale according to the following procedure. Chamber A of a flame-dried small two-chamber was filled with 1,1'-sulfonyldiimidazole (SDI, 1.5 g, 7.5 mmol, 1.5 eq. TCI, #S0803), and potassium fluoride (KF, 1.2 g, 20 mmol, 4.0 eq., Wako). Next, chamber B was charged with 4-aminophenol (0.5 g, 5.0 mmol, 1.0 eq., TCI), *N,N*-diisopropylethylamine (DIPEA, 2.5 mL, 15 mmol, 3.0 eq., Watanabe Chem.), and dichloromethane (DCM, 10 mL). Finally, 5 mL trifluoroacetic acid was added by injection through a septum in chamber A. The reaction was stirred for 18 hours at 25°C. The crude reaction mixture was mixed with ethyl acetate (15 mL), and successively washed with saturated NaHCO<sub>3</sub> aq. (5.0 mL), brine (5.0 mL), dried over Na<sub>2</sub>SO<sub>4</sub>, and evaporated. Then, it was purified by a flash column chromatography on silica gel (hexane/ethyl acetate, 2/1). The title compound was obtained as a white solid (0.76 g, yield 80%). Identification of the purified warhead precursor was performed by <sup>1</sup>H, <sup>13</sup>C, and <sup>19</sup>F NMR (Fig. S2.1).

Warhead precursor: <sup>1</sup>H NMR (CDCl<sub>3</sub>, 500 MHz) δ 7.11 (d, *J* = 9.5 Hz, 2H), 6.68 (dd, *J* = 2.0 and 6.5 Hz, 2H); <sup>13</sup>C NMR (CDCl<sub>3</sub>, 125 MHz) δ 146.8, 142.2, 121.9, 115.6; <sup>19</sup>F NMR (CDCl<sub>3</sub>, 470 MHz) δ 36.08.

#### Synthesis of Br-AFS

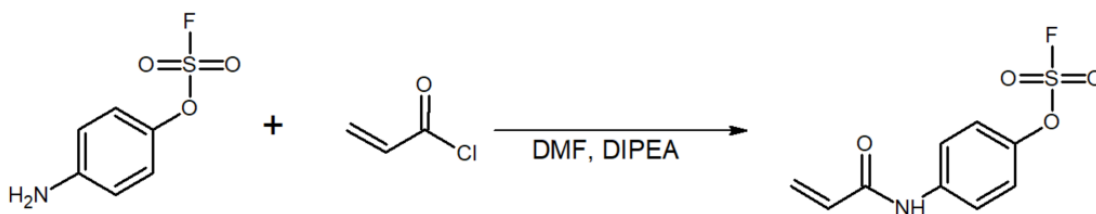


A cysteine reactive warhead, 4-bromoacetamide-aryl-fluorosulfate (Br-AFS), was synthesized on a preparative scale according to a following procedure. The warhead precursor (33 mg, 0.17 mmol, 1.0 eq.), DIPEA (0.10 mL, 0.59 mmol, 3.4 eq.) and bromoacetyl bromide (22 μL, 0.25

mmol, 1.5 eq., TCI, #B0539, Japan) were mixed in 3.0 mL of DCM. After stirring for 12 hours at 25°C, the reaction mixture was mixed with ethyl acetate (10 mL), and successively washed with water (5 mL), 0.10 M HCl aq. (5 mL), saturated NaHCO<sub>3</sub> aq. (5 mL), brine (5 mL), dried over Na<sub>2</sub>SO<sub>4</sub>, and evaporated. Then, it was purified by the flash column chromatography on silica gel (hexane/ethyl acetate, 2/1). The title compound was obtained as a brown solid (15 mg, yield 30%). Identification of the purified Br-AFS was performed by <sup>1</sup>H, <sup>13</sup>C, and <sup>19</sup>F NMR (Fig. S2.2).

Br-AFS: <sup>1</sup>H NMR (CDCl<sub>3</sub>, 500 MHz) δ 7.68 (dd, *J* = 2.0 and 7.0 Hz, 2H), 7.34 (d, *J* = 8.5 Hz, 2H), 4.04 (s, 2H); <sup>13</sup>C NMR (CDCl<sub>3</sub>, 125 MHz) δ 163.7, 146.5, 137.3, 121.9, 121.6, 29.3; <sup>19</sup>F NMR (CDCl<sub>3</sub>, 470 MHz) δ 37.504; HRMS (ESI) Found *m/z* 309.9229, 311.9245 [(M-H)<sup>-</sup>]; calculated for C<sub>8</sub>H<sub>7</sub>BrFNO<sub>4</sub>S: 309.9190, 311.9170].

### Synthesis of MAFS



The Michael-acceptor type aryl-fluorosulfate (MAFS) warhead was synthesized on a preparative scale according to a following procedure. The warhead precursor (0.12 g, 0.60 mmol, 1.0 eq.), DIPEA (0.17 ml, 1.8 mmol, 3.0 eq.) and acryloyl chloride (54 μl, 0.70 mmol, 1.1 eq., TCI, #A0147) were mixed in 1.2 mL of *N,N*-dimethylformamide (DMF). After stirring for 3 hours at 25°C, the reaction mixture was mixed with ethyl acetate (10 mL), washed successively with saturated NaHCO<sub>3</sub> aq. (5 mL), 0.10 M HCl aq. (5 mL), brine (5 mL), dried over Na<sub>2</sub>SO<sub>4</sub>, and evaporated to yield a white solid pure product (0.11 g, yield 76%). Identification of the purified warhead was performed by <sup>1</sup>H, <sup>13</sup>C, and <sup>19</sup>F NMR (Fig. S2.3).

MAFS: <sup>1</sup>H NMR (CD<sub>3</sub>OD, 500 MHz) δ 7.82 (dt, *J* = 10.1 and 2.6 Hz, 2H), 7.41 (dd, *J* = 11.7 and 3.2 Hz, 2H), 6.46–6.37 (m, 2H), 5.80 (dd, *J* = 9.2 and 2.9 Hz, 1H); <sup>13</sup>C NMR (CD<sub>3</sub>OD, 125 MHz) δ 164.9, 145.9, 139.1, 130.8, 127.2, 121.3, 121.2; <sup>19</sup>F NMR (CD<sub>3</sub>OD, 470 MHz) δ 35.21; HRMS (ESI) Found *m/z* 244.0087 [(M-H)<sup>-</sup>]; calculated for C<sub>9</sub>H<sub>8</sub>FNO<sub>4</sub>S: 244.0085].

***Identification of covalently-binding position on GST with AFS-modified LNYCDGW peptide***  
***Synthesis of AFS-modified LNYCDGW peptide***

The peptide (LNYCDGW, 50 mM) was dissolved in 20 mM phosphate buffer (PB, Na<sub>2</sub>HPO<sub>4</sub>/NaH<sub>2</sub>PO<sub>4</sub>, pH 7.4 at 25°C) / 50% (v/v) dimethyl sulfoxide (DMSO), and reacted with Br-AFS (80 mM) in the presence of neutralized tris(2-carboxyethyl)phosphine (TCEP; 2.0 mM). The mixture was reacted for more than 4 hours at 25°C in the dark with vigorous shaking, and purified by the reverse-phase HPLC (yield 30%), and identified with MS and MS/MS analyses (Fig 2.2A).

***Identification of covalently-binding position by tandem MS analysis***

The AFS-modified LNYCDGW peptide (0.50 mM) was mixed with GST (0.15 mM) in Dulbecco's Phosphate-Buffered Saline (D-PBS) and incubated for 12 hours at 37°C. It was mixed with 1 × sample buffer, denatured at 95°C, separated by 12% (w/v) SDS-PAGE, followed by trypsinization/LC-MS/MS analysis. The covalently-binding site was determined to be the glutathione binding pocket; the covalently bound amino acid was tyrosine located at the 111<sup>th</sup> position<sup>36</sup> from the N-terminus (Fig. 2.2B).

***Molecular docking simulation using MolDesk Basic***

For the docking simulation, the structure of the covalent binder (*i.e.*, LNYC\*DGW, C\* represents AFS-modified cysteine) was created by ChemDraw Ultra (version 11.0) and converted to mol file. Docking of the GST (PDB: 1UA5) was performed with MolDesk Basic (version 1.1.45, Imsbio Inc.) under a graphical-user interface (GUI) of several myPresto programs<sup>45, 49</sup> as follows. First, the mol file was further converted to a mol2 file. Second, the target GST protein was stripped out of the co-crystallized glutathione and converted to a pdb file format. Finally, the binder and the glutathione-subtracted GST input file were entered and docked using sievгене program of myPresto (version 5.000).<sup>45, 49</sup> For the docking, 13 separate poses were taken. The binding geometry of the best docking model was supported experimentally by an exclusive covalent binding of the warhead, which was proved by MS/MS analysis of the trypsinized fragment of the conjugated GST (Fig. 2.2C).

***Evaluation of reaction conversion yield of each warhead-modified LNYCDGW peptide***

AFS- or ethene sulfonyl fluoride- (ESF) modified LNYCDGW peptide (1.0 mM; the latter has been already reported in a previous work<sup>36</sup>) and GST (0.15 mM) were mixed in D-PBS, respectively, and incubated for 12 hours at 37°C. It was mixed with 1 × sample buffer, denatured at 95°C, separated by 12% (w/v) SDS-PAGE, followed by trypsinization/LC-MS/MS analysis (Fig. 2.3).

### ***Evaluation of thioetherification between each warhead and designated cysteines of model peptide on T7 phage***

For evaluation of a successful introduction of the turn-on warhead to designated cysteines (underlined) of a model monoclonal peptide (-GSRVS-C-GGRDRPG-C-LSV; fused at the C-terminal region of gp10) on T7 phage via the gp10 based-thioetherification (10BASE<sub>d</sub>-T)<sup>39</sup>, I mixed each warhead (*i.e.*, Br-AFS or MAFS; 1.0 mM) and the model peptide on T7 phage ( $1.0 \times 10^{11}$  plaque forming units) in 0.70 mL of 1.0 M NaCl / 0.50 mM neutralized TCEP in D-PBS containing 10% (v/v) DMSO at ice temperature or 55°C. After 3 hours of the reaction, the peptide was further treated with 5-(iodoacetamido)fluorescein (FL-IA; 0.20 mM) for 3 hours at ice temperature. The latter reaction with FL-IA blocks all of the unreacted cysteines of the model peptide on T7 phage after the introduction with Br-AFS. It is demonstrated that FL-IA was conjugated to at least 95% of the designated cysteines of the model peptide on T7 phage under the condition.<sup>46</sup> Thus, I can indirectly estimate introduction yield of Br-AFS by the fluorescent densitometric analysis. After the 10BASE<sub>d</sub>-T, the T7 phage particles were precipitated by centrifugation with a mixture of polyethylene glycol 6000 and sodium chloride to final concentrations of 5% (w/v) and 0.5 M, respectively.<sup>39</sup> The precipitate was dissolved in the sample buffer, and whole T7 phage proteins were subjected to 12% (w/v) SDS-PAGE after the denaturation, followed by the in-gel fluorescence imaging and CBB staining (Fig. 2.5).

### ***Direct screening of covalent binder***

#### ***Biotinylation of GST<sup>39</sup>***

GST (1.4 mM) in 20 mM PB (pH 7.4) was mixed with *N*-succinimidyl 6-(biotinamido)hexanoate (TCI, #S0490,) at a final concentration of 2.8 mM and incubated at ice temperature overnight. For desalination, Zeba<sup>TM</sup> Spin Desalting Columns (Thermo Fisher Scientific, USA) was used with centrifugation at 800g for 4 minutes at ice temperature. The biotinylation of GST was confirmed by Western blotting; from the densitometric quantification reported previously<sup>44</sup>, it was estimated that ca. 0.5 molecules of biotin were conjugated to a single GST molecule (data not shown). The biotinylated GST was incubated with streptavidin-coupled magnetic nanoparticles (Dynabeads<sup>TM</sup> MyOne<sup>TM</sup> Streptavidin T1, Invitrogen), to obtain GST-immobilized beads.

### ***Determination of stringent washing condition during biopanning***

The model monoclonal- or library (-SGGG-X<sub>3</sub>-C-X<sub>4-10</sub>-C-X<sub>3</sub>; X represents any randomized amino acid; diversity:  $8.6 \times 10^9$ )-peptide on T7 phage ( $1.0 \times 10^{11}$  plaque forming units)<sup>1</sup> was reacted with MAFS (1.0 mM) for 3 hours at 37°C. After the 10BASE<sub>d</sub>-T, the warhead-modified monoclonal- or polyclonal phages were precipitated by centrifugation with a mixture of

polyethylene glycol 6000 and sodium chloride to final concentrations of 5% (w/v) and 0.5 M, respectively, and dissolved in a selection buffer (D-PBS supplemented with 1.0% (v/v) Tween-20). Then, each phage was incubated with the GST-immobilized beads for 1 hour at 37°C using a rotator. The beads were washed with 0.20 mL of a stringent wash buffer (1.0% (w/v) SDS, 4.0 M urea, 0.15 M NaCl, 50 mM DTT in D-PBS) under sonication (10 minutes), and this washing process was repeated four times. Then, numbers of the GST-conjugated phages on the beads were directly counted by a plaque assay<sup>39</sup>.

### ***Biopanning against GST by using turn-on type covalently-binding peptide library***

The peptide library on T7 phage ( $1.0 \times 10^{11}$  plaque forming units) was modified via the 10BASE<sub>i</sub>-T. After the MAFS modification and the phage precipitation, it was dissolved in the selection buffer. To remove non-specific binders (*i.e.*, beads-, streptavidin-, plastic-, and BSA-binders), the library was pre-incubated with streptavidin-coupled beads for 1 hour at 37 °C, and then the supernatant was further incubated with the GST-immobilized beads for 1 hour at 37 °C. The latter beads were washed with 0.20 mL of a stringent wash buffer under sonication (10 minutes), and this washing process was repeated four times. Then, the GST-bound phages were directly infected with *E. coli* BLT5403 strain, and the amplified phages were used for the next round of biopanning. In the second round, biopanning was performed as same above, except containing 1% (w/v) BSA in the selection buffer.

### ***Next generation sequencing (NGS) analysis***

The phages ( $1.0 \times 10^{11}$  plaque forming units) recovered from the second round of biopanning were twice subjected to the phenol / chloroform treatment to purify phage DNA. After the ethanol precipitation, DNA was dissolved in water and 10 ng of it was used for polymerase chain reaction (PCR; 18 cycles repeating three steps of denaturation at 94°C for 30 seconds, annealing at 58°C for 30 seconds, and extension at 72°C for 1 minutes) as a template to amplify the library-coding region using a forward primer (TCGTCGGCAGCGTCAGATGTGTATAAGAGACAGCGCTAAGTACGCAATGGGCC) and a reverse primer (GTCTCGTGGGCTCGGAGATGTGTATAAGAGACAGGTCTCAACGTTTCATATGGTATGAGCG). The product was twice subjected to the phenol / chloroform treatment to purify. After the ethanol precipitation, DNA was dissolved in water. The purified DNA was ligated with adapter DNA (Nextera XT Index Kit, illumine) harbored with the appropriate index sequences and purified on Agencourt AMPure XP Beads, according to the protocols of QIA seq 1-Step Amplificon Library Kit (QIAGEN). The adaptor-ligated amplicon was again amplified by PCR (8 cycles repeating 3 steps of denaturation at 95°C for 30 seconds, annealing at 55°C for 30

seconds, and extension at 72°C, 30 seconds) using the primer mix in the kit and purified on Agencourt AMPure XP Beads. The adaptor-ligated DNA prepared thus was supplied to NGS analysis on Illumina Miseq using Miseq v3 reagent. About twenty amplicon samples, which were indexed by the barcode, were mixed, and analyzed. The NGS data collected on Miseq were transformed to FastQ format, and sorted by the barcode. The nucleotide data were quality-checked, merged, and translated into amino acid sequences to determine the representative peptide.

### ***Identification of covalently-binding position of covalent binder***

#### ***Synthesis of covalent binder***

The representative peptide (*i.e.*, LESCAWY, 50 mM) was dissolved in 20 mM PB (pH 7.4) / 50% (v/v) DMSO, and reacted with MAFS (80 mM) in the presence of neutralized TCEP (2.0 mM). The mixture was reacted for more than 12 hours at 25°C in the dark with vigorous shaking, purified by the reverse-phase HPLC (yield 60%), and identified with MS and MS/MS analyses (Fig. S2.4).

#### ***Identification of covalently-binding position by tandem MS analysis***

The covalent binder (0.40 mM) was mixed with GST (0.10 mM) in D-PBS and incubated for 12 hours at 37°C. It was mixed with 1 × sample buffer, denatured at 95°C, separated by 12% (w/v) SDS-PAGE, followed by trypsinization/LC-MS/MS analysis. As shown in Fig. 2.7 in the main text, the covalently-binding site was determined to be the glutathione binding pocket; the covalently bound amino acid of GST was tyrosine which was located at the 111<sup>th</sup> position from the N-terminus.

#### ***Molecular docking simulation of covalent binder***

The docking simulation was performed as described in Section "Molecular docking simulation using MolDesk Basic" except using a structure of the covalent binder (*i.e.*, LEYC\*AWY, C\* represents MAFS-modified cysteine). The binding geometry of the best docking model was supported experimentally by the exclusive covalent conjugation of the warhead, which was proved by MS/MS analysis of the trypsinized fragment of the conjugated GST.

### ***Evaluation of reaction conversion yield and protein-specificity of covalent binder***

#### ***Evaluation of concentration-dependent conversion***

For assessment of concentration-dependent conversion of the covalent binder, I mixed it at various molar concentrations with GST (0.10 mM) in D-PBS and incubated it for 24 hours at 37°C. It was mixed with the sample buffer, denatured at 95°C, separated by 12% (w/v) SDS-PAGE followed by trypsinization/LC-MS/MS analysis. The reaction conversion yield was calculated as mean ± SD (n = 3) from the absorbance peak ratios between the remaining GST fragment containing 111<sup>th</sup> tyrosine (*i.e.*, IAYSK at 6.7 minutes in Fig. 2.8A; Y should react with the warhead) (Fig. S2.5A) and a different GST fragment as an internal standard (*i.e.*, YGVSR at 6.9 minutes) (Fig. S2.5B).

### ***Evaluation of time-dependent conversion***

For assessment of time-dependent conversion of the covalent binder, I incubated the covalent binder (0.20 mM) and GST (0.10 mM) for arbitrary time in D-PBS at 37°C. After the incubation, it was mixed with the sample buffer, and quantified in the same procedure as described in Section “Evaluation of concentration-dependent conversion”.

### ***Kinetic evaluation of covalent binder***<sup>27</sup>

GST activity inhibition by the covalent binder was measured by a colorimetric assay. GST catalyzes conjugation of 1-chloro-2,4-dinitrobenzene (CDNB) with glutathione and the resulting reaction product has a molar absorption at 340 nm<sup>46</sup>. The enzymatic activity was determined by monitoring the change in NanoPhotometer (Implen) using a 1 mm lid for the NanoPhotometer submicroliter cell.

For kinetic evaluation of the covalent binder on the basis of the assay, I mixed the covalent binder at various molar concentrations with GST (60 μM) in D-PBS and incubated for arbitrary time at 37°C. After the incubation, it was 50-fold diluted by 100 mM PB (K<sub>2</sub>HPO<sub>4</sub>/KH<sub>2</sub>PO<sub>4</sub>, pH 6.5 at room temperature) and mixed with CDNB (1.0 mM) and glutathione (0.30 g/L). Then, it was incubated for 30 seconds at 25°C, and the maximum absorbance (340 nm) was measured by the absorbance spectrophotometer. In each incubation time, the maximum absorbance in the absence of the covalent binder was normalized to 100%, and the relative absorbance of each concentration was quantified. The degree of GST-activity inhibition (DoI) was calculated as mean ± SD (n = 3) from the quantified values and plotted against time. Exponential curve fitting of the plot by GraphPad Prism 6 (MDF Co., Ltd.) gave us the value of  $k_{\text{obs}}$  at each covalent-binder concentration by using an equation of  $\text{DoI (\%)} = v_i / k_{\text{obs}} \times -1 - \exp(-k_{\text{obs}} \times t)$ ;  $v_i$  = initial velocity (Fig. 2.8D). Finally, the values of  $k_{\text{obs}}$  (*i.e.*, pseudo-first-order rate constant) were plotted against the covalent-binder concentrations, and the values of  $K_i$  and  $k_{\text{inact}}$  (*i.e.*, inhibition constant and inactivation rate constant, respectively) were determined by the curve fitting of  $k_{\text{obs}} = (k_{\text{inact}} \times [I]) / (K_i + [I])$ ;  $[I]$  = covalent-binder concentration.

### ***Evaluation of protein-specificity***

The fluorescent peptide possessing the representative sequence (*i.e.*, Fam-GG-LESCAWY, 10 mM) was dissolved in 20 mM PB (pH 7.4) / 50% (v/v) DMSO, and reacted with MAFS (20 mM) in the presence of neutralized TECP (2.0 mM) for more than 4 hours at 25°C with vigorous shaking. Then it was monitored / purified by the reverse-phase HPLC. The purified Fam-modified covalent binder (Fig. S2.6; 0.30 mM) was mixed with GST (0.30 mM) in D-PBS in the presence of 40% (v/v) human serum (Sigma, H4522), and incubated for 12 hours at 37°C. It was mixed with 1 × sample buffer, denatured at 95°C, and separated by 12% (w/v) SDS-PAGE. Proteins,

which were conjugated with the fluorescent covalent binder, were detected by the fluorescence imaging, and the whole proteins were visualized by CBB staining.

Supplementary figures

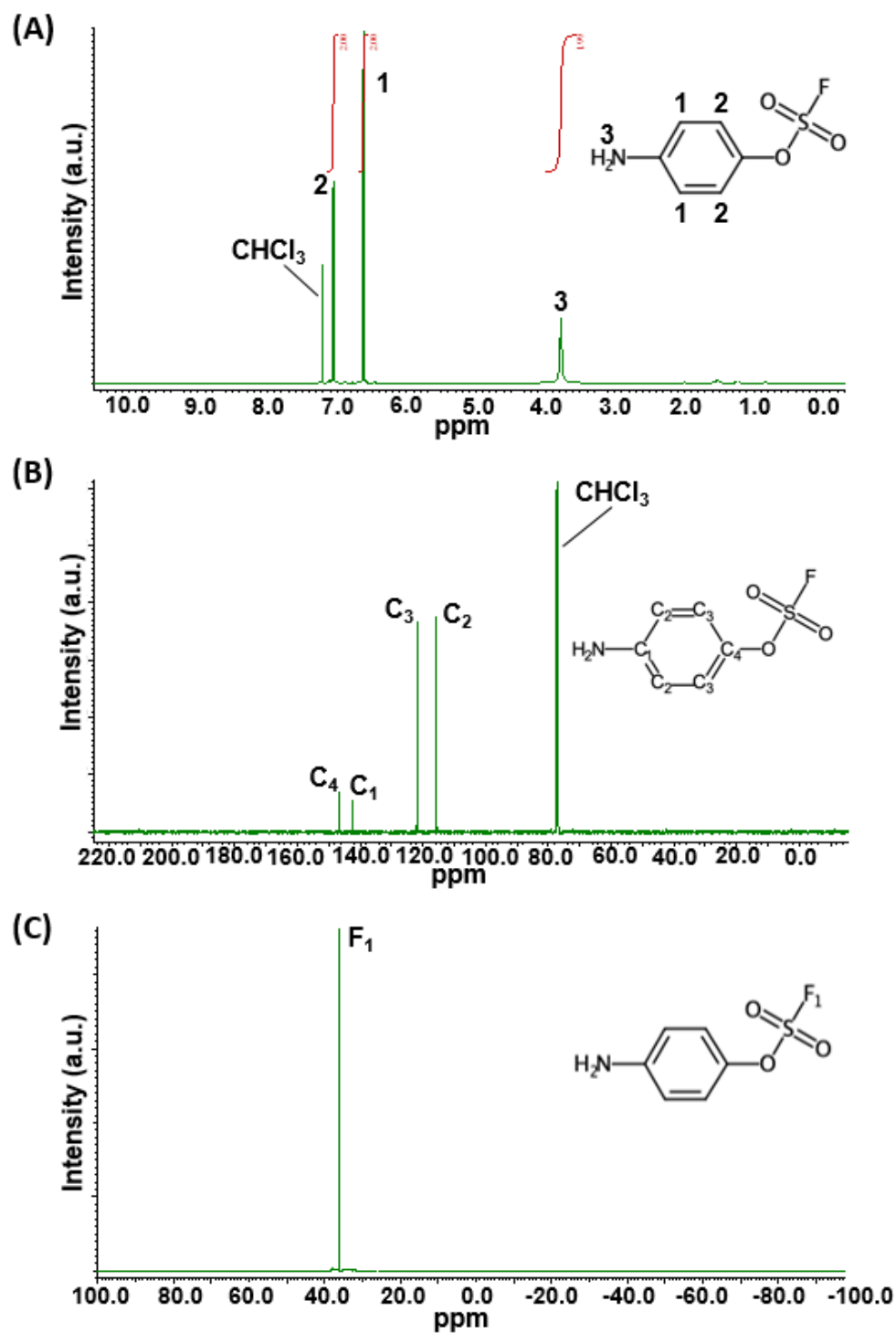
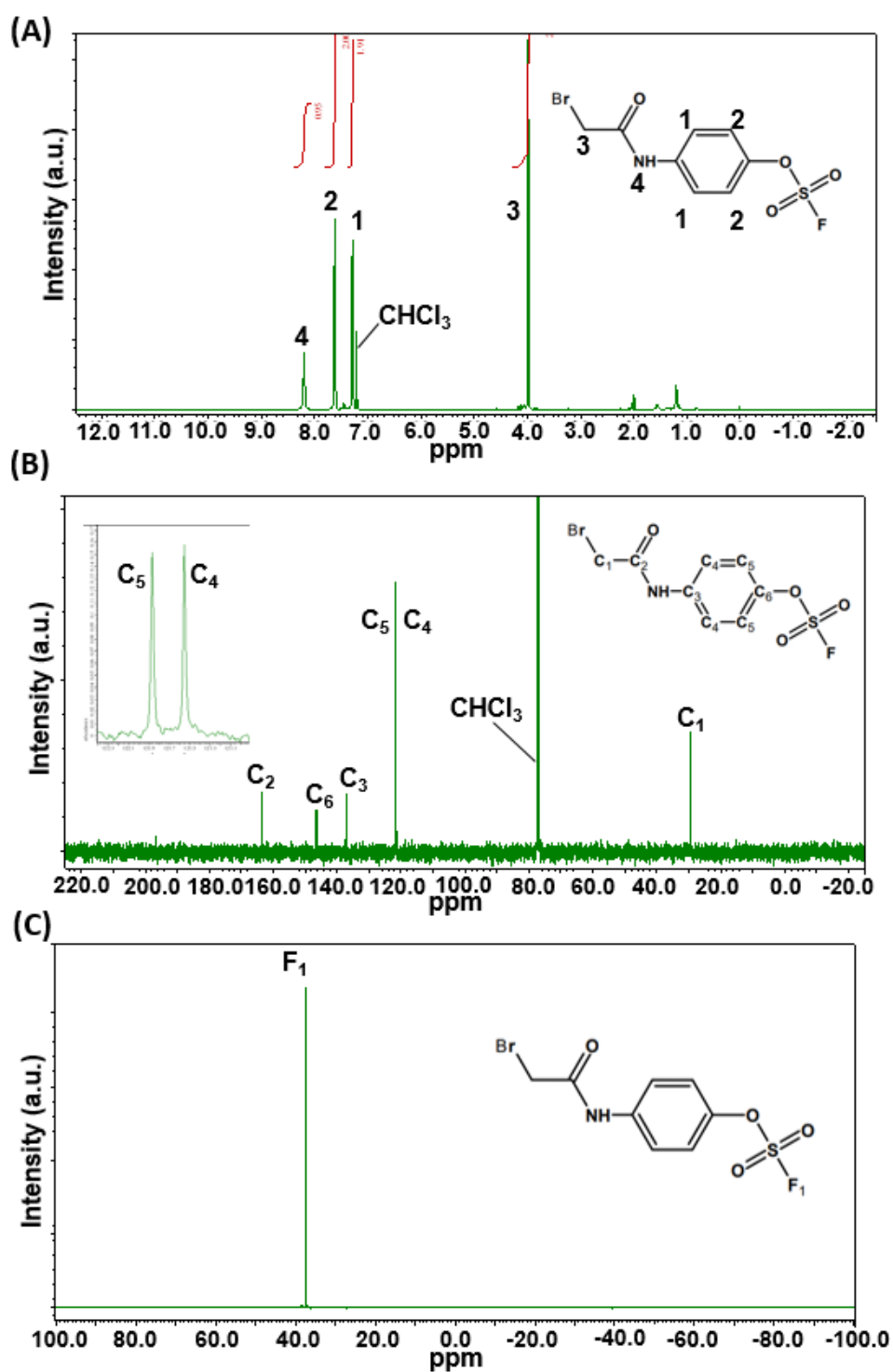
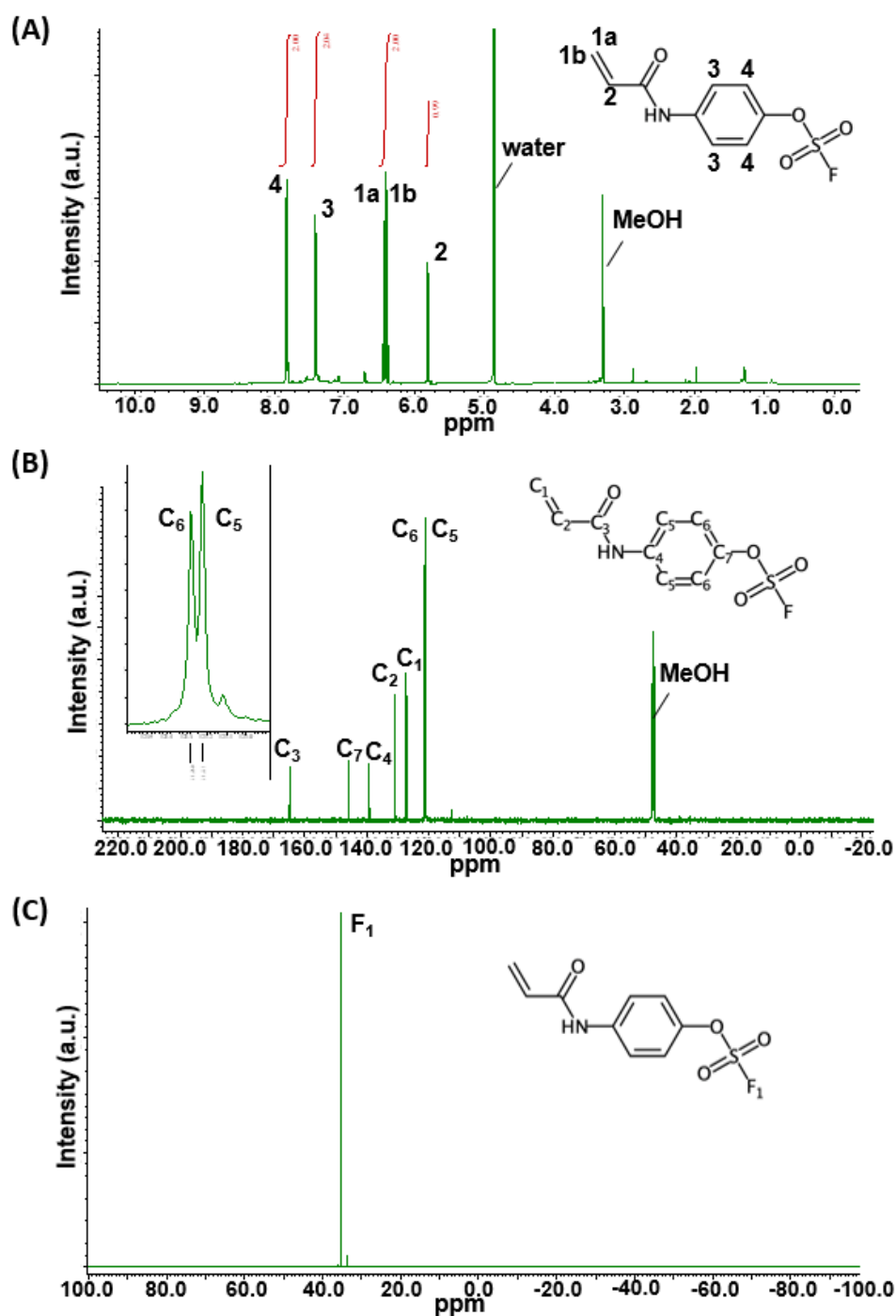


Fig. S2.1 Identification of the purified warhead precursor.<sup>43</sup> (A) <sup>1</sup>H NMR spectrum. (B) <sup>13</sup>C NMR spectrum. (C) <sup>19</sup>F NMR spectrum.



**Fig. S2.2** Identification of the purified Br-AFS. (A)  $^1\text{H}$  NMR spectrum. (B)  $^{13}\text{C}$  NMR spectrum. (C)  $^{19}\text{F}$  NMR spectrum.



**Fig. S2.3** Identification of the purified MAFS. (A)  $^1\text{H}$  NMR spectrum. (B)  $^{13}\text{C}$  NMR spectrum. (C)  $^{19}\text{F}$  NMR spectrum.

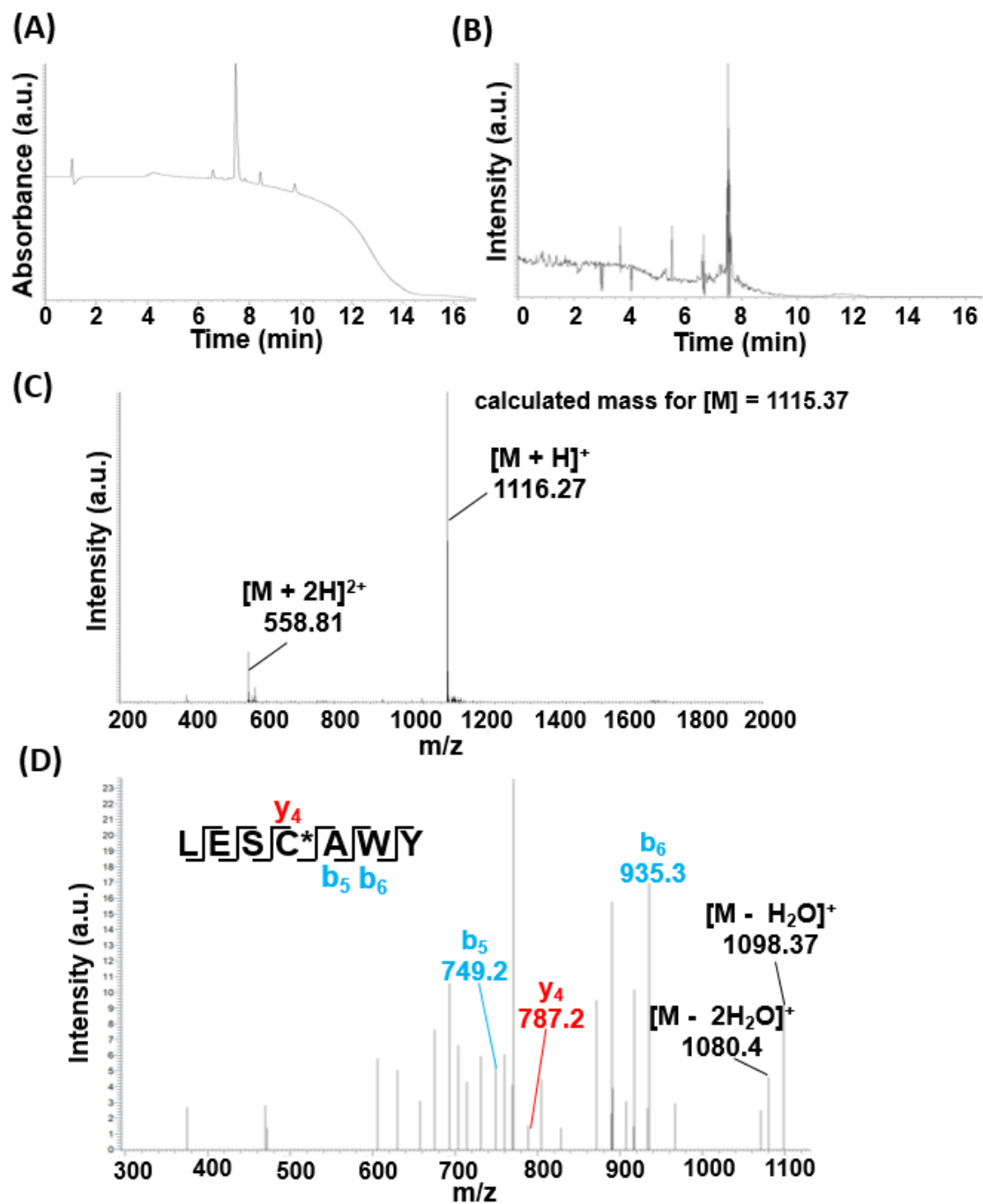


**Fig. S2.4** Identification of the purified covalent binder (*i.e.*, LESC\*AWY, C\* represents MAFS-modified cysteine) via (A) LC absorbance profile, (B) LC-MS total ion profile, (C) MS, and (D) MS/MS analyses.

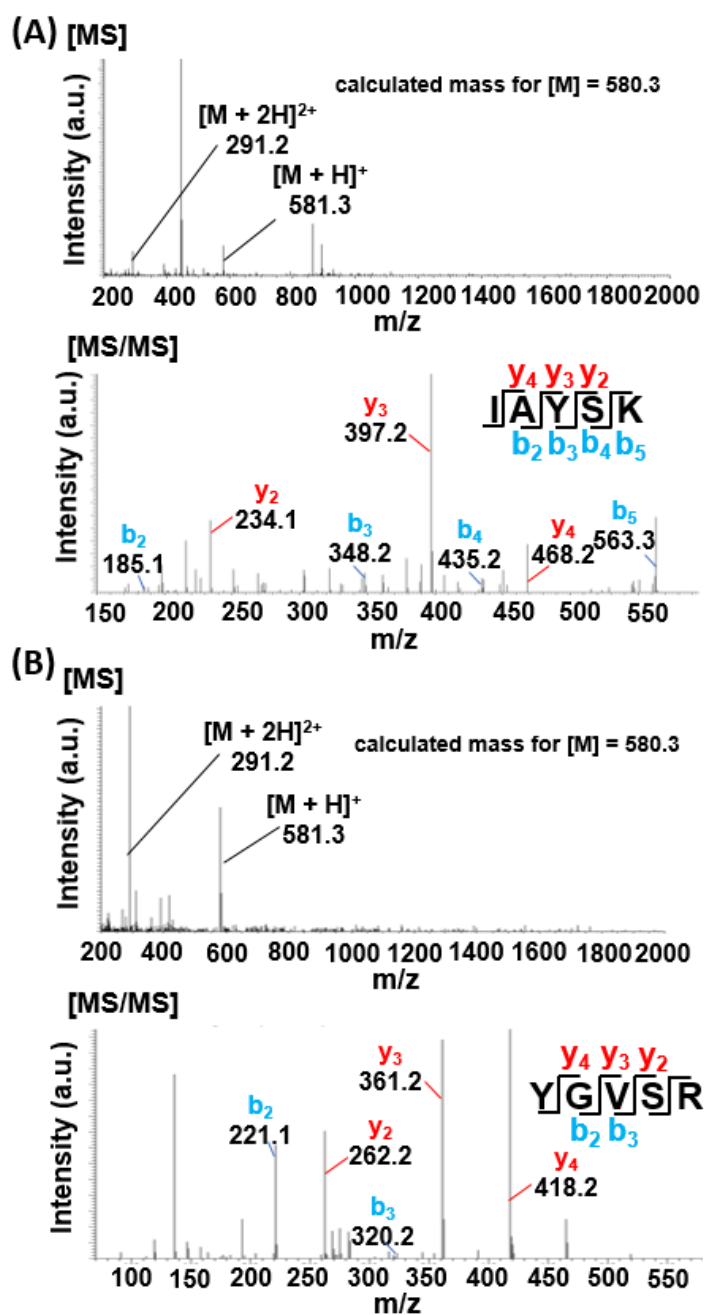


**Fig. S2.5** MS and MS/MS identifications of trypsinized peptide fragments of GST, (A) IAYSK and (B) YGVSR, which correspond to the LC absorbance profiles in Fig. 4A (*i.e.*, 6.7 and 6.9 minutes, respectively).

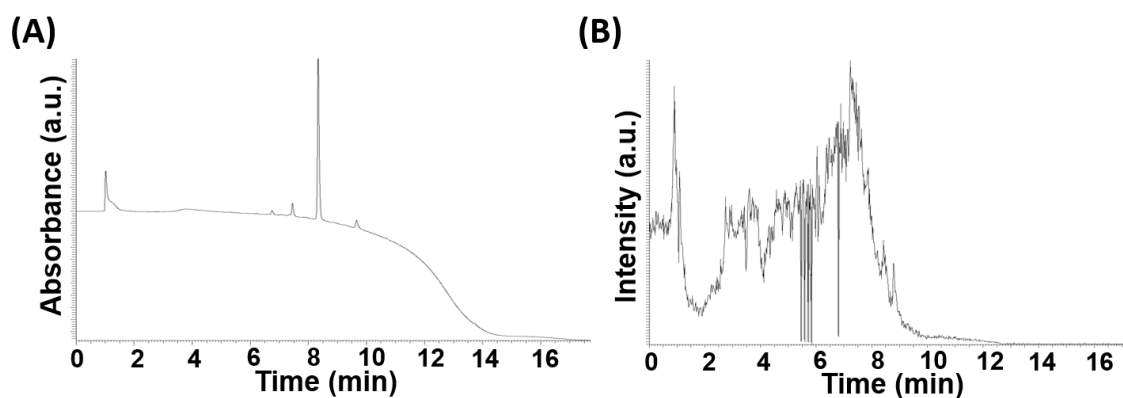


**Fig. S2.6** Identification of the purified Fam-modified covalent binder (Fam-GG-LESC<sup>\*</sup>AWY; Fam, GG, and C<sup>\*</sup> represent carboxyfluorescein, glycylglycine spacer, and MAFS-modified cysteine, respectively) via (A) LC absorbance profile, and (B) LC-MS total ion profile. I could not observe an expected  $m/z$  value of the purified Fam-modified covalent binder presumably because of the low ionization efficiency of the fluorine derivative both in positive and negative ionization mode.<sup>23</sup> Nevertheless, I suppose MAFS was successfully introduced, because a single peptide peak of Fam-GG-LESCAWY on the LC absorbance shifted to a longer retention time after the reaction.

## **CHAPTER 3**

### **Inhibition of thrombin activity by a covalently-binding aptamer and reversal by the complementary strand antidote**

### ■ 3.1 Introduction

As described in Chapters 1 and 2, many developments of covalent drugs have been conducted using a small molecule, peptide, and protein as its modality.<sup>8,15-18</sup> In particular, biologics type covalent inhibitors would reduce the side effects induced by the off-target reaction due to high target specificity. Nevertheless, the potential risk of unintended irreversible adverse drug effects (ADEs) have still existed, and to the best of my knowledge, there have been no covalent drugs that overcame such risks.

Nucleic acid aptamers (*i.e.*, single-stranded oligonucleotides) are emerging as an attractive class of drugs.<sup>50-54</sup> Aptamers have been shown to exhibit high binding affinity and selectivity<sup>55</sup> with dissociation constants typically in the nM and even pM ranges when properly selected against a target.<sup>56,57</sup> As the target affinity arises from the correct folding of the single-stranded aptamer, the addition of the complementary strand (CS) oligonucleotide as an antidote results in the formation of a double-strand (DS), and release the aptamer drug from the target.<sup>53</sup> The kinetics of DS formation are rapid and effective *in vivo*, and the reversal of an anticoagulant aptamer has been demonstrated.<sup>52,58</sup>

Here I report the creation of an aptamer-type covalent drug that covalently conjugates to thrombin, inhibiting its enzymatic activity while retaining on-demand reversal by a CS antidote. I started with the well-characterized thrombin binding aptamer (TBA) which is a 15-base DNA oligonucleotide identified by SELEX (Systematic Evolution of Ligands by EXponential enrichment).<sup>57,59-61</sup> TBA inhibits thrombin enzymatic activity which results in the prolongation of the clotting time, *in vitro*,<sup>60,62</sup> and effective anticoagulation, *in vivo*.<sup>63</sup> A warhead (*i.e.*, sulfonyl fluoride<sup>28,29</sup>) with a relatively long spacer was introduced at appropriate positions of TBA to create the weaponized covalent drugs. The linker was placed outside the presumed TBA/thrombin interaction interface in order to minimize its potential interference with the binding of TBA to thrombin. The reactive warhead placed at the end of the extended linker maximized the chances of covalent bond formation at sites away from the enzyme catalytic active site and the TBA binding site. Upon addition of the CS antidote, TBA was dislodged from thrombin, reversing the anticoagulant effect while still covalently binding to the target protein (Fig. 3.1).

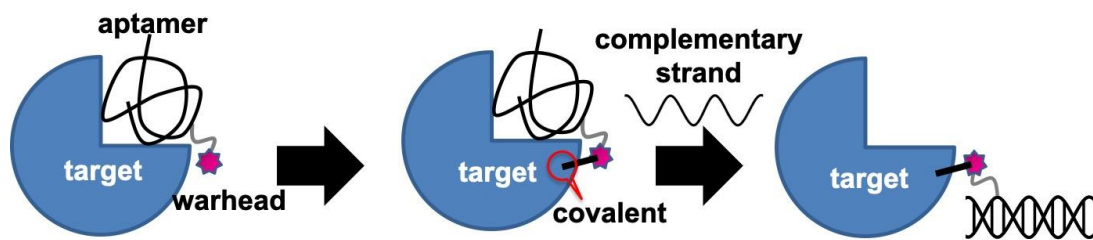


**Fig. 3.1** Summary of a covalently-binding DNA aptamer. A warhead (red star) conjugated aptamer (folded string) binds to its target protein (blue) (left). A covalent-bond is formed between the warhead-conjugated aptamer and the target (middle), resulting in a semi-permanent drug action. Introduction of the CS antidote removes the aptamer from the binding site and reverses the semi-permanent drug action (right).

### ■ 3.2 Results and discussion

To create the covalently-binding TBA, I introduced an azidated (*i.e.*,  $N_3^-$ ) warhead to an alkyne-containing TBA by the copper(I)-catalyzed azide–alkyne cycloaddition (CuAAC) reaction.<sup>64</sup> As the warhead, I chose an aryl-sulfonyl fluoride ( $Ar-SO_2F$ ) derivative to maximize the potential of covalent binding with the target protein without the lack of protein-specificity; it spontaneously forms a covalent bond with a proximal nucleophilic amino acid (*i.e.*, serine, threonine, lysine, tyrosine, cysteine, or histidine) via a reaction.<sup>26-29</sup> As identified in Fig. S3.2,  $N_3-Ar-SO_2F$  was synthesized (Fig. 3.2A), and it was introduced on designated thymine residues ( $T_x$ ) to obtain TBA isomers ( $TBA_x$ ) (Fig. 3.2B left).  $TBA_3$  and  $TBA_{12}$ , in which the warhead is attached to  $T_3$  and  $T_{12}$ , respectively, facing the TBA-thrombin interaction interface, were designed on the basis of the known crystal structure<sup>36</sup> (Fig. 3.2B right).  $TBA_9$  was also created in which  $T_9$  modified by the warhead faced the side opposite from the interaction interface. The purity of each warhead-conjugated TBA was determined to be ca. 95% by liquid chromatography (Fig. 3.3). Invariant circular dichroism spectra (Fig. 3.4) showed that introducing the warhead did not hardly change the folded structure of TBA.

Next, I evaluated the covalently-binding ability of each warhead-conjugated TBA.  $TBA_3$  and  $TBA_{12}$ , incubated with thrombin, induced persistent mobility shift of the protein on gel electrophoresis where the protein bands were visualized by Coomassie Brilliant Blue (CBB) staining. This suggests that a stable covalent bond was formed between the respective modified aptamers and thrombin. On the contrary, native TBA (*i.e.*, negative control possessing no warhead) and  $TBA_9$  did not induce the significant mobility shift (Fig. 3.5). The warhead location-dependent covalent binding with thrombin also strongly suggests that the SuFEx reaction is target-specific and not due to a non-specific interaction of the warhead. For further experiments, I solely used  $TBA_3$  because its covalently-binding efficiency was the highest among them. The covalently-binding efficiency was improved by increasing the molar concentration of  $TBA_3$  against a fixed thrombin amount. At higher molar concentrations of  $TBA_3$ , two separated bands were seen (Fig. 3.6A). Of note, the competition assay with native TBA demonstrated a decrease in both of the separated bands (Fig. 3.7), suggesting that the  $TBA_3$ -mono-adduct and bis-adduct form covalent-bond formation at two distinct thrombin residues while sharing the same binding site with native TBA (*i.e.*, exosite I<sup>36</sup>). I suppose that  $TBA_3$  tethered to thrombin exhibits a finite off-rate from exosite I, allowing the entry of a second  $TBA_3$  that covalently conjugates to a different residue in thrombin, resulting in the bis-adduct. The covalently-binding efficiency increased with time up to ca. 90% within 60–120 minutes. The final covalently-

binding efficiency of TBA<sub>3</sub> to thrombin proceeded to 90% in time- and concentration-dependent manners (Fig. 3.6B and C).

The potential covalently-binding site with TBA<sub>3</sub> was explored by trypsinization of the covalently bound molecule followed by liquid chromatography-tandem mass spectrometry (LC-MS/MS). Because of the technical difficulty in identifying a peptide-oligonucleotide complex by MS analysis<sup>65</sup>, I monitored the disappearance of a specific peak among the trypsinized fragments of thrombin on the LC profile. A significant decrease in a peptide fragment corresponding to the IYIHPR sequence was observed only when TBA<sub>3</sub> was present (Fig. 3.6D and E), suggesting that the location of the putative covalently-binding site with TBA<sub>3</sub> is within this peptide span and outside of the thrombin catalytic site (Fig. 3.6F).

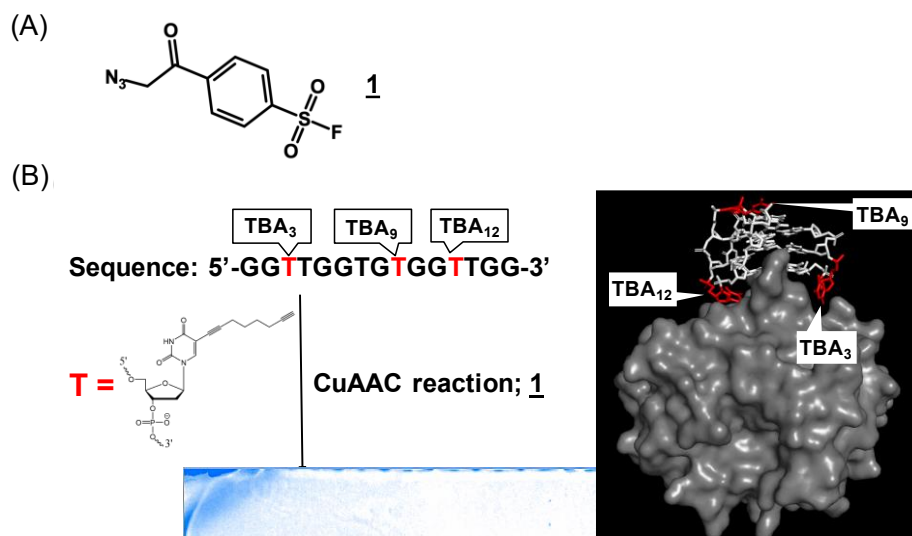


**Fig. 3.2** Identification of covalent-binding TBA. (A) Chemical structure of the azidated warhead. (B) Creation of the warhead-conjugated TBA. Azidated warhead was introduced to an appropriate position of TBA; an alkyne-containing thymine whose position is highlighted in red was conjugated with the azidated warhead by the CuAAC reaction. The location of each designated thymine residue visualized in PyMOL. TBA (white), thrombin (gray surface) (PDB: 1HAO), and each designated thymine residue (red).

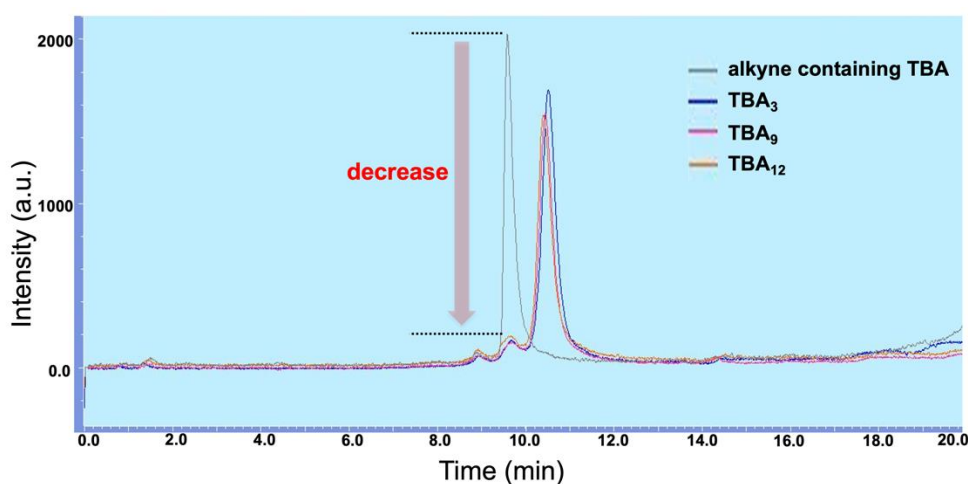


**Fig. 3.3** LC profiles of the crude CuAAC-reaction mixture of each alkyne-containing TBA isomer and the warhead. (A) TBA<sub>3</sub> (blue line), (B) TBA<sub>12</sub> (yellow line), and (C) TBA<sub>9</sub> (pink line), respectively, were monitored using absorbance above 270 nm. Peak areas of unreacted alkyne-containing TBAs were compared with alkyne-containing TBA before the CuAAC reaction (gray line) to estimate the conjugation reaction yields. Reaction yields were estimated ca. 95% from the peak area ratios.

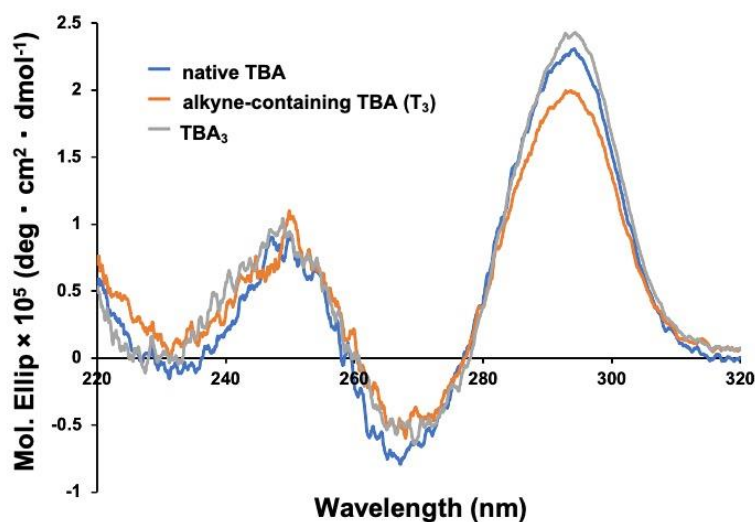


**Fig. 3.4** CD spectra of native TBA, alkyne-containing TBA (T<sub>3</sub>), and TBA<sub>3</sub>. Native TBA, alkyne-containing TBA (T<sub>3</sub>), or TBA<sub>3</sub> at 10  $\mu$ M in D-PBS held at 37°C and spectrum scanned between 220 to 340 nm at 100 nm per minutes (Jasco Corporation J-720W spectrometer). Triplicate measurements were averaged for the plot. The CD spectrum of the native TBA was consistent with a previous report<sup>66</sup> indicating that a G-quadruplex structure was present in the solution state. The introduction of an alkyne linker or a warhead did not alter the 3D structure of TBA.

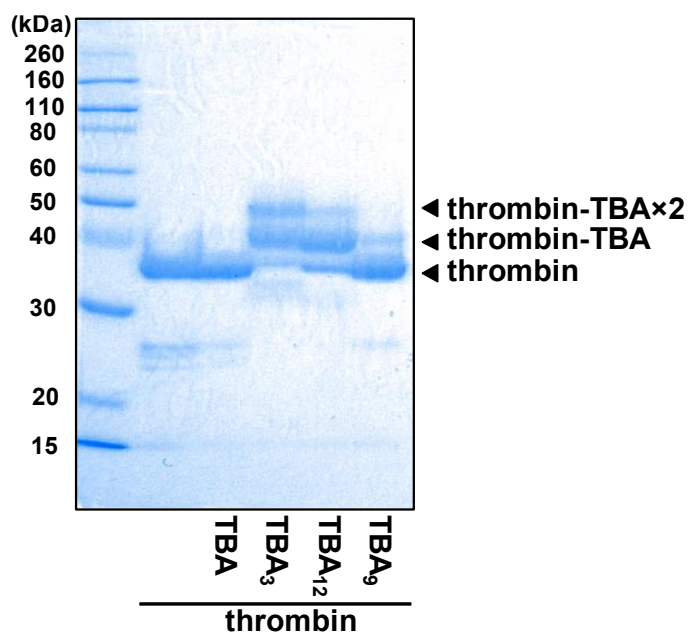


**Fig. 3.5** Covalent binding between each warhead-conjugated TBA and thrombin, confirmed by 13% SDS-PAGE, followed by CBB staining. Each black arrow represents the band of the thrombin and thrombin-TBA conjugate, respectively.

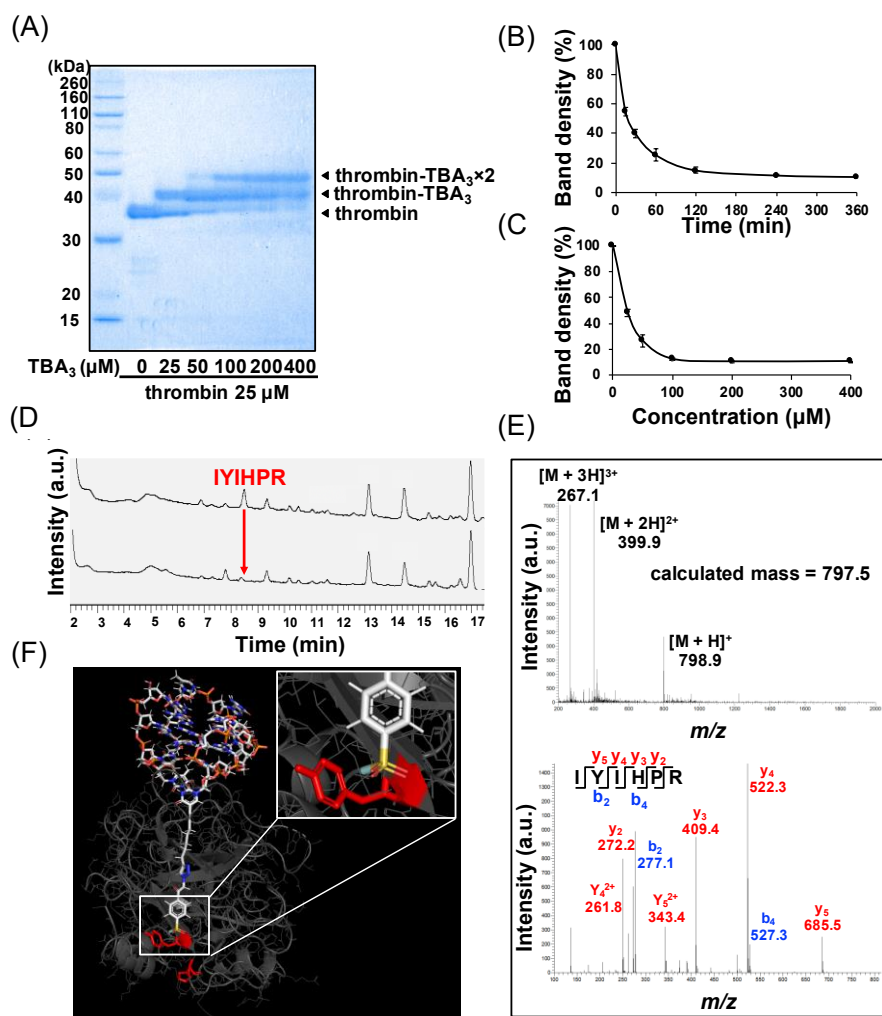


**Fig. 3.6** Covalent-binding ability of TBA<sub>3</sub>. (A) Concentration-dependent mobility shift of thrombin on gel, confirmed by 13% SDS-PAGE followed by CBB staining. (B) Time-dependent change of covalent-binding efficiency. The density of the unreacted-thrombin band at 0 minute was normalized to 100%, and the relative density of each incubation time was quantified. (C) Concentration-dependent change of covalent-binding efficiency. The density of the unreacted-thrombin band in the absence of TBA<sub>3</sub> was normalized to 100%, and the relative density of each concentration of TBA<sub>3</sub> was quantified. (D) LC profile of trypsinized fragments of thrombin without (top) or with (bottom) TBA<sub>3</sub>. A single fragment peak of thrombin, identified as IYIHPR by MS and MS/MS, disappeared after the covalent binding of TBA<sub>3</sub>. (E) MS and MS/MS spectra of the reduced peak. (F) Docking simulation of the TBA<sub>3</sub> (shown as a stick) to thrombin (PDB ID: 1HAO) using cosgene of myPresto. Fluorine atom in the warhead (cyan) and a folded ribbon cartoon thrombin (grey) with the putative TBA<sub>3</sub> covalently bound residues Y88 and H91 (red).

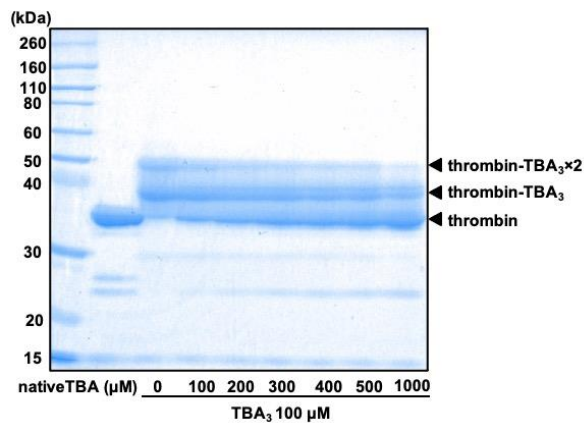


**Fig. 3.7** Determine of TBA<sub>3</sub> binding site of mono- and bis-adducts by competition assay with native TBA. The indicated amounts of native TBA were pre-incubated with thrombin (25 μM) in D-PBS for 10 minutes at 25°C. After addition of TBA<sub>3</sub> (100 μM), the mixture was incubated for an additional 3 hours at 37°C. The covalent modification of thrombin was monitored by SDS-PAGE followed by CBB staining.

Thrombin activity inhibition by TBA<sub>3</sub> was monitored by a time-dependent change of optical density at 288 nm (*i.e.*, turbidimetric assay), which corresponds to thrombin-induced fibrin aggregation.<sup>67</sup> The activity decreased in a concentration-dependent manner with an IC<sub>50</sub> of  $3.5 \pm 0.1$  nM for native TBA (Fig. 3.8A and B), whereas TBA<sub>3</sub> showed a 3-fold greater potency with an IC<sub>50</sub> of  $1.2 \pm 0.1$  nM (N = 3, P = 0.00048) (Fig. 3.8C and D). It is plausible that the tethered TBA<sub>3</sub> covalently bound to thrombin increased the effective local concentration,<sup>68</sup> allowing the desired thrombin inhibition to be achieved at a lower bulk concentration. An automated coagulometer monitored the change in the thrombin-dependent clotting time, and as I expected, the mean clotting times in the presence of TBA<sub>3</sub> at 5 nM and 1 nM were obviously increased compared to native TBA (Table 2.1).

Finally, the on-demand reversal property of TBA<sub>3</sub> was confirmed by the following experiments. A carboxyfluorescein (Fam)-labeled CS incubated with TBA<sub>3</sub> covalently bound thrombin resulted in a fluorescent signal at the expected molecular mass consistent with the Fam-CS forming a double strand with the thrombin bound-TBA (Fig. 3.9A). Such fluorescent bands did not appear on serum proteins, indicating the high specificity of TBA<sub>3</sub> toward thrombin (Fig. 3.9B). A turbidimetric thrombin enzymatic assay confirmed a CS antidote concentration-dependent reactivation of thrombin with an EC<sub>50</sub> of  $2.3 \pm 0.2$  nM for native TBA (Fig. 3.9C and D), and an EC<sub>50</sub> of  $4.6 \text{ nM} \pm 0.3$  for TBA<sub>3</sub> (Fig. 3.9E and F). The difference in the CS antidote EC<sub>50</sub> was statistically significant (N = 3, P = 0.015) by a paired t-test. As I expected, the clotting times increased by native TBA or TBA<sub>3</sub> were completely normalized by the CS antidote (Table 2.1).

In conclusion, I created a covalently-binding DNA aptamer that targets thrombin by introducing a sulfonyl fluoride warhead into appropriate positions of the TBA. The covalently-binding TBA showed high-affinity inhibition of the thrombin activity and an on-demand reversal property of this drug action by the CS antidote. I suppose that our concept and findings will be valuable for developing a safe class of covalent drugs, and weaponizing aptamers with a SuFEx-warhead will likely be applicable in developing covalent aptamers targeting a wide range of target proteins as a general method.

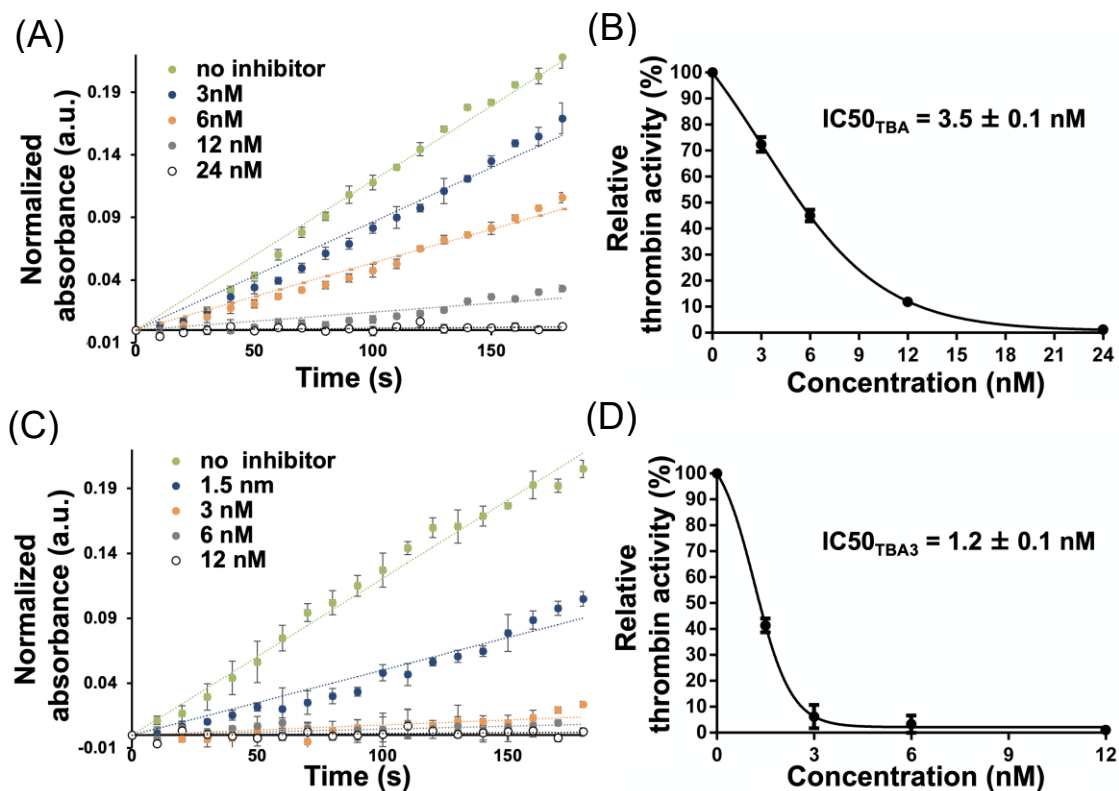


**Fig. 3.8** Comparison of thrombin inhibition activity between native TBA and TBA<sub>3</sub> by turbidimetric assay. (A) Time-dependent thrombin inhibition by native TBA with different concentration. The maximum absorbance (288 nm) of fibrin polymerization at 0 second was normalized to 0% and plotted against time. The plot was fit by a line, and the slope value was quantified as a thrombin activity. (B) The thrombin activity in the absence of inhibitor was normalized to 100%, and the relative thrombin activity of each concentration was quantified. (C) and (D) were performed as above but using TBA<sub>3</sub>.

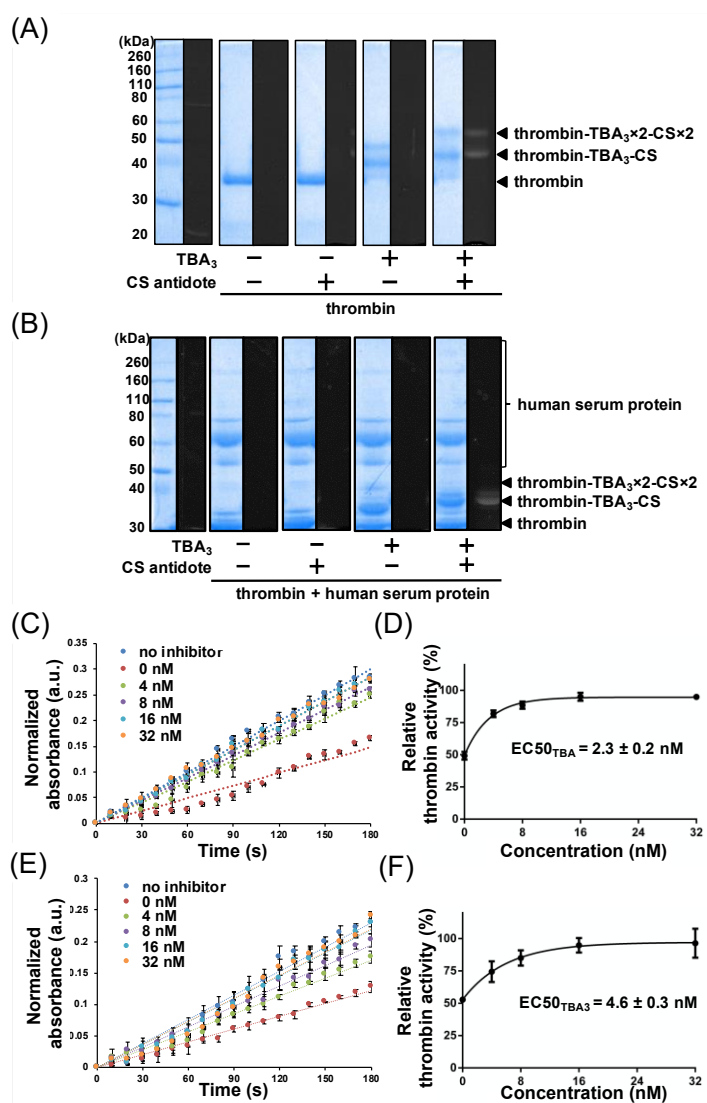


**Fig. 3.9** On-demand reversal property of TBA<sub>3</sub> by CS antidote. (A) TBA<sub>3</sub>-specific duplex formation of CS antidote confirmed by 13% SDS-PAGE/fluorescence imaging. Whole proteins were visualized by CBB staining (left panel of each lane), and a complex of TBA<sub>3</sub> covalently bound for thrombin and Fam-CS was visualized by fluorescence in the same gel (right panel of each lane). (B) Specific covalent binding between TBA<sub>3</sub> and thrombin, confirmed by the same procedure as in (A) except in the presence of human serum (40% v/v). (C) The reversal of thrombin inhibition activity of native TBA confirmed by the turbidimetric assay with increasing concentrations of CS antidote. All runs contained IC<sub>50</sub> concentration of native TBA, which resulted in approximately 50% thrombin activity in the absence of CS antidote. The maximum absorbance (288 nm) of fibrin polymerization at 0 second was normalized to 0% and plotted against time. The plot was fit by a line and the slope quantified as thrombin activity. (D) The thrombin activity in the absence of inhibitor was normalized to 100%, and relative thrombin activity at each concentration of CS antidote was quantified. (E) and (F) were performed as in (C) and (D) but by using TBA<sub>3</sub>.

**Table 2.1.** Elongation of clotting time by native TBA and TBA<sub>3</sub>.

<b>Sample</b>	<b>Concentration<sup>a</sup></b>	<b>CS antidote</b>	<b>Clotting time (s)<sup>b</sup></b>	<b>P value<sup>c</sup></b>
<b>No inhibitor</b>	<b>-</b>	<b>-</b>	<b>21 ± 1</b>	<b>0</b>
<b>native TBA</b>	<b>1 nM</b>	<b>-</b>	<b>26 ± 2</b>	<b>0.0065</b>
<b>TBA<sub>3</sub></b>	<b>1 nM</b>	<b>-</b>	<b>41 ± 3</b>	<b>0.00016</b>
<b>native TBA</b>	<b>5 nM</b>	<b>-</b>	<b>40 ± 3</b>	<b>-</b>
<b>TBA<sub>3</sub></b>	<b>5 nM</b>	<b>-</b>	<b>200 ~</b>	<b>-</b>
<b>TBA<sub>3</sub></b>	<b>1 nM</b>	<b>5 nM</b>	<b>21 ± 1</b>	<b>0.80</b>
<b>TBA<sub>3</sub></b>	<b>1 nM</b>	<b>20 nM</b>	<b>20 ± 1</b>	<b>0.86</b>
<b>TBA<sub>3</sub></b>	<b>5 nM</b>	<b>5 nM</b>	<b>39 ± 1</b>	<b>0.0080</b>
<b>TBA<sub>3</sub></b>	<b>5 nM</b>	<b>20 nM</b>	<b>22 ± 2</b>	<b>0.19</b>

<sup>a</sup>Native TBA or TBA<sub>3</sub> was incubated with thrombin for 3 hours at 37°C and fibrinogen solution was added to give a final concentration of 13 nM thrombin, 2 mg/mL fibrinogen, and native TBA or TBA<sub>3</sub> varied as shown. <sup>b</sup>Clotting times were measured using an automated coagulometer. <sup>c</sup>Values are mean ± S.E.M. from 6 independent experiments. All groups were compared with the group of no inhibitor by a paired t-test. P < 0.05 was considered to be statistically significant.

### ■ 3.3 Experimental procedures and additional figures

#### General

All the reagents and solvents were commercially available and used without further purification. Native TBA, TBA with introduction of a relatively long spacer and a terminal alkyne replacing a thymine residue ( $T_x$ ), complementary strand (CS) antidote, and carboxyfluorescein (Fam)-tagged CS were obtained from Integrated DNA Technologies (IDT) Inc. (Table S1).

**Table S1.** Nucleic acids purchased from IDT.

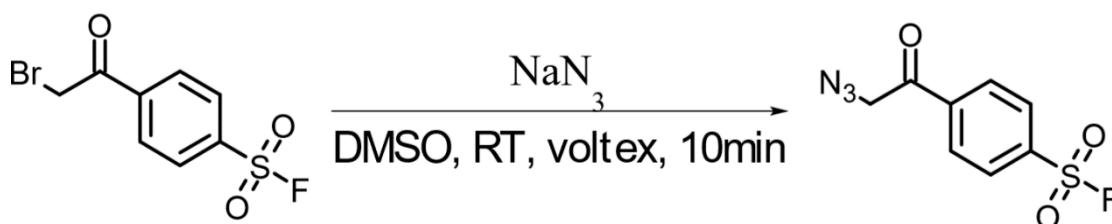
sample	sequence
native TBA	5'-GGTTGGTGTGGTTGG-3'
alkyne-containing TBA ( $T_3$ )	5'-GGXTGGTGTGGTTGG-3'
alkyne-containing TBA ( $T_9$ )	5'-GGTTGGTGXGGTTGG-3'
alkyne-containing TBA ( $T_{12}$ )	5'-GGTTGGTGTGGXTGG-3'
CS antidote	5'-CCAACCACACCAACC-3'
FAM-tagged CS	FAM-5'-CCAACCACACCAACC-3'

Human  $\alpha$ -thrombin (Haematologic Tech Inc, # HCT-0020) and fibrinogen from human plasma (Aldrich, #9001-32-5) were purchased commercially.

NMR experiments were performed at 25°C using a 500 MHz spectrometer (JNM-ECA500, Jeol Resonance). Liquid chromatography (LC) analysis was performed on an Agilent 1100 HPLC system (Agilent Technologies) using a 0–100% gradient of acetonitrile containing 0.1% formic acid at a flow rate of 300  $\mu$ L per minutes, equipped with a C18 reverse-phase column (Hypersil GOLD, 2.1  $\times$  100 mm, Thermo Fisher Scientific) connected to a photodiode array (PDA) and/or a LCQ-Fleet ion trap mass spectrometer. A small scale quantitative analysis of aptamers was carried out by using a reversed-phase semi-micro HPLC system (PU-2085 with C18 column, JASCO) connected to a fluorescence detector followed by a PDA. The aptamers were separated using a 0–60% gradient of acetonitrile containing 20 mM triethylamine acetate aqueous solution (pH 7.4) for 26 minutes at a flow rate of 200  $\mu$ L per minutes. Electrospray ionization-time-of-flight-mass spectrometry (ESI-TOF-MS; JMS-T100 AccuTOF, Jeol Resonance) was performed by dissolving the analyte in methanol and directly injecting into the instrument. The trypsinized peptides were analyzed by matrix-assisted laser desorption/ionization time-of-flight mass spectrometry (MALDI-TOF/MS, UltrafleXtreme, Bruker) with several matrices (*e.g.*, 2,5-dihydroxybenzoic acid, 3-amino-4-hydroxybenzoic acid).

All images of stained gel and in-gel fluorescence were captured by ChemDoc XRS+ (Bio-Rad Laboratories Inc.) and band intensities were quantified using Image Lab™ software (Bio-Rad).

### ***Synthesis of warhead; 1***



The warhead 1 was synthesized on a preparative scale according to the following procedure. 4-(2-bromoacetyl)-benzene-1-sulfonyl fluoride (71  $\mu$ mol, Aldrich #00364) and sodium azide (65  $\mu$ mol, WAKO #195-11092) were mixed in 0.32 mL of dimethyl sulfoxide (DMSO). The reaction mixture was vortexed for 10 minutes at 25°C, then mixed with cold water (0.5 mL) and extracted with ethyl acetate (1 mL). The collected organic phase was washed with saturated NaHCO<sub>3</sub> (0.5 mL  $\times$  2) and brine (0.5 mL  $\times$  2), dried over Na<sub>2</sub>SO<sub>4</sub>, and evaporated to yield a yellow solid pure product (12 mg, yield 49%). Confirmation of the purified warhead 1 was performed by <sup>1</sup>H and <sup>13</sup>C NMR (Fig. S3.2).

### ***Synthesis of warhead-conjugated TBA via CuAAC reaction***

Tris (3-hydroxypropyl) triazolylmethyl) amine (in water, 0.50  $\mu$ mol, Aldrich # 762342) and copper (II) sulfate (in water, 0.25  $\mu$ mol, Aldrich # 451657) were mixed. Then, each alkyne-containing TBA (in water, 10 nmol) and warhead (in DMSO, 0.50  $\mu$ mol) was added, and the mixture was reacted for 1 hour at 25°C after addition of ascorbic acid (in water, 0.40  $\mu$ mol, Aldrich # A92902). The crude reaction product was purified by ethanol precipitation. To the crude product, sodium acetate (in water, 9  $\mu$ mol) and cold ethanol were added and incubated at -20°C for 1 hour. After centrifugation (15000 rpm, 20 minutes, ice temperature), the supernatant was removed, and the pellet washed with 70% ethanol. The residue was dissolved in nuclease-free water and the purified warhead-conjugated TBA was identified by LC analysis (Fig. 3.3). I also tried to identify the warhead-conjugated TBA by MS analysis (*e.g.*, ESI-TOF/MS, MALDI-TOF/MS, LC-MS). However, I could not observe the expected *m/z* value of the warhead-conjugated TBA most probably due to the low ionization efficiency of the fluorine derivative both in positive and negative ionization modes.

### ***Optimization of warhead position***

Native TBA and each warhead-conjugated TBA (*i.e.*, TBA<sub>3</sub>, TBA<sub>12</sub>, TBA<sub>9</sub>) (0.33 mM) were mixed with thrombin (25 μM) in Dulbecco's phosphate-buffered saline (D-PBS), and incubated for 12 hours at 37°C. The samples were mixed with SDS-PAGE Sample Buffer (Wako) and separated by 13% sodium dodecyl sulfate-polyacrylamide gel electrophoresis (SDS-PAGE). Whole proteins were visualized by Coomassie Brilliant Blue (CBB) staining.

### ***TBA<sub>3</sub>-concentration dependent mobility shift of thrombin on gel electrophoresis***

Various molar concentrations of TBA<sub>3</sub> and a constant molar concentration of thrombin (25 μM) were mixed in D-PBS and incubated for 12 hours at 37°C. After addition of the Sample Buffer and separation by 13% SDS-PAGE, proteins were visualized by CBB staining.

### ***Time-dependent change of covalently-binding efficiency***

For assessment of time-dependent bond formation of TBA<sub>3</sub>, I mixed TBA<sub>3</sub> (100 μM) and thrombin (25 μM) with various incubate time in D-PBS at 37°C. It was mixed with the Sample Buffer, separated by 13% SDS-PAGE. Whole proteins were visualized CBB staining. The unreacted-thrombin band was quantified by Image Lab software and the density of unreacted-thrombin band at 0 minute was normalized to 100% and the relative density at each time was quantified.

### ***Concentration-dependent change of covalently-binding efficiency***

For assessment of concentration-dependent change of covalently-binding efficiency, I mixed various molar concentrations of TBA<sub>3</sub> and constant molar concentrations of thrombin (25 μM) in D-PBS and incubated for 3 hours at 37°C. It was mixed with the Sample Buffer, separated by 13% SDS-PAGE. Whole proteins were visualized by CBB staining. The unreacted-thrombin band was quantified by Image Lab software and the density of unreacted-thrombin band in 0 molar of TBA<sub>3</sub> was normalized to 100% and the relative density of each molar concentration was quantified.

### ***Trypsin digestion and analysis by LC-MS/MS***

For LC-MS/MS analysis, TBA<sub>3</sub> (0.10 mM) was mixed with thrombin (25 μM) in D-PBS and incubated for 3 hours at 37°C. After addition of a sample buffer and separation by 13% SDS-PAGE, whole protein were visualized by CBB staining. The stained protein bands were excised from the gel, reduced with 25 mM dithiothreitol at 65°C for 10 minutes, and alkylated with 55 mM iodoacetamide at 25°C for 1 hour in the dark. Digestion was carried out with modified trypsin (Promega # V5111) with 25 mM n-Octyl-beta-D-thioglucoiside (WAKO # 349-05361)

for 12 hours at 37°C. The resulting peptides were analyzed using LC-MS/PDA system. The trypsinized peptides were separated using a 0-50% gradient of acetonitrile containing 0.1% formic acid during 55 minutes at a flow rate of 300  $\mu$ L per minutes, and the eluted peptides were directly sprayed into the mass spectrometer. The mass spectrometer was operated in the data-dependent mode and externally calibrated. Survey MS scans were acquired in the 200-2000  $m/z$  ranges. Multiply charged ions of high intensity per scan were fragmented with collision-induced dissociation in the ion trap. A dynamic exclusion window was applied within 30 seconds. All tandem mass spectra were collected using normalized collision energy of 40%. Data were acquired and analyzed with Xcalibur software v.2.07 (Thermo Scientific). I also tried to analyze the trypsinized peptides by MALDI-TOF/MS, however, I could not observe the ionization of the peptide-TBA<sub>3</sub> complex.

#### ***Monitor of thrombin inhibition activity by turbidimetric assay***

I mixed various molar concentrations of native TBA or TBA<sub>3</sub> and constant molar concentrations of thrombin (25  $\mu$ M) in D-PBS and incubated for 3 hours at 37°C. Then, each reaction mixture was added into fibrinogen solution (in D-PBS) to give a final concentration of 2.5 nM thrombin and 1 mg/mL fibrinogen, the maximum absorbance of polymerized fibrin (288 nm) was measured every 10 seconds by NanoPhotometer (Implen) using 10-mm plastic cell. In each experiment, the maximum absorbance of polymerized fibrin at 0 second was normalized to 0, and the relative absorbance of each second was quantified.

#### ***Monitor of thrombin inhibition activity by clotting time change***

Various molar concentrations of native TBA or TBA<sub>3</sub> and a constant molar concentration of thrombin (25  $\mu$ M) in D-PBS were incubated for 3 hours at 37°C. Each reaction mixture was supplemented with a fibrinogen solution (in D-PBS) to give a final concentration of 13 nM thrombin and 2 mg/mL fibrinogen<sup>23</sup>, and the clotting time was measured by a BFT II Analyzer (Siemens Healthineers).

#### ***Double strand formation between TBA and CS antidote***

Thrombin (25  $\mu$ M) with or without TBA<sub>3</sub> (100  $\mu$ M) in D-PBS were incubated for 3 hours at 37°C. The mixture was supplemented with or without Fam-labeled CS (400  $\mu$ M) for 30 minutes at 37°C, mixed with the sample buffer, separated by 13% SDS-PAGE, followed by an in-gel fluorescence imaging. Specificity of the covalent binding between TBA<sub>3</sub> and thrombin was examined, as above, but in the presence of 40% (v/v) human serum (Aldrich #H4522). Whole proteins were visualized by CBB staining.

### ***Evaluation of the reversal of thrombin inhibition by turbidimetric assay***

Native TBA (3.5 nM) or TBA<sub>3</sub> (1.2 nM) and a constant molar concentration of thrombin (25 μM) in D-PBS was incubated for 3 hours at 37°C. To each reaction mixture, various molar concentration of the CS antidote was added and incubated for 30 minutes at 37°C. Fibrinogen solution (in D-PBS) was added to each reaction mixture to give a final concentration of 2.5 nM thrombin and 1 mg/mL fibrinogen and absorbance (288 nm) was measured every 10 seconds by NanoPhotometer (Implen) using a 10-mm plastic cell. Time dependent absorbance values were plotted with baseline absorbance at 0 second taken as 0.

### ***Evaluation of the reversal of thrombin inhibition by clotting time***

Native TBA (3.5 nM) or TBA<sub>3</sub> (1.2 nM) and thrombin (25 μM) in D-PBS were incubated for 3 hours at 37°C. CS antidote (5.3 or 21 nM) was added and further incubated for 30 minutes at 37°C. Fibrinogen solution (in D-PBS) to give a final concentration of 13 nM thrombin and 2 mg/mL fibrinogen was added and the clotting time measured by the BFT II Analyzer.

### ***Molecular docking simulations of the TBA<sub>3</sub> to thrombin***

TBA<sub>3</sub> was created in Avogadro<sup>69</sup> (version 1.2.0) from native TBA (PDB ID = 1HAO). Docking of TBA<sub>3</sub> to thrombin (PDB ID = 1HAO) was performed with MolDesk Basic (version 1.1.45, ImSBio Inc.) graphical user interface of several myPresto programs<sup>45</sup>. Docking model (*i.e.*, globally minimized structure) of TBA<sub>3</sub> on thrombin was calculated by the Cosgene program of myPresto (version 5.000) using the universal force field.

### ***Statistical calculations***

Values are presented as mean ± S.D. Statistical significance of differences between groups was estimated by a paired t-test. A P-value < 0.05 was considered statistically significant (\*P < 0.05, \*\*P < 0.01, \*\*\*P < 0.001). Analyses were performed using GraphPad Prism 6.0 software (GraphPad Software).

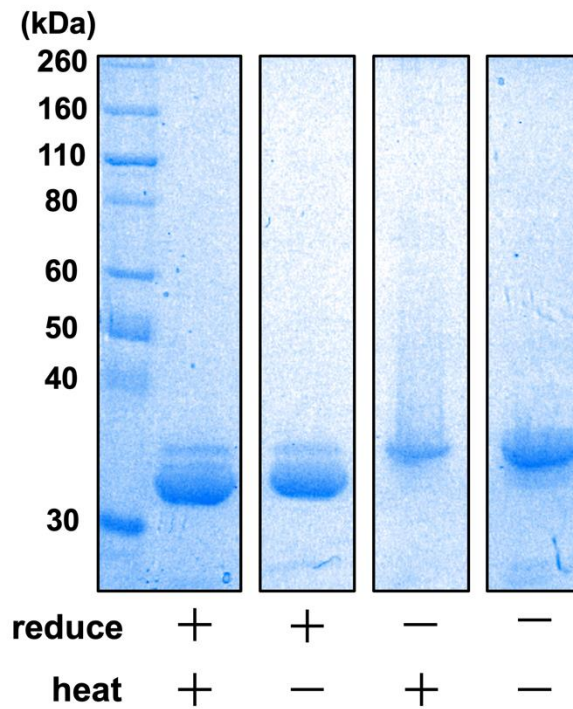


**Fig. S3.1** *Optimization of sample preparation for SDS-PAGE.* Thrombin was prepared with or without boiling or reducing, separated by SDS-PAGE followed by CBB staining. A single thrombin band was seen without heating or reducing. I chose this simplest low-temperature and non-reducing condition for the sample preparation because it minimized potential artifacts from promiscuous covalent reactions of the warhead to the target protein.

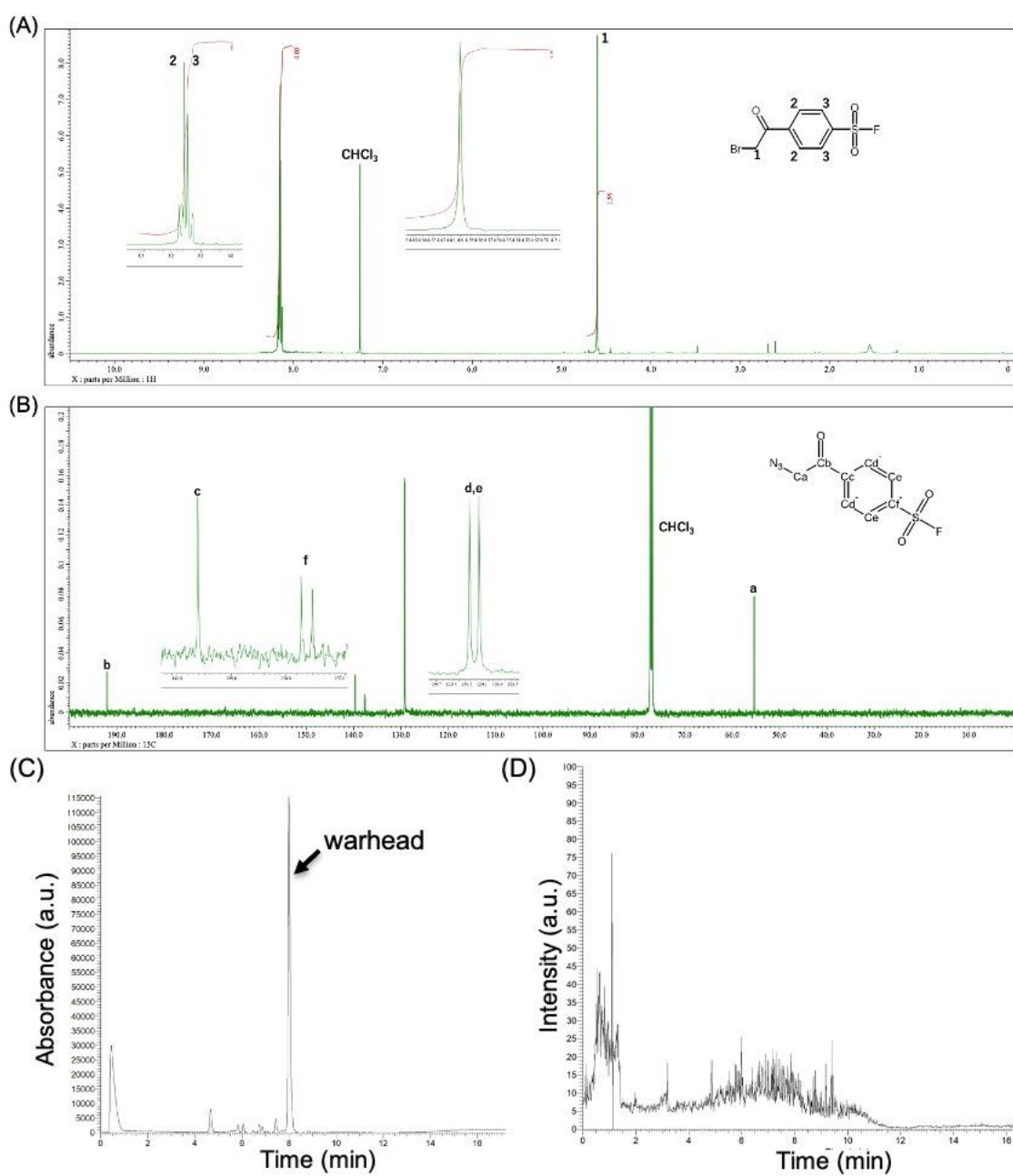


**Fig. S3.2** Identification of the purified warhead. (A) <sup>1</sup>H NMR spectrum. (B) <sup>13</sup>C NMR spectrum. (C) LC-absorbance (240 - 260 nm) profile of the purified warhead. (D) LC-MS total ion profile. I could not observe an expected  $m/z$  value of the purified warhead because of the low ionization efficiency of the fluorine derivative both in positive and negative ionization modes.

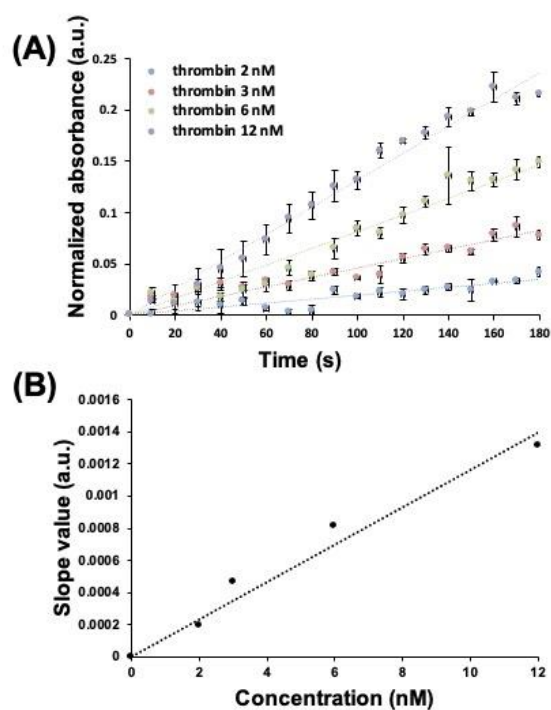


**Fig. S3.3** *Standard curve of thrombin-activity.* Thrombin-activity was monitored by the turbidimetric assay. (A) Time-dependent change in absorbance for different thrombin concentrations. The baseline absorbance (288 nm) at 0 second was subtracted and the time dependent absorbance values plotted and a line fit by linear regression. (B) The slope values were plotted against concentration to yield the standard curve of thrombin activity as determined by this assay. The slope value (*i.e.*, thrombin-activity) was linearly correlated with thrombin concentration within the range examined.

## **CHAPTER 4**

**Relative nuclease resistance of DNA-aptamer  
covalently conjugated to a target protein**

## ■ 4.1 Introduction

Modifications of the molecular structures of nucleic-acid aptamers<sup>51, 53-56, 70-72</sup> such as the use of a non-natural phosphorothioate backbone, and manipulation of the sugar structure, are often used to reduce rapid hydrolysis by nucleases and to increase the *in vivo* circulation half-life.<sup>70, 72, 73</sup> It has been also well known that natural DNA aptamers can be protected from hydrolysis by nucleases when they are tightly bound to the target proteins; nuclease resistance of a DNA aptamer depends on its affinity to the target protein.<sup>74-78</sup>

As I described in the previous chapter, I created a covalently-binding DNA aptamer, as a novel covalent-drug modality, by introducing a warhead (*i.e.*, reactive group) into designated position(s) on the aptamer.<sup>19</sup> The covalently-binding aptamer could form a permanent bond to a target protein with an effective zero dissociation constant ( $K_D$ ) rate resulting in a left-shifted concentration-dependent inhibition activity. Here I demonstrate that the covalent binding also confers relative nuclease resistance to the DNA aptamer presumably because of the effectively zero  $K_D$  rate (Fig. 4.1).

**(A) Conventional aptamer**



**(B) Covalent binding aptamer**

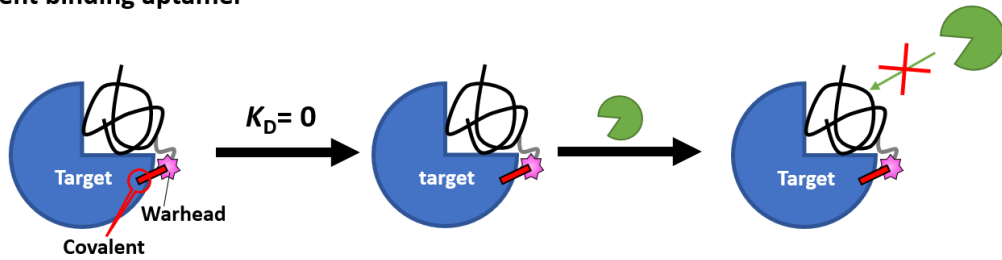


**Fig. 4.1** Susceptibility mechanism to the hydrolysis mediated by a nuclease. (A) Conventional aptamer: aptamer (fold string) binds to its target protein (blue) (left). The aptamer dissociates from the target protein (middle). The free state of the aptamer is recognized by the nuclease (right). (B) Covalently-binding aptamer: a warhead (red star) conjugated aptamer forms a covalent bond (left) and permanently conjugates to the target protein (middle), which would result in semi-permanent nuclease resistance.

## ■ 4.2 Results and discussion

As described previously, I introduced the sulfonyl fluoride warhead, which can react with any nucleophilic amino acid residues (*i.e.*, serine, threonine, lysine, tyrosine, cysteine, and histidine)<sup>25-32</sup>, into the third thymine residue from the five-prime end of the thrombin binding aptamer (TBA) to create the covalently-binding TBA (TBA<sub>3</sub>).<sup>19</sup> I hypothesize that TBA<sub>3</sub> reversibly docks to thrombin prior to forming an irreversible covalent bond; such a two-step process is observed to many known conventional covalent drugs<sup>1-6, 8</sup> (Fig. 4.2A). First, I proved that the TBA<sub>3</sub> showed a time-dependent inhibition activity which supports the hypothesized two-step process (Fig. 4.2B). Furthermore, TBA<sub>3</sub> showed an ideal  $k_{\text{inact}}/K_I$  value of  $0.21 \pm 0.06 \mu\text{M}^{-1}\text{s}^{-1}$ , which was in the same order of approved covalent drugs.<sup>79</sup>

Next, I evaluated the nuclease resistance of TBA<sub>3</sub> in the presence of human serum or DNases. As a preliminary experiment, the hydrolysis of TBA was monitored by liquid chromatography (LC). After the serum treatment of the TBA in the presence of thrombin, the TBA peak completely disappeared and a low molecular-weight nucleotide peak was detected at the void volume (Fig. 4.3A). As expected, TBA with a finite off rate dissociated from the target thrombin was digested by the nuclease in the human serum. Since it is hard to monitor the hydrolysis of the covalently conjugated TBA<sub>3</sub> by LC because of chimeric formation with the target protein, I did it by the mobility shift of thrombin induced by the TBA<sub>3</sub> binding with sodium dodecyl sulfate polyacrylamide gel electrophoresis (SDS-PAGE). Thrombin incubated with TBA<sub>3</sub> resulted in a persistent mobility shift on gel electrophoresis where the protein bands were visualized by Coomassie Brilliant Blue (CBB) staining. An equal amount of the mobility shift was observed even in the presence of human serum (Fig. 4.3B), which suggests that thrombin was covalently conjugated to TBA<sub>3</sub> and resisted against the nuclease digestion for a prolonged time. To assess the nuclease resistance mechanism, I used recombinant Exo VII exonuclease and S1-endonuclease instead of the crude nuclease mixtures (*i.e.*, human serum) for further experiments.

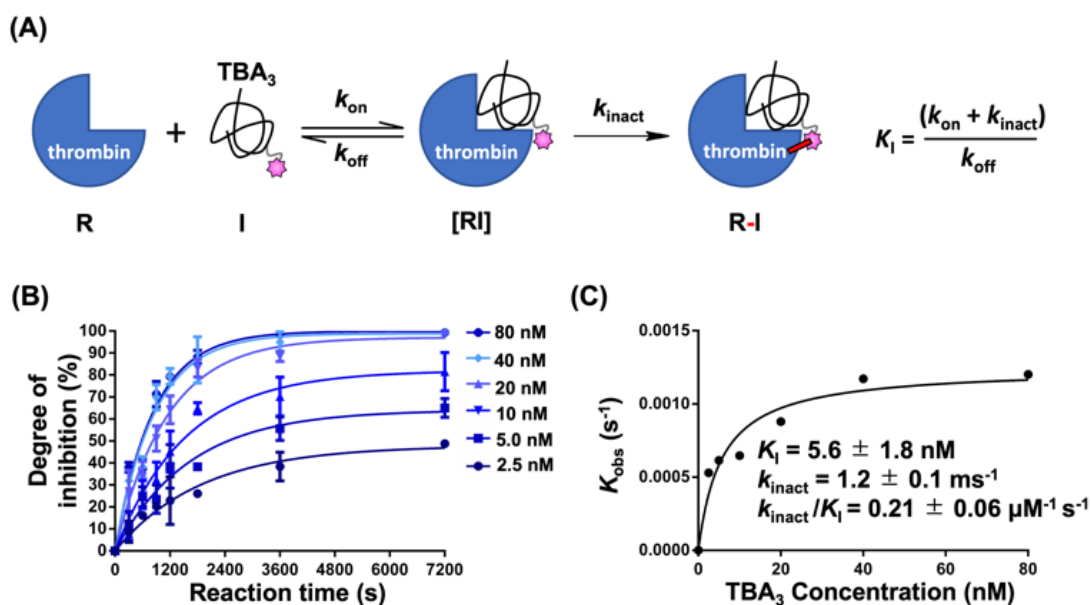


**Fig. 4.2** (A) Reaction kinetics of TBA<sub>3</sub>: a reversible interaction between TBA<sub>3</sub> and thrombin is described as rate constants of association ( $k_{on}$ ) and dissociation ( $k_{off}$ ). Inactivation rate of thrombin by the covalent binding of TBA<sub>3</sub> is described as  $k_{inact}$ . The resulting  $k_{inact}:K_I$  ratio is generally preferred to rank the potency of covalent inhibitors against a target, rather than using IC<sub>50</sub> values.<sup>8</sup> (B) The degree of thrombin inhibition at each reaction time was monitored by a turbidimetric assay for different concentrations of TBA<sub>3</sub>. The pseudo-first-order rate constant,  $k_{obs}$  was calculated for each TBA<sub>3</sub> concentration using nonlinear regression analysis in GraphPad Prism 6. (C) The obtained  $k_{obs}$  were plotted against each covalent binder concentration to afford the second-order rate constant  $k_{inact}/K_I$ .

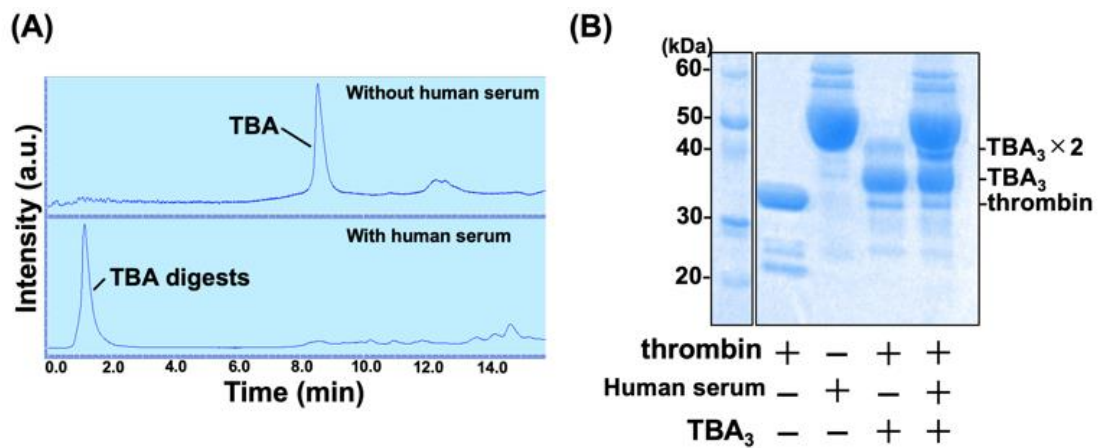


**Fig. 4.3** Nuclease resistance of naïve TBA and TBA<sub>3</sub> in the presence of human serum. (A) LC absorbance profiles of naïve TBA incubated with thrombin in the presence/absence of human serum. (B) Nuclease resistance of TBA<sub>3</sub> in the presence of human serum, confirmed by 12% (w/v) native PAGE. Whole proteins were visualized by CBB staining. The band density of the TBA<sub>3</sub>–conjugated thrombin did not change after the serum incubation for 24 hours at 37°C.

The nuclease resistance of naïve TBA or TBA<sub>3</sub> were evaluated by native and SDS-PAGEs which reflect the *bound* and the *conjugated* states of the aptamer/thrombin (*i.e.*, [RI] and [R-I] states in Fig. 2A), respectively. The bands of TBA/thrombin disappeared when treated with Exo VII exonuclease or S1 endonuclease, whereas those of TBA<sub>3</sub>/thrombin did not (Fig. 4.4A–D). TBA<sub>3</sub> induced two distinct mobility-shift corresponding to the TBA<sub>3</sub>-monoadduct and bisadduct by covalent binding. For the bisadduct, two equimolar TBA<sub>3</sub> were conjugated to different residues in a thrombin while both TBA<sub>3</sub> seemed to recognize the same TBA-binding site.<sup>15</sup> In the presence of nucleases, the band of monoadduct remained dense whereas that of bisadduct almost disappeared. This suggests that while one of the conjugated TBA<sub>3</sub> was in the bound-state on thrombin, the other one was microscopically in the unbound-state and recognized by the nucleases (Fig. 4.5). Furthermore, the conjugated bisadduct was digested with S1 endonuclease rather than Exo VII (Fig. 4.4A–D), suggesting that the thrombin-conjugated TBA<sub>3</sub> provides greater steric hindrance to the latter nuclease which recognizes the terminal regions of the aptamer.

A desirable property of the aptamer drugs is the inherent reversibility by the addition of the complimentary strand (CS) antidote. In the previous chapter, I demonstrated that the inhibition of the thrombin enzymatic activity by TBA<sub>3</sub> is reversed by the CS, and here I investigated the effect of CS on nuclease resistance of TBA<sub>3</sub>. An addition of CS to TBA<sub>3</sub>-conjugated thrombin resulted in a band appearance at the expected molecular mass consistent with the CS forming a double strand with the thrombin conjugated TBA<sub>3</sub>. The density of the shifted bands were greatly reduced when treated with DNA duplex-specific nucleases (*i.e.*, exonuclease III and DNase I) (Fig. 4.6). This indicates that the double-strand state TBA<sub>3</sub> became microscopically in the unbound-state and hydrolyzed by the nucleases. (Fig. 4.7).

Finally, thrombin inhibition by naïve TBA and TBA<sub>3</sub> in the presence of nuclease or human serum was monitored by a time-dependent change of optical density at 288 nm (*i.e.*, turbidimetric assay), which corresponds to thrombin-induced fibrin aggregation.<sup>15, 32</sup> The thrombin inhibition activity of naïve TBA was decreased when incubated with nucleases or human serum, whereas that of TBA<sub>3</sub> was not (Fig. 4.8). This indicates that TBA<sub>3</sub> resisted nuclease digestion and maintained the target inhibition activity when covalently conjugated to the target protein.

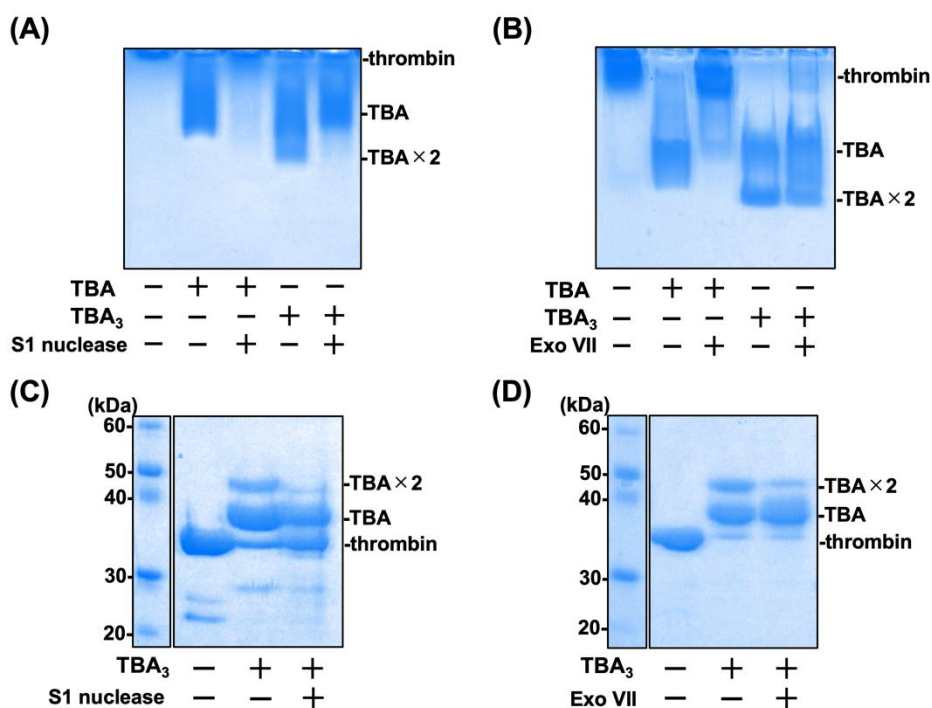


**Fig. 4.4** Nuclease resistance of naïve TBA and TBA<sub>3</sub> against S1- and Exo VII-nucleases were confirmed by 12% native PAGE (A and B) and 12% SDS-PAGE (C and D), respectively. Whole proteins were visualized by CBB staining.

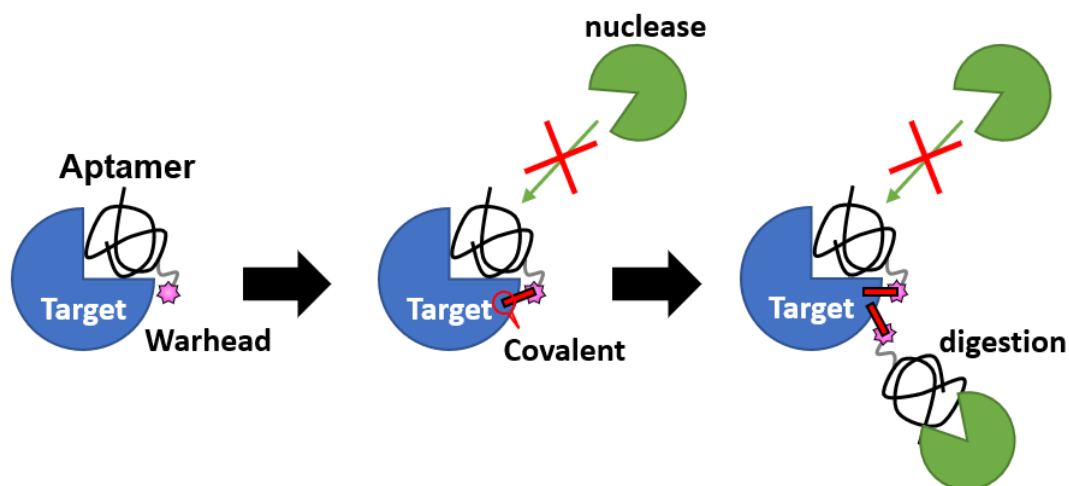


**Fig. 4.5** The expected nuclease resistance mechanism of TBA<sub>3</sub>. A warhead conjugated aptamer forms a covalent bond and permanently conjugates to the target protein, resulting in semi-permanent nuclease resistance (left and middle). When thrombin is conjugated with an additional TBA<sub>3</sub>, one of the TBA<sub>3</sub> is microscopically bound to thrombin, whereas the other one is in the unbound state and recognized by the nuclease (right).

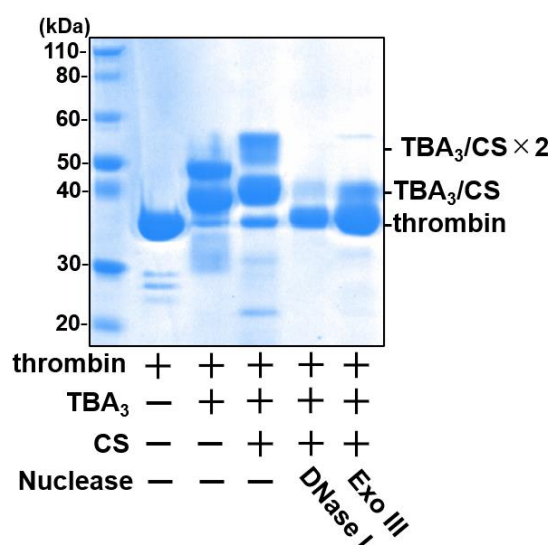


**Fig. 4.6** Nuclease resistance of double-strand state TBA<sub>3</sub> against DNase I- or Exo III-nuclease was confirmed by 12% SDS-PAGE. Whole proteins were visualized by CBB staining.

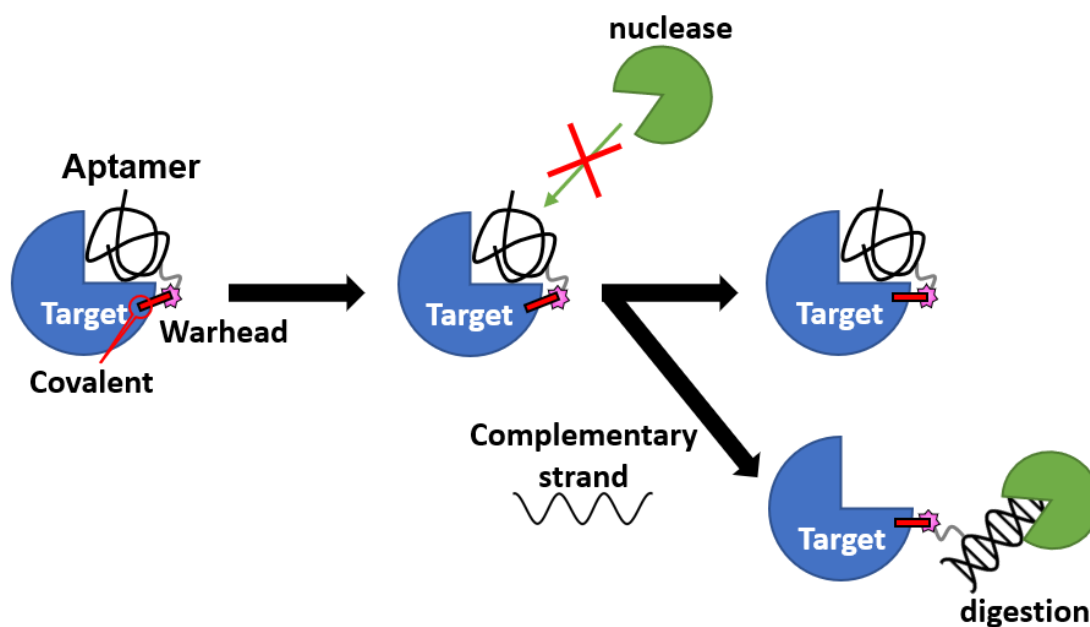


**Fig. 4.7** Nuclease digestion of double-stranded TBA<sub>3</sub>. A warhead conjugated aptamer forms a covalent bond and permanently conjugates to the target protein (left), resulting in semi-permanent nuclease resistance (middle). Introduction of the CS removes the aptamer from the binding site, and the double-stranded TBA<sub>3</sub> is recognized by the nuclease.

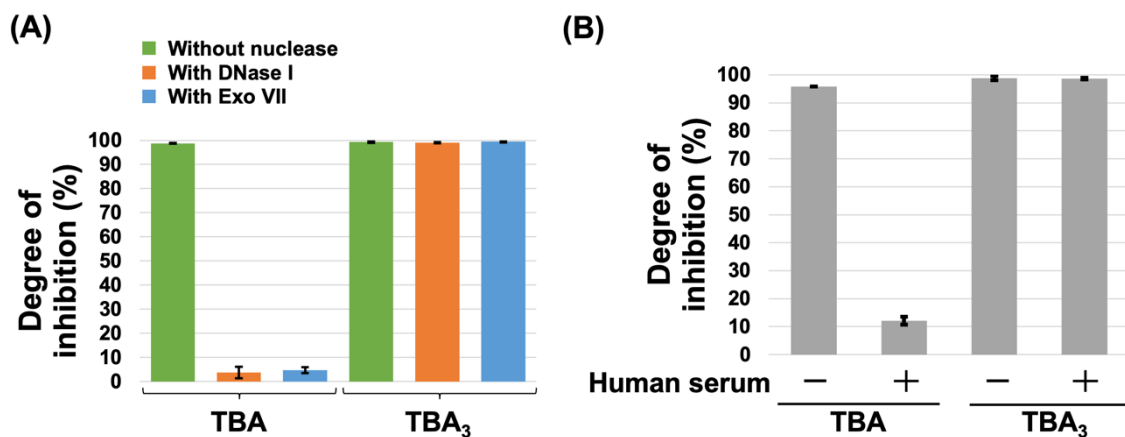


**Fig. 4.8** Comparison of thrombin inhibition activity between naïve TBA and TBA<sub>3</sub> by the turbidimetric assay. (A) Thrombin inhibition activity of each aptamer in the presence of DNase I- or Exo VII-nuclease. The maximum absorbance (288 nm) of fibrin polymerization at 0 second was normalized to 0%. (B) Thrombin inhibition activity of each aptamer in the presence of human serum. The degree of inhibition was calculated as above (A).

In conclusion, I demonstrated a novel methodology to endow nuclease resistance to a DNA aptamer. TBA<sub>3</sub> formed a permanent bond to thrombin, resulting in a drug-protein complex that is not affected by classical equilibrium kinetics of binding (*i.e.*,  $K_D = 0$ ). As a result, TBA<sub>3</sub> showed a long-term relative nuclease resistance against nucleases and maintained the desired thrombin inhibition activity. While I did not examine *in vivo* pharmacokinetics of TBA<sub>3</sub>, a prolonged inhibition of the target protein is expected from the extension of the pharmacological half-life due to the covalent binding, regardless of the macroscopically observable pharmacokinetic half-life of the free TBA<sub>3</sub>. I suppose that these advantages provided by the covalently binding aptamer will mitigate the major obstacles to the therapeutic application of aptamers, such as susceptibility to hydrolysis by nucleases and rapid clearance through glomerular filtration, and accelerate the translation of aptamer therapeutics to clinical applications.

### ■ 4.3 Experimental procedures and additional figures

#### *General*

All the reagents and solvents were purchased commercially and used without further purification. Human  $\alpha$ -thrombin (Haematologic Tech Inc, # HCT-0020, USA) and fibrinogen from human plasma (Aldrich, #9001-32-5, USA), human serum (Sigma, #H422, USA), Exonuclease III (Biolabs, #M0206S, USA), Exonuclease VII (Biolabs. #M0379S, USA), S1 nuclease (TaKaRa, #2410A, Japan), and DNase I (Nippon gene, #314-08071, Japan) were purchased commercially. TBA, TBA with introduction of a relatively long spacer and a terminal alkyne replacing a thymine residue ( $T_3$ ), and complementary strand (CS) were synthesized by Integrated DNA Technologies (IDT) Inc. (Table S1).

**Table S1.** Nucleic acids purchased from IDT.

Sample	Sequence
TBA	5'-GGTTGGTGTGGTTGG-3'
Alkyne-containing TBA ( $T_3$ )	5'-GGXTGGTGTGGTTGG-3'
CS	5'-CCAACCACACCAACC-3'

A small scale quantitative analysis of aptamers was carried out by using a reversed-phase semi-micro HPLC system (PU-2085 with C18 column, JASCO, Japan) connected to a fluorescence detector followed by a photodiode array (PDA). The aptamers were separated using a 0–60% gradient of acetonitrile containing 20 mM triethylamine acetate aqueous solution (pH 7.4) for 26 minutes at a flow rate of 200  $\mu$ L per minutes.

All images of stained gel and in-gel fluorescence were captured by ChemDoc XRS+ (BioRad Laboratories Inc., USA) and band intensities were quantified using Image Lab software (BioRad Laboratories Inc., USA).

### ***Synthesis of TBA<sub>3</sub>***

TBA<sub>3</sub> was synthesized according to the following procedure<sup>19</sup>. Tris(3-hydroxypropyltriazolylmethyl)amine (in water, 0.50 μmol, Aldrich # 762342, USA) and copper (II) sulfate (in water, 0.25 μmol, Aldrich # 451657, USA) were mixed. Then, each alkyne-containing TBA (T<sub>3</sub>) (in water, 10 nmol) and an azidated warhead<sup>1</sup> (in DMSO, 0.50 μmol) was added, and the mixture was reacted for 1 hour at ice temperature after addition of ascorbic acid (in water, 0.40 μmol, Aldrich # A92902, USA). The crude reaction product was purified by ethanol precipitation. To the crude product, sodium acetate (in water, 9 μmol) and cold ethanol were added and incubated at -20°C for 1 hour. After centrifugation (13000 g, 20 minutes, 4°C), the supernatant was removed, and the pellet washed with 70% ethanol. The residue was dissolved in nuclease-free water.

### ***Kinetics evaluation of TBA<sub>3</sub>***

Thrombin activity inhibition by TBA<sub>3</sub> was measured by a turbidimetric assay. I mixed various molar concentrations of TBA<sub>3</sub> and constant molar concentrations of thrombin (25 μM) with various incubate time in Dulbecco's Phosphate-Buffered Saline (D-PBS) at 37°C. Then, each reaction mixture was added into fibrinogen solution (in D-PBS) to give a final concentration of 2.5 nM thrombin and 1 mg/mL fibrinogen, the maximum absorbance of polymerized fibrin (288 nm) was measured after three minutes by NanoPhotometer (Implen, German) using 10-mm plastic cell. In each experiment, the maximum absorbance of polymerized fibrin at 0 second was normalized to 0, and the relative absorbance was quantified. The degree of thrombin-activity inhibition (DoI) was calculated as mean ± SD (n = 3) from the quantified values and plotted against time. Exponential curve fitting of the plot by GraphPad Prism 6 (MDF Co., Ltd.) gave us the value of  $k_{\text{obs}}$  at each TBA<sub>3</sub> concentration by using an equation of DoI (%) =  $v_i / k_{\text{obs}} \times [1 - \exp(-k_{\text{obs}} \times t)]$ ;  $v_i$  = initial velocity (Fig. 2B). Finally, the values of  $k_{\text{obs}}$  (i.e, pseudo-first-order rate constant) were plotted against the TBA<sub>3</sub> concentrations, and the values of  $K_i$  and  $k_{\text{inact}}$  (i.e., inhibition constant and inactivation rate constant, respectively) were determined by the curve fitting of  $k_{\text{obs}} = (k_{\text{inact}} \times [I]) / (K_i + [I])$ ;  $[I]$  = TBA<sub>3</sub> concentration (Fig. 2C).

***Evaluation of nuclease resistance of naïve TBA and TBA<sub>3</sub> in the presence of human serum***  
***Liquid-chromatography analysis***

For assessment of nuclease resistance, naïve TBA (0.10 mM) was mixed with thrombin (25 µM) in D-PBS and incubated for 3 hours at 37°C. It was mixed with human serum (40 % (v/v)) for 24 hours at 37°C. Then, the reaction mixture was heated at 95°C for 10 minutes and centrifuged at 10000 g for 10 minutes. The supernatant was analyzed by liquid-chromatography (LC) analysis (Fig. 3A).

***Gel electrophoresis analysis***

For assessment of nuclease resistance, TBA<sub>3</sub> (0.10 mM) was mixed with thrombin (25 µM) in D-PBS in the presence of human serum (40% (v/v)) and incubated for 3 hours at 37°C. After addition of the sample buffer and separation by 12% sodium dodecyl sulfate polyacrylamide gel electrophoresis (SDS-PAGE), whole proteins were visualized by Coomassie Brilliant Blue (CBB) staining (Fig. 3B).

***Evaluation of nuclease resistance of naïve TBA and TBA<sub>3</sub> in the presence of exo- and endo-nucleases by gel electrophoresis analysis***

For assessment of nuclease resistance, naïve TBA or TBA<sub>3</sub> (0.10 mM) was mixed with thrombin (25 µM) in D-PBS and incubated for 3 hours at 37°C. It was mixed with ten-units of each nuclease (DNase I, S1 nuclease, Exonuclease VII) for 24 hours at 37°C. After addition of the loading buffer or sample buffer and separation by 12% native PAGE or SDS-PAGE, whole proteins were visualized by CBB staining (Fig. 4, Fig. S4.2).

***Evaluation of nuclease resistance of double strand state TBA<sub>3</sub> by gel electrophoresis analysis***

Thrombin (25 µM) with or without TBA<sub>3</sub> (0.10 mM) in D-PBS were incubated for 3 hours at 37°C. The mixture was supplemented with or without complementary strand (CS, 400 µM) for 30 minutes at 37°C. Then, it was mixed with ten-units of each nuclease (DNase I, S1 nuclease, Exonuclease VII) for 24 hours at 37°C. After addition of the loading buffer or sample buffer and separation by 12% SDS-PAGE, whole proteins were visualized by CBB staining (Fig. 5).

### ***Evaluation of thrombin inhibition activity***

#### ***Evaluation of thrombin inhibition activity in the presence of exo- and endo-nucleases***

For assessment of thrombin inhibition activity, naïve TBA or TBA<sub>3</sub> (0.10 mM) was mixed with thrombin (25 µM) in D-PBS and incubated for 3 hours at 37°C. It was mixed with ten-units of each nuclease (DNase I, Exonuclease VII) for 24 hours at 37°C. Then, each reaction mixture was analyzed the turbidimetric assay. Each reaction mixture was added into fibrinogen solution (in D-PBS) to give a final concentration of 2.5 nM thrombin and 1 mg/mL fibrinogen, the maximum absorbance of polymerized fibrin (288 nm) was measured after three minutes by NanoPhotometer (Implen, German) using 10-mm plastic cell. In each experiment, the maximum absorbance of polymerized fibrin at 0 second was normalized to 0, and the relative absorbance was quantified.

#### ***Evaluation of thrombin inhibition activity in the presence of human serum***

For assessment of thrombin inhibition activity, naïve TBA or TBA<sub>3</sub> (0.10 mM) was mixed with thrombin (25 µM) in D-PBS in the presence of human serum (40% (v/v)) and incubated for 3 hours at 37°C. Then, each reaction mixture was analyzed the turbidimetric assay. Each reaction mixture was added into fibrinogen solution (in D-PBS) to give a final concentration of 2.5 nM thrombin and 1 mg/mL fibrinogen, the maximum absorbance of polymerized fibrin (288 nm) was measured after three minutes by NanoPhotometer (Implen, German) using 10-mm plastic cell. In each experiment, the maximum absorbance of polymerized fibrin at 0 second was normalized to 0, and the relative absorbance was quantified.

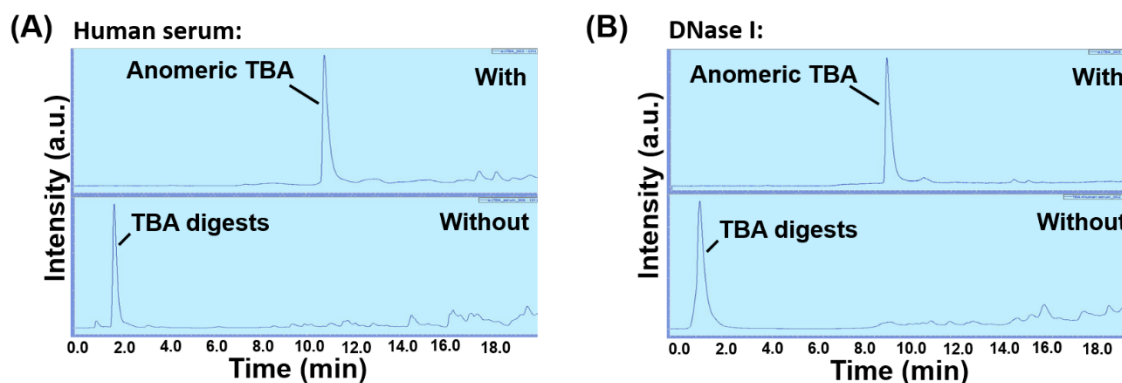


**Fig. S4.1** Nuclease resistance of anomeric TBA. Anomeric TBA (0.10 mM) was mixed with thrombin (25  $\mu$ M) in D-PBS and incubated for 3 hours at 37°C. It was mixed with human serum (40% (v/v)) or with ten units of DNase I for 24 hours at 37°C. Then, the reaction mixture was heated at 95°C for 10 minutes and centrifuged at 10000 g for 10 minutes. The supernatant was analyzed by LC analysis. LC profile treated with (A) human serum and (B) DNase I.

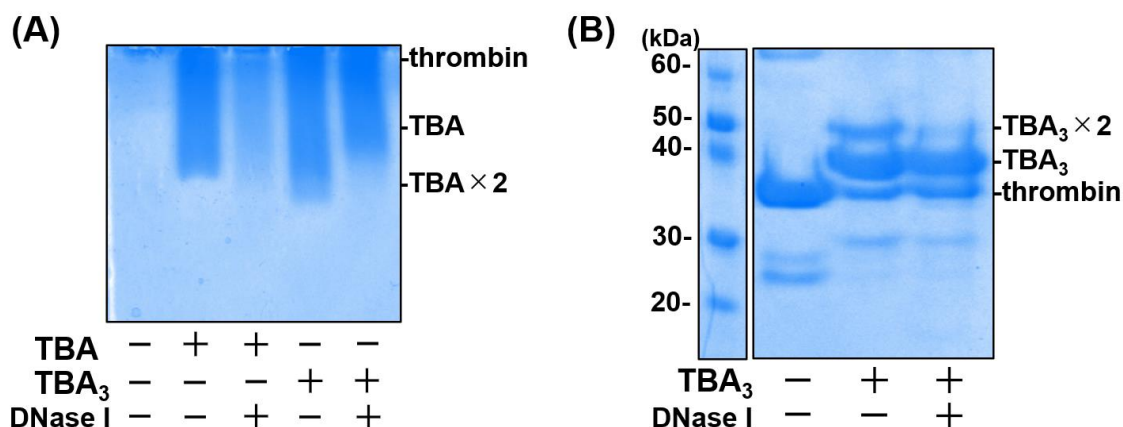


**Fig. S4.2** Evaluation of nuclease resistance of naive TBA and TBA<sub>3</sub> in the presence of DNase I. TBA or TBA<sub>3</sub> (0.10 mM) was mixed with thrombin (25  $\mu$ M) in D-PBS and incubated for 3 hours at 37°C. It was mixed with ten-units of DNase I for 24 hours at 37°C. After addition of the loading buffer or sample buffer, the mixture was separated by (A) 12% native PAGE or (B) SDS-PAGE, and whole proteins were visualized by CBB staining.

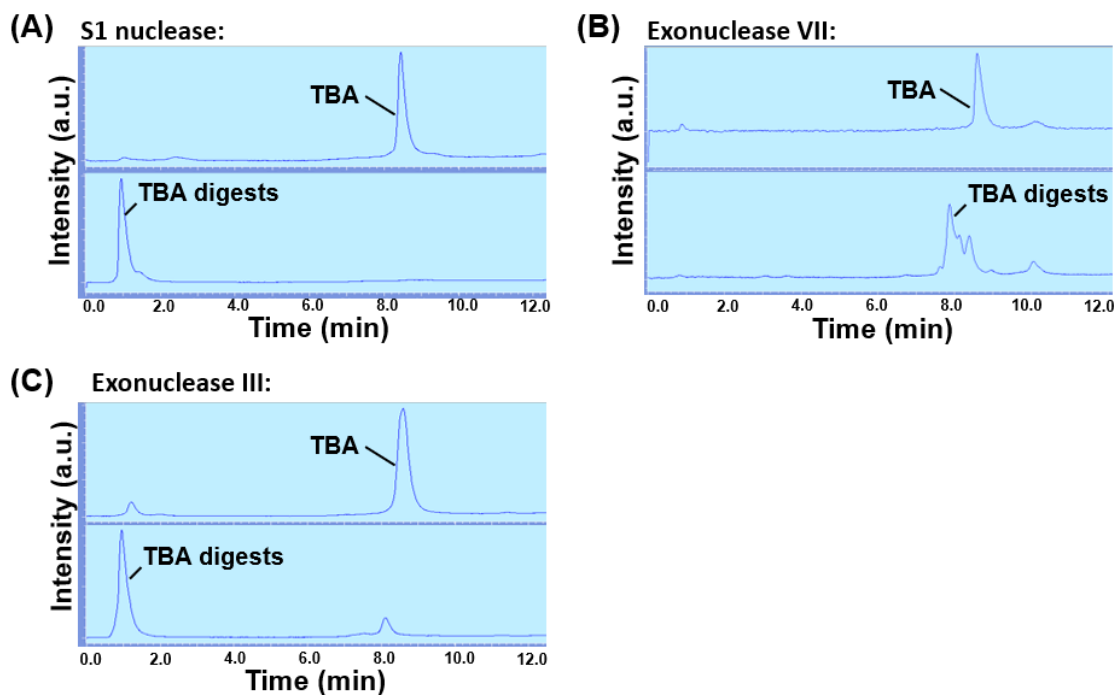


**Fig. S4.3** *Confirmation of nuclease activity.* Naïve TBA (0.10 mM) was mixed with ten units of each nuclease (DNase I, Exonuclease VII) for 24 hours at 37 °C. Then, the reaction mixture was heated at 95°C for 10 minutes and centrifuged at 10,000g for 10 minutes. The supernatant was analyzed by LC analysis. LC profiles treated with (A) S1 nuclease, (B) Exonuclease VII, and (C) Exonuclease III were shown, respectively.

# **CHAPTER 5**

## **Concluding remarks**

Biologics is one of the ideal modalities of covalent drugs for alleviating off-target reactions. However, biologics-type covalent drugs are in the dawning phase; the development method of the modality is not established enough, and further, it is difficult to overcome the potential risk of irreversible ADEs yet. To address the problem, 1) a novel direct and stringent screening method to obtain a peptidic-covalent binder using T7 phage display, and 2) a novel covalent drug modality that allows the neutralization of permanent drug action at an arbitrary time using the DNA aptamer, were developed in this study. In addition, I demonstrated a novel nuclease resistance mechanism of the DNA aptamer due to the covalent-binding to the target protein.

Middle-biologics (*i.e.*, peptides and nucleic acid) are generally recognized as unsuitable modalities for drugs because of the very short half-life *in vivo* derived from nuclease digestion and rapid renal clearance. However, applying covalent-binding ability against target proteins to middle-biologics, could result in prolonged drug action, regardless of the macroscopically observable pharmacokinetic half-life, due to covalent-binding to the target protein. Furthermore, chapter 3 suggested that middle-biologics might obtain the nuclease resistance by covalent-binding to the target protein. Considering the above, middle-biologics would be withstood use *in vivo* by applying covalent-binding ability. In the future, I will continue to challenge the development of biologics type covalent drugs, and prove how suitable are biologics and covalent drugs for clinical application.

# **CHAPTER 6**

## **References**

## ■ References

1. T. A. Baillie, *Angew. Chem. Int. Ed. Engl.*, 2016, **55**, 13408.
2. J. Gan, H. Zhang and W. G. Humphreys, *Chem. Res. Toxicol.*, 2016, **29**, 2040.
3. A. J. Smith, X. Zhang, A. G. Leach and K. N. Houk, *J. Med. Chem.*, 2009, **52**, 225.
4. D. S. Johnson, E. Weerapana and B. F. Cravatt, *Future Med. Chem.*, 2010, **2**, 949.
5. R. Lagoutte, R. Patouret and N. Winssinger, *Curr. Opin. Chem. Biol.*, 2017, **39**, 54.
6. J. Singh, R. C. Petter, T. A. Baillie and A. Whitty, *Nat. Rev. Drug. Discov.*, 2011, **10**, 307.
7. R. A. Copeland, *Methods Biochem. Anal.*, 2005, **46**, 1.
8. R. A. Bauer, *Drug Discov. Today*, 2015, **20**, 1061.
9. A. J. Claxton, J. Cramer and C. Pierce, *Clin. Ther.*, 2001, **23**, 1296.
10. W. J. Pichler, D. J. Naisbitt and B. K. Park, *J. Allergy Clin. Immunol.*, 2011, **127**, S74.
11. H. Cao, K. Wang, Y. L. Ye and J. H. Shen, *Curr. Med. Chem.*, 2017, **24**, 3921.
12. H. F. Zhu and Y. Li, *Nat. Prod. Bioprospect.*, 2018, **8**, 297.
13. R. Ferreira de Freitas and M. Schapira, *Medchemcomm.*, 2017, **8**, 1970.
14. M. S. Rao, R. Gupta, M. J. Liguori, M. Hu, X. Huang, S. R. Mantena, S. W. Mittelstadt, E. A. G. Blomme and T. R. Van Vleet, *Front Big Data*, 2019, **2**, 25.
15. T. Zhang, J. M. Hatcher, M. Teng, N. S. Gray and M. Kostic, *Cell. Chem. Biol.*, 2019, **26**, 1486.
16. L. Gambini, C. Baggio, P. Udompholkul, J. Jossart, A. F. Salem, J. J. P. Perry and M. Pellicchia, *J. Med. Chem.*, 2019, **62**, 5616.
17. Q. Li, Q. Chen, P. C. Klauser, M. Li, F. Zheng, N. Wang, X. Li, Q. Zhang, X. Fu, Q. Wang, Y. Xu and L. Wang, *Cell*, 2020, **182**, 85.
18. V. Y. Berdan, P. C. Klauser and L. Wang, *Bioorg. Med. Chem.*, 2021, **29**, 115896.
19. Y. Tabuchi, J. Yang and M. Taki, *Chem. Commun.*, 2021, **57**, 2483.
20. R. B. Merrifield, *J. Am. Chem. Soc.*, 1963, **85**, 5.
21. L. Wang, A. Brock, B. Herberich and P. G. Schultz, *Science*, 2001, **292**, 498.
22. L. Wang and P. G. Schultz, *Angew. Chem. Int. Ed. Engl.*, 2004, **44**, 34.
23. L. Wang, *Acc. Chem. Res.*, 2017, **50**, 2767.
24. Z. Xiang, H. Ren, Y. S. Hu, I. Coin, J. Wei, H. Cang and L. Wang, *Nat. Methods*, 2013, **10**, 885.
25. Q. Zheng, J. L. Woehl, S. Kitamura, D. Santos-Martins, C. J. Smedley, G. Li, S. Forli, J. E. Moses, D. W. Wolan and K. B. Sharpless, *Proc. Natl. Acad. Sci. U S A*, 2019, **116**, 18808.
26. J. Dong, L. Krasnova, M. G. Finn and K. B. Sharpless, *Angew. Chem. Int. Ed. Engl.*, 2014, **53**, 9430.

27. A. S. Barrow, C. J. Smedley, Q. Zheng, S. Li, J. Dong and J. E. Moses, *Chem. Soc. Rev.*, 2019, **48**, 4731.
28. A. Narayanan and L. H. Jones, *Chem. Sci.*, 2015, **6**, 2650.
29. H. Mukherjee, J. Debreczeni, J. Breed, S. Tentarelli, B. Aquila, J. E. Dowling, A. Whitty and N. P. Grimster, *Org. Biomol. Chem.*, 2017, **15**, 9685.
30. B. Yang, N. Wang, P. D. Schnier, F. Zheng, H. Zhu, N. F. Polizzi, A. Ittuveetil, V. Saikam, W. F. DeGrado, Q. Wang, P. G. Wang and L. Wang, *J. Am. Chem. Soc.*, 2019, **141**, 7698.
31. R. Xu, T. Xu, M. Yang, T. Cao and S. Liao, *Nat. Commun.*, 2019, **10**, 3752.
32. Y. Shishido, F. Tomoike, Y. Kimura, K. Kuwata, T. Yano, K. Fukui, H. Fujikawa, Y. Sekido, Y. Murakami-Tonami, T. Kameda, S. Shuto and H. Abe, *Chem. Commun.*, 2017, **53**, 11138.
33. C. Hoppmann and L. Wang, *Chem. Commun.*, 2016, **52**, 5140.
34. R. Liu, X. Li and K. S. Lam, *Curr. Opin. Chem. Biol.*, 2017, **38**, 117.
35. Y. Tabuchi and M. Taki, *Anal. Bioanal. Chem.*, 2018, **410**, 6713.
36. S. Uematsu, Y. Tabuchi, Y. Ito and M. Taki, *Bioconjug. Chem.*, 2018, **29**, 1866.
37. S. Chen, S. Lovell, S. Lee, M. Fellner, P. D. Mace and M. Bogoy, *Nat. Biotechnol.*, 2020, **39**, 490.
38. Y. Tabuchi, T. Watanabe, R. Katsuki, Y. Ito and M. Taki, *Chem. Commun.*, 2021, **57**, 5378.
39. K. Fukunaga, T. Hatanaka, Y. Ito and M. Taki, *Mol. Biosyst.*, 2013, **9**, 2988.
40. K. Fukunaga, T. Hatanaka, Y. Ito, M. Minami and M. Taki, *Chem. Commun.*, 2014, **50**, 3921.
41. G. T. James, *Anal. Biochem.*, 1978, **86**, 574.
42. K. Fukunaga and M. Taki, *J. Nucleic. Acids*, 2012, **2012**, 295719.
43. M. Lunder, T. Bratkovic, U. Urleb, S. Kreft and B. Strukelj, *Biotechniques*, 2008, **44**, 893.
44. Y. Tokunaga, Y. Azetsu, K. Fukunaga, T. Hatanaka, Y. Ito and M. Taki, *Molecules*, 2014, **19**, 2481.
45. Y. Fukunishi, Y. Mikami and H. Nakamura, *J. Phys. Chem. B*, 2003, **107**, 13201.
46. W. H. Habig, M. J. Pabst and W. B. Jakoby, *J. Biol. Chem.*, 1974, **249**, 7130.
47. C. Baggio, P. Udompholkul, L. Gambini, A. F. Salem, J. Jossart, J. J. P. Perry and M. Pellicchia, *J. Med. Chem.*, 2019, **62**, 9188.
48. C. Veryser, J. Demaerel, V. Bieliu Nas, P. Gilles and W. M. De Borggraeve, *Org. Lett.*, 2017, **19**, 5244.
49. Y. Fukunishi, Y. Mikami and H. Nakamura, *J. Mol. Graph. Model*, 2005, **24**, 34.

50. K. Wakui, T. Yoshitomi, A. Yamaguchi, M. Tsuchida, S. Saito, M. Shibukawa, H. Furusho and K. Yoshimoto, *Mol. Ther. Nucl. Acids*, 2019, **16**, 348.
51. C. P. Rusconi, E. Scardino, J. Layzer, G. A. Pitoc, T. L. Ortel, D. Monroe and B. A. Sullenger, *Nature*, 2002, **419**, 90.
52. H. Stoll, H. Steinle, N. Wilhelm, L. Hann, S. J. Kunnakattu, M. Narita, C. Schlensak, H. P. Wendel and M. Avci-Adali, *Molecules*, 2017, **22**, 954.
53. K. M. Bompiani, R. S. Woodruff, R. C. Becker, S. M. Nimjee and B. A. Sullenger, *Curr. Pharm. Biotechnol.*, 2012, **13**, 1924.
54. T. Adachi and Y. Nakamura, *Molecules*, 2019, **24**, 4229.
55. X. Chen, L. Qiu, R. Cai, C. Cui, L. Li, J. H. Jiang and W. Tan, *ACS Appl. Mater. Interfaces*, 2020, **12**, 37845.
56. Y. Zhang, B. S. Lai and M. Juhas, *Molecules*, 2019, **24**, 941.
57. J. Zhou and J. Rossi, *Nat. Rev. Drug Discov.*, 2017, **16**, 181.
58. C. P. Rusconi, J. D. Roberts, G. A. Pitoc, S. M. Nimjee, R. R. White, G. Quick, Jr., E. Scardino, W. P. Fay and B. A. Sullenger, *Nat. Biotechnol.*, 2004, **22**, 1423.
59. A. D. Ellington and J. W. Szostak, *Nature*, 1990, **346**, 818.
60. L. C. Bock, L. C. Griffin, J. A. Latham, E. H. Vermaas and J. J. Toole, *Nature*, 1992, **355**, 564.
61. M. Blind and M. Blank, *Mol. Ther. Nucleic Acids*, 2015, **4**, e223.
62. W. X. Li, A. V. Kaplan, G. W. Grant, J. J. Toole and L. L. Leung, *Blood*, 1994, **83**, 677.
63. L. C. Griffin, G. F. Tidmarsh, L. C. Bock, J. J. Toole and L. L. Leung, *Blood*, 1993, **81**, 3271.
64. V. V. Rostovtsev, L. G. Green, V. V. Fokin and K. B. Sharpless, *Angew. Chem. Int. Ed. Engl.*, 2002, **41**, 2596.
65. I. Russo Krauss, A. Merlino, A. Randazzo, E. Novellino, L. Mazzarella and F. Sica, *Nucleic Acids Res.*, 2012, **40**, 8119.
66. S. Nagatoishi, Y. Tanaka and K. Tsumoto, *Biochem. Bioph. Res. Co.*, 2007, **352**, 812.
67. E. G. Zavyalova, A. D. Protopopova, I. V. Yaminsky and A. M. Kopylov, *Anal. Biochem.*, 2012, **421**, 234.
68. R. Hansen, U. Peters, A. Babbar, Y. Chen, J. Feng, M. R. Janes, L. S. Li, P. Ren, Y. Liu and P. P. Zarrinkar, *Nat. Struct. Mol. Biol.*, 2018, **25**, 454.
69. M. D. Hanwell, D. E. Curtis, D. C. Lonie, T. Vandermeersch, E. Zurek and G. R. Hutchison, *J. Cheminform.*, 2012, **4**, 17.
70. F. Odeh, H. Nsairat, W. Alshaer, M. A. Ismail, E. Esawi, B. Qaqish, A. A. Bawab and S. I. Ismail, *Molecules*, 2019, **25**, 3.
71. J. W. Weisel and R. I. Litvinov, *Blood*, 2013, **121**, 1712.

72. J. Byun, *Life*, 2021, **11**, 193.
73. S. Ni, H. Yao, L. Wang, J. Lu, F. Jiang, A. Lu and G. Zhang, *Int. J. Mol. Sci.*, 2017, **18**, 1683.
74. S. E. Smith and A. G. Papavassiliou, *Nucleic Acids Res.*, 1992, **20**, 5239.
75. D. J. Galas and A. Schmitz, *Nucleic Acids Res.*, 1978, **5**, 3157.
76. X. L. Wang, F. Li, Y. H. Su, X. Sun, X. B. Li, H. J. Schluesener, F. Tang and S. Q. Xu, *Anal. Chem.*, 2004, **76**, 5605.
77. Y. Liu, C. Wang, F. Li, S. Shen, D. L. Tyrrell, X. C. Le and X. F. Li, *Anal. Chem.*, 2012, **84**, 7603.
78. H. W. Hu, Y. J. Ding, Z. H. Gao and H. Li, *Sensor Actuat. B-Chem.*, 2021, **331**.
79. P. A. Schwartz, P. Kuzmic, J. Solowiej, S. Bergqvist, B. Bolanos, C. Almaden, A. Nagata, K. Ryan, J. Feng, D. Dalvie, J. C. Kath, M. Xu, R. Wani and B. W. Murray, *Proc. Natl. Acad. Sci. U S A*, 2014, **111**, 173.

## ■ List of publications

### Chapter 1

**Y. Tabuchi**, M. Taki\*, Fluorescent 'keep-on' type pharmacophore obtained from dynamic combinatorial library of Schiff bases, *Anal. Bioanal. Chem.*, **410**, 6713 (2018).

### Chapter 2

**Y. Tabuchi**, T. Watanabe, R. Katsuki, Y. Ito, M. Taki\*, Direct screening of a target-specific covalent binder: stringent regulation of warhead reactivity in a matchmaking environment, *Chem. Commun.*, **57**, 5378 (2021), selected as HOT article and cover article.

### Chapter 3

**Y. Tabuchi**, J. Yang\*, M. Taki\*, Inhibition of thrombin activity by a covalent-binding aptamer and reversal by the complementary strand antidote, *Chem. Commun.*, **57**, 2483 (2021), selected as cover article.

### Chapter 4

**Y. Tabuchi**, J. Yang\*, M. Taki\*, *to be submitted*.

### Others

**田淵雄大\***, 瀧真清\*, 薬効の中和が可能なアプタマー型共有結合性薬剤の開発, 日本生物工学会誌, 第 99 卷, 第 4 号, 172 (2021); invited.

**田淵雄大\***, 瀧真清\*, Covalent Biologics: 中・高分子型共有結合性薬剤, ファルマシア, 第 57 卷, 第 11 号, 1024 (2021); invited.

S. Uematsu, **Y. Tabuchi**, Y. Ito, and M. Taki\*, Combinatorially Screened Peptide as Targeted Covalent Binder: Alteration of Bait-Conjugated Peptide to Reactive Modifier, *Bioconjug. Chem.*, **29**, 1866 (2018).

K. Yatabe, M. Hisada, **Y. Tabuchi**, and M. Taki\*, A Cysteine-Reactive Small Photo-Crosslinker Possessing Caged-Fluorescence Properties: Binding-Site Determination of a Combinatorially-

Selected Peptide by Fluorescence Imaging / Tandem Mass Spectrometry, *Int. J. Mol. Sci.*, **19**, 3682 (2018).

谷田部和貴, 田淵雄大, 望月和人, 瀧真清\*, フェージディスプレイ法を利用した機能性ペプチドスクリーニング, 医薬品開発における中分子領域 (核酸医薬・ペプチド医薬) の開発戦略, pp.139-143 (2019); invited.

\*Corresponding author

## ■ List of presentations

1. **Y. Tabuchi**, J. Yang, M. Taki, Covalent-binding aptamer: a new covalent drug modality for control of irreversible inhibition activity, The 48th International Symposium on Nucleic Acids Chemistry 2021, P-20, Online, October 2021 (Poster).
2. **Y. Tabuchi**, M. Taki, Fluorescent “keep-on” type pharmacophore: a novel principle of fluorescence detection for improving the signal-to-noise ratio, Irago conference 2019, #251, August, 2019 (Poster).
3. **Y. Tabuchi**, S. Uematsu, Y. Ito, M. Taki, Combinatorial Screened biologics as Targeted Covalent Binder, Gordon research conference: Biotherapeutics and Vaccines Development, #6, January 2019 (Poster).
4. S. Uematsu, **Y. Tabuchi**, Y. Ito, M. Taki, COMBINATORIALLY SCREENED PEPTIDE AS TARGETED COVALENT BINDER, 35th European Peptide Symposium (2018), #251, August, 2018 (Poster).
5. **田淵雄大**, Jay Yang, 瀧真清, 『コバレントドラッグ化によるアプタマーの機能拡張』、第 44 回日本分子生物学会年会、1PWS1-09、オンライン開催、2021 年 12 月 (口頭発表)。
6. **田淵雄大**, 渡辺嵩人, 勝木陸, 伊東祐二, 瀧真清, 『拡張ファージディスプレイ法によるペプチド型コバレントドラッグの直接的な取得』、第 58 回ペプチド討論会、Y-06、オンライン開催、2021 年 10 月 (口頭発表)。
7. **田淵雄大**, 『中分子バイオリジクス型共有結合性薬剤』、第 15 回バイオ関連化学シンポジウム、1C-15、オンライン開催、2021 年 9 月 (口頭発表)。
8. **田淵雄大**, Jay Yang, 瀧真清, 『薬効の中和が可能なアプタマー型コバレントドラッグの開発』、若手ペプチド夏の勉強会、オンライン開催、2021 年 8 月 (ポスター発表)。
9. **田淵雄大**, 渡辺嵩人, 勝木陸, 伊東祐二, 瀧真清, 『拡張ファージディスプレイ法による直接的なペプチド型コバレントドラッグの取得』、若手ペプチド夏の勉強会、オンライン開催、2021 年 8 月 (口頭発表)。
10. **田淵雄大**, 瀧真清, 『薬効の中和が可能なアプタマー型コバレントドラッグの開発』、日本核酸化学会若手フォーラム、オンライン開催、2021 年 8 月 (口頭発表)。
11. **田淵雄大**, 瀧真清, 『中分子を用いたバイオリジクス型コバレントドラッグの開発』、生体機能関連化学部会若手の会 第 32 回サマースクール、P-43、オンライン開催、2021 年 7 月 (ポスター発表)。

12. **田淵雄大**、Jay Yang、瀧真清、『Inhibition of thrombin activity by a covalent-binding aptamer and reversal by the complementary strand antidote』、日本核酸医薬品学会 第 6 回年会 サテライト若手シンポジウム (2021)、WT-02、オンライン開催、2021 年 6 月 (口頭発表).
13. **田淵雄大**、Jay yang、瀧真清、『Inhibition of thrombin activity by a covalent-binding aptamer and reversal by the complementary strand antidote』、日本核酸医薬品学会第 6 回年会 (2021)、P-15、オンライン開催、2021 年 6 月 (ポスター発表).
14. **田淵雄大**、谷田部和貴、瀧真清、加水分解型蛍光分子を用いた蛋白質検出法の開発、日本化学会第 98 回春季年会, 1D4-42、日本大学理工学部船橋キャンパス、2018 年 3 月(口頭発表).

## ■ List of grants and awards

### Grants

1. JSPS KAKENHI grant (#20J22890), Yudai Tabuchi
2. Sasakawa scientific research grant from Japan science society, Yoshiki Nara, Yudai Tabuchi

### Awards

1. 田淵雄大 「ペプチド討論会 若手口頭発表優秀賞」2021年10月.
2. 田淵雄大 「若手ペプチド夏の勉強会 ポスター発表優秀賞」2021年8月.
3. 田淵雄大 「日本核酸医薬品学会第6回年会 川原賞」2021年6月.
4. 田淵雄大 「文科省データ関連人材育成プログラム 最優秀賞」2021年3月.
5. 田淵雄大 「電気通信大学 学生表彰」2020年3月.
6. 田淵雄大 「電気通信大学 優秀発表賞」2020年3月.
7. 田淵雄大 「第一回基礎理工学研究会 口頭発表優秀賞」2020年1月.
8. 田淵雄大 「第24回冬季複合材料研究会 口頭発表優秀賞」2019年12月.
9. 田淵雄大 「電気通信大学 学生表彰」2019年3月.
10. 田淵雄大 「日本ペプチド学会 2018年度 JPS Travel Award」2018年8月.
11. 田淵雄大 「第21回夏季複合材料研究会 口頭発表優秀賞」2018年7月.
12. 田淵雄大 「トビタテ！留学 JAPAN 日本代表プログラム 採択」2018年6月.
13. 田淵雄大 「電気通信大学 目黒会賞」2018年3月.
14. 田淵雄大 「電気通信大学 優秀発表賞」、2018年3月.
15. 田淵雄大 「第20回冬季複合材料研究会 口頭発表特別賞」2017年12月.
16. 田淵雄大 「第19回夏季複合材料研究会 ポスター発表優秀賞」2017年7月.

## ■ Acknowledgments

I would like to thank Prof. Masumi Taki for allowing me to work in his laboratory even though my grade was bottom in UEC. His constant support, philosophy, and encouragement have been extremely helpful for the development of this work and for my life as a scientist and a person.

I would also like to thank Prof. Jay Yang for allowing me to work in his laboratory at the University of Wisconsin-Madison. The idea of this work was born by a fruitful discussion with him. He taught me the fun of research, not only research techniques.

I am grateful to Prof. Yuji Ito (Kagoshima University) for providing T7 phage peptide libraries, Prof. Youngsook Lee (Wisconsin University) and Prof. Ying Ge for providing me with experimental facilities, and Dr. Yanglong Zhu for the technical assistance, respectively.

Financially, this work was supported by grants of Japan Society for the Promotion of Science - KAKENHI grant (#20J22890) and an internal UEC grant for promoting research integration (originating in the MEXT, the program for promoting the enhancement of research universities) to Yudai Tabuchi and Masumi Taki, respectively.

Finally, I would like to thank my wife and parents, who supported my research life at the graduate school(s).